Evaluation of Lipid-Based Nanoparticles for the Treatment of Cardiovascular Diseases

by

Kristen Wai Yan Hong Dorsey

A dissertation submitted in partial fulfillment
of the requirements for the degree of
Doctor of Philosophy
(Pharmaceutical Sciences)
in the University of Michigan
2024

Doctoral Committee:

Professor Anna Schwendeman, Chair
Professor Y. Eugene Chen
Professor James Moon
Professor Duxin Sun

Kristen Hong Dorsey

kwhong@umich.edu

ORCID ID: 0000-0003-2742-4658

Dedication

To my amazing mother, Sauling. Without you, I wouldn't be where I am today.

With love, always.

Acknowledgements

I first want to express my sincerest gratitude to my mentor, Dr. Anna Schwendeman, for all the scientific and life advice you have provided me in the last five years. Thank you for always being supportive of my academic and career goals and for helping me grow into a better scientist and a better person. I would also like to extend a huge thank you to the rest of my committee, Dr. James Moon, Dr. Duxin Sun and Dr. Eugene Chen for their time and invaluable guidance throughout my PhD career.

I would like to thank the past and present members of the Schwendeman labs that have made the lab such an enjoyable place to be. I will always cherish the time I spent with all of you and appreciate all the chats and fun we had. I would especially like to thank Karl Olsen for his help on my animal studies. It was a pleasure hearing all your life stories during our long hours with the rats. To Brian, thank you for teaching me everything I know about mass spectrometry. Your patience and guidance were crucial to me as I worked to finish my last chapter, and for that, I am incredibly grateful for you. Special thanks to Dr. Minzhi Yu, Dr. Troy Halseth, Dr, Mark Vander Roest, Hannah Naldrett, and Julia Crowther, Dr. Jingyao Gan, and Youngseo Na for working with me on my projects. Thank you to Troy, Corrine, Jill, John, Mark, Cameron, and Swetha for all the interesting lunch conversations we've had. To everyone in the lab who has helped me through tough times, I will forever be thankful for you.

Additionally, I would also like to thank the College of Pharmacy and all my funding sources that made this research possible. I was fortunate to be funded by two NIH T32 training

programs at the University of Michigan, the Pharmacological Sciences Training Program (NIH T32 GM140223) and the Training Program in Translational Cardiovascular Research and Entrepreneurship (NIH T32 HL125242). I would also like to thank my funding from the American Foundation for Pharmaceutical Education Pre-Doctoral Fellowship.

To my support system in Columbus, thank you for being here since day one of my graduate school journey. To Leah, Monica, Kelsey, Ashley and Bri, thank you for all our girls' trips and always welcoming me back home. I am incredibly grateful for all our crazy nights, funny stories, and unforgettable memories in Vegas. Thank you for supporting me, celebrating me, and helping me through life over the past 5.5 years.

To my Michigan family, I am so happy this experience brought us together. I am so thankful to have celebrated birthdays, engagements, weddings, graduations, and all the big life events with all of you. For all the tailgates, times at Hill house, trips around Michigan, bar hangs, etc., grad school wouldn't have been the same without you all. To the Michigan girls – Mery, Corrine, Jill, and Meg, I am so grateful that you were brought into my life. Thank you for laughing with me, crying with me, and letting me express my emotions to you all the time. To Luis, thank you for always being willing to talk and providing support in times of need.

To my family, thank you for the support and unconditional love you have provided me. Thank you to the Dorsey's for allowing me to be a part of your family. To my dad, thank you for all your wisdom you have imparted to me. I have enjoyed all our chats about PhD life. To my siblings and siblings-in-law: Andrea, Kevin, Matt, and Martha, I am so grateful for all the family time we have spent together over the last few years. To my husband, Owen, thank you for all the sacrifices you have made for me and for being by my side through this whole journey. Special

shout out to my beautiful and wonderful Rhodesian ridgebacks, Nacho and Cheddar, for being the best therapy dogs in the world.

Last but not least, I would not be here without the love and support of my mom. Mom- thank you everything you did for me. I believe that all the hours spent at CVS as a child and times in the pharmacy with you led me to pursue this field of study. Thank you for being the perfect role model, for showing me that kindness can take you far, and for supporting me every step of the way. Without you, I wouldn't be who I am today.

Table of Contents

Dedication ii

Acknowledgements iii

List of Tables viii

List of Figures ix

Abstract xiii

Chapter 1 - Introduction 1

1.1 High-density lipoprotein 1

1.2 HDL structure and composition 2

1.3 HDL transformations and plasma stability in circulation 5

1.4 HDL biological functions 7

1.5 Disease implications: endothelial dysfunction and atherosclerosis 10

1.6 Synthetic high-density lipoproteins (sHDL) and clinical trials 16

1.7 sHDL As a drug delivery vehicle 19

1.8 sHDL mimetic nanoparticles 20

1.9 Research scope 29

1.10 Dissertation overview 30

1.11 References 32

Chapter 2 Effect of Lipid Composition of the Atheroprotective Properties of HDL-Mimicking Micelles 39

2.1 Abstract 39

2.2 Introduction 40

2.3 Material and methods 41

2.4 Results 46

2.5 Discussion 56

2.6 Conclusion 58

2.7 References 59

Chapter 3 – Evaluation of Synthetic High-Density Lipoproteins for the Protection of Endothelial Function 63

3.1 Abstract 63

3.2 Introduction 64

3.3 Materials and methods 66

3.4 Results 69

3.5 Discussion 76

3.6 Conclusion 79

3.7 References 80

Chapter 4 - Understanding Synthetic High-Density Lipoprotein Remodeling Ex Vivo Using Human Serum 84

4.1 Abstract 84

4.2 Introduction 85

4.3 Materials and methods 86

4.4 Results 91

4.5 Discussion 104

4.6 Conclusion 109

4.7 References 110

Chapter 5 Conclusions and Perspectives 114

List of Tables

Table 1.1 Breakdown of endogenous lipoprotein populations found in blood circulation. Derived from Ginsberg et.al. [25]. 5

Table 1.2 Characteristics and clinical updates of apolipoprotein A-I-based rHDL infusion therapeutics. 17

Table 2.1 Average particle size of different micelles measured by DLS (n = 3, mean ± SD). Micelles were diluted to a 2mM concentration with PBS and size was determined using Malvern Zetasizer Nano ZSP. 47

Table 2.2 Pharmacokinetic parameters (% CV) of phospholipids after a 136 μmol/kg dose of micelles containing different PC lipids. 52

Table 2.3 Pharmacodynamic parameters (% CV) of total cholesterol (TC), free cholesterol (FC) and cholesterol ester (CE) after 136 μmol/kg doses of micelles containing different PC lipids. 53

Table 2.4 Pharmacokinetic parameters (% CV) of phospholipids for micelles containing different ratios of DMPC:DSPE-PEG2k lipid dosed at 136 μmol/kg. 54

Table 2.5 Pharmacodynamic parameters (% CV) of total cholesterol (TC), free cholesterol (FC) and cholesterol ester (CE) for DMPC micelles containing different ratios of PC:DSPE-PEG lipid dosed at 136 μmo/kg. 55

List of Figures

Figure 1.1 HDL remodeling by HL, CETP, PLTP and SR-BI [30]..... 7

Figure 1.2 Endothelial dysfunction is the first step of atherosclerosis development [46]. 12

Figure 1.3 Schematic representation of atheroma plaque formation from a healthy artery to plaque rupture underlying the most important vents that contribute to its development in each stage [37]..... 14

Figure 1.4 Types of HDL mimics and HDL-mimicking nanoparticles. 21

Figure 1.5 PLGA HDL-like nanoparticles. (a)"Schematic depiction of the synthesis of PLGA–HDL by microfluidic technology. PLGA–HDL nanoparticles target atherosclerotic plaques. (b) The preferential interaction of PLGA–HDL with macrophages was confirmed with flow cytometry analysis. Fluorescence of macrophages, pancreatic endothelial cells, smooth muscle cells, and hepatocytes incubated with PEG–PLGA NP (white) and PLGA–HDL (black). (c) Cholesterol efflux assay of native-HDL, PLGA–HDL, and microfluidic-synthesized HDL on human macrophage-like THP-1 cells at 50 μg/ml. (d) Fluorescence imaging of excised aortas of ApoE-/- mice injected with placebo or PLGA–HDL nanoparticles. (e) Fluorescent activated cell sorting of digested aortas injected with PLGA–HDL; the label DiR is mainly associated with monocytes and macrophages in the aorta." Figures combined and reprinted with permission from Sanchez-Gaytan et al. (2015). Copyright 2015. American Chemical Society. . 24

Figure 1.6 (a) "Synthesis of biomimetic HDL using an Au NP core for use as a therapeutic. Au NPs of 5 nm in diameter were surface-functionalized with ApoA-I and then with two phospholipids, 1,2-dipalmitoyl-sn-glycero-3-phosphoethanolamine-N-[3-(2-pyridyldithio) propionate (yellow) and 1-2-dipalmitoyl-sn-glycero-3-phosphocholine (green)." Reprinted with permission from Thaxton et al. (2009). Copyright 2009. American Chemical Society. (b) "Self-assembly of a mixture of DPPC/MPDP PE/2-MPT (175:175:175) on three apoA-I loaded AuNPs." Reprinted with permission from Lai et al. (2017). Copyright 2017. American Chemical Society. (c) "Representative synthesis of the three nanocrystal HDLs for imaging atherosclerotic plaque and their imaging of atherosclerosis. Confocal microscopy images of aortic sections of mice injected with nanocrystal HDL. Red is nanocrystal HDL, macrophages are green, and nuclei are blue. Yellow indicates colocalization of nanocrystal HDL with macrophages and is indicated by arrowheads." Reprinted with permission from Cormode et al. (2008). Copyright 2008. American Chemical Society..... 27

Figure 2.1 Micelle size and morphology analyzed by DLS (A) and TEM (B). Malvern Zetasizer Nano ZSP was used to determine the size of micelles diluted with PBS to a 2mM

concentration. Micelles were diluted to 10 μM in PBS and TEM images were taken on a 100kV Morgagni TEM equipped with a Gatan Orius CCD. 47

Figure 2.2 Cholesterol crystal dissolution after 7 days of incubation with different PC lipids (A) and different ratios of DMPC:DSPE-PEG2k (C). Effect of 4 hour incubation of different PC lipids (B) and different ratios of DMPC:DSPE-PEG2k (D) on the cholesterol efflux of J774A.1 macrophage cells containing radiolabeled cholesterol. ***P < 0.001, ****P < 0.0001 when compared to untreated PBS group. (n = 3, mean ± SD. $^{\#}$P < 0.05, $^{\#\#\#\#}$P < 0.0001 when compared to DMPC or 1:2 group). 48

Figure 2.3 TNF-α and IL-6 pro-inflammatory cytokine release was measured after induction of inflammation with LPS endotoxin in Raw 264.7 macrophage cells with simultaneous addition of micelles composed of different PC lipids (A,B) and micelles composed of different ratios of DMPC:DSPE-PEG2k lipid (C,D). *P < 0.05; **P < 0.01; ***P < 0.001: ****P < 0.0001 when compared to untreated LPS+ group. $^{\#}$P < 0.05; $^{\#\#}$P < 0.01; $^{\#\#\#}$P < 0.001: $^{\#\#\#\#}$P < 0.0001 when compared to DMPC group (n = 3, mean ± SD). 50

Figure 2.4 A pharmacokinetic/pharmacodynamic study was completed using Sprague Dawley Rats. Micelles were injected via tail vein injection and blood was collected from the jugular vein at various time points between 0 and 48 hours post-injection. The concentration of a) phospholipid, b) total cholesterol (TC), c) free cholesterol (FC), and d) cholesterol ester (CE), over a 48-hour time frame were measured using commercially available kits. Profiles of concentration vs. time are displayed over a 48 hour time period (n = 4, mean ± SD). 51

Figure 2.5 A pharmacokinetic/pharmacodynamic study was completed using Sprague Dawley Rats. Micelles were injected via tail vein injection and blood was collected from the jugular vein. The concentration of a) phospholipid, b) total cholesterol (TC), c) free cholesterol (FC), and d) cholesterol ester (CE), over a 48-hour time frame were measured using commercially available kits. Profiles of concentration vs. time are displayed over a 48 hour time period to examine the effect of DMPC:DSPE-PEG2k ratio on the phospholipid pharmacokinetics and cholesterol mobilization ability of the micelles (n = 4, mean ± SD). 54

Figure 3.1 Average particle size, size distribution and purity of sHDLs were analyzed by (A) dynamic light scattering (DLS) and (B) gel permeation chromatography (GPC). sHDLs were diluted to a 1 mg/mL concentration of PBS. 70

Figure 3.2 Expression levels of eNOS (A), E-selectin (B), ICAM1, (C) and VCAM1 (D) were measured after pretreatment with different sHDLs (0.2 mg/mL) for 18 hours, then with or without LPS endotoxin addition (1 μg/mL) to HUVECs. ****P < 0.0001 when compared to untreated LPS+ group. 72

Figure 3.3 Expression levels of eNOS (A), E-selectin (B), ICAM1 (C) and VCAM1 (D) were measured after pretreatment with different sHDLs and addition of TNF- α to HUVECs. **P < 0.01; ***P < 0.001: ****P < 0.0001 when compared to untreated TNF-α + group. 73

Figure 3.4 Nitrite concentrations measured by NOA in the media of HUVEC cells after incubation with various L-arginine concentrations for 15 minutes (A) and the presence or

absence of L-NAME pretreatment (1 hour) and DMPC-sHDL treatment (1hour) (B).*P<0.05 and **P < 0.01 when compared to control group. 74

Figure 3.5 Evans blue dye leakage past the blood brain barrier was assessed after no treatment or treatment with DMPC sHDL in mice with induced traumatic brain injury. (A) Photos of full brains after injury, treatment and IV injection of Evans blue dye. (B) Evans blue dye absorbance measured at 620 nm normalized by brain weight of injured hemisphere. (C) Evans blue dye absorbance measured at 620 nm normalized by brain weight for non-injured contralateral hemisphere. 76

Figure 4.1 Characterization of blank sHDLs, DiD-sHDLs and GW3965-sHDLs. Particle size distribution determined by dynamic light scattering (DLS) for blank sHDLs (A) and GW3965-sHDLs (C). Purity of sHDLs determined using gel permeation chromatography (GPC) analysis for blank sHDLs (B), GW3965-sHDLs (D) and DiD-sHDLs (E). 92

Figure 4.2 Percent of initial concentrations of 22A peptide (A) and PC lipid (B) measured by LC-MS after incubation of sHDLs with human serum at 37°C for various timepoints between 0 and 24 hours. The data represent mean ± SD (n =3). 93

Figure 4.3 PC lipid concentrations in human serum alone, sHDLs alone, and after incubation of sHDLs with human serum for 0, 2 and 24 hours. SEC was used to separate out different lipoprotein populations found in human serum and concentrations of PC lipid in elution fractions were measured for POPC-sHDL (A), DMPC-sHDL (B), DPPC-sHDL (C), and DSPC-sHDL (D) by LC-MS analysis. Data is represented as the mean (n=3). 94

Figure 4.4 Percent of PC lipids measured within HDL, LDL, VLDL or other elution times for POPC-sHDL (A), DMPC-sHDL (B), DPPC-sHDL (C) and DSPC-sHDL (D), and after incubation of sHDLs with human serum for 0, 2 and 24 hours with subsequent separation of lipoprotein populations by SEC. Data is represented as the mean (n=3). 95

Figure 4.5 Detection of 22A peptide in fractions resulting from separation of lipoprotein populations by SEC for human serum alone, sHDLs alone, and after incubation of sHDLs with human serum for 0, 2 and 24 hours. Movement of 22A was measured for POPC-sHDL (A), DMPC-sHDL (B), DPPC-sHDL (C), and DSPC-sHDL (D) in the conditions described above. Data is represented as the mean (n=3). 97

Figure 4.6 Percent of total 22A measured within HDL, LDL, VLDL or other elution times for POPC-sHDL (A), DMPC-sHDL (B), DPPC-sHDL (C) and DSPC-sHDL (D) alone, and after incubation of sHDLs with human serum for 0, 2 and 24 hours with subsequent separation of lipoprotein populations by SEC. Data is represented as the mean (n=3). 98

Figure 4.7 DiD fluorescence measured during SEC separation in human serum alone, DiD-sHDLs alone, and after incubation of DiD-sHDLs with human serum for 0, 2, and 24 hours for DiD-POPC-sHDL (A), DiD-DMPC-sHDL (B), DiD-DPPC-sHDL (C), and DiD-DSPC-sHDL (D). DiD fluorescence was measured at an excitation wavelength of 646 nm and emission wavelength of 663 nm. Data is represented as the mean (n=3). 100

Figure 4.8 Percent of total DiD fluorescence measured within HDL, LDL, VLDL or other elution times for POPC-sHDL (A), DMPC-sHDL (B), DPPC-sHDL (C) and DSPC-sHDL (D) alone, and after incubation of sHDLs with human serum for 0, 2 and 24 hours with subsequent separation of lipoprotein populations by SEC. Data is represented as the mean (n=3). 101

Figure 4.9 Percent of initial concentrations of GW3965 determine by LC-MS after incubation of GW3965-sHDLs with human serum at 37°C for various timepoints between 0 and 24 hours. The data represent mean ± SD (n =3). 103

Figure 4.10 GW3965 concentrations in human serum alone, GW3965-sHDLs alone, and after 0-, 2- and 24-hour incubation of GW3965-sHDLs with human serum. POPC-sHDL (A), DMPC-sHDL (B), DPPC-sHDL (C), and DSPC-sHDL (D) were subjected to the conditions above, lipoprotein populations were separated out by SEC, and concentrations of GW3965 were measured by LC-MS analysis. Data is represented as the mean (n=3). 103

Figure 4.11 Percent of total GW3965 measured within HDL, LDL, VLDL or other elution times for POPC-sHDL (A), DMPC-sHDL (B), DPPC-sHDL (C) and DSPC-sHDL (D) alone, and after incubation of sHDLs with human serum for 0, 2 and 24 hours with subsequent separation of lipoprotein populations by SEC. Data is represented as the mean (n=3). 104

Abstract

Nearly 17.9 million people die every year from cardiovascular-related diseases, which accounts for 31% of all deaths worldwide. Endogenous high-density lipoproteins (HDL) are natural cardioprotective particles that have been shown to reduce cardiovascular related risks, such as progression of atherosclerosis, inflammation, and endothelial dysfunction. Therefore, synthetic high-density lipoproteins (sHDL) have been synthesized to mimic the natural cardioprotective behaviors of endogenous HDL. In this work, we investigated the therapeutic potential of both sHDL and HDL-mimetic micelles for improving endothelial function and treating atherosclerosis, respectively, and understand how the lipid composition affects the activity of particles in vitro and in vivo, and the remodeling of the particle in the presence of other endogenous lipoproteins contained in human serum.

In chapter 2, we synthesized a library of micelles composed of different phosphatidylcholine (PC) lipids and ratios of PC to PEGylated lipids and tested these micelles in vitro and in vivo to better understand how lipid properties influence the physiochemical activity and therapeutic potential of our micelles for the treatment of atherosclerosis. Overall, micelle composition did not affect the cholesterol efflux capabilities of the particles in vitro. Micelles composed of more fluid lipids and micelles containing less PEG lipid had a more potent effects on cytokine levels in vitro, while more PEGylated micelles had a longer circulation half-life and mobilized more cholesterol in vivo. Therefore, a fine balance must be achieved to determine the composition of micelles with optimal therapeutic benefit and favorable pharmacokinetics.

In Chapter 3, we investigated the potential therapeutic benefit of sHDLs on endothelial function. sHDLs were prepared using 22A, an ApoA-1 mimetic peptide, and different PC lipids. In lipopolysaccharide (LPS) activated human umbilical vein endothelial cells (HUVECs), sHDL decreased the expression of adhesion molecules, including VCAM-1, ICAM-1, and E-selectin. DMPC-sHDLs showed the ability to increase nitric oxide release from HUVECs. Furthermore, DMPC-sHDL treatment slightly reduced Evans blue dye leakage through the blood brain barrier on the injured hemisphere in a traumatic brain injury murine model, suggesting positive effects of sHDLs on endothelial integrity. Further studies will need to be completed to determine the optimal composition of sHDL and to explore its potential in improving endothelial function.

In Chapter 4, we evaluated the effect of lipid composition on the stability and remodeling of sHDL in human serum containing other endogenous lipoprotein populations. Blank sHDLs, as well as sHDLs encapsulating DiD or GW3965, were prepared with different PC lipids (POPC, DMPC, DPPC and DSPC) and 22A. Lipoprotein populations were separated out by size exclusion chromatography (SEC) after incubation of sHDL with human serum and concentration of sHDL components within each fraction was measured by liquid chromatography-mass spectrometry (LCMS). Overall, DSPC-sHDLs remained the most intact with sHDL components and cargo staying within HDL elution times to the largest extent after incubation with human serum. POPC-sHDLs showing the most remodeling and movement of components to larger lipoprotein populations over time. Together, our findings show that the lipid composition of sHDLs affects the remodeling in human serum, suggesting that lipid composition must be considered when designing sHDLs as therapeutics and drug delivery systems.

In summary, we found that the lipid composition of HDL-mimicking micelles and sHDL affects the particle's overall activity, pharmacokinetics, stability and remodeling, making

composition a crucial factor to consider when optimizing lipid-based nanoparticles as therapeutics.

Chapter 1 - Introduction

1.1 High-density lipoprotein

High-density lipoproteins (HDL) are endogenous, nanosized, protein–lipid particles that circulate in blood and play a role in the transport and metabolism of triglycerides, phospholipids, and cholesterol [1,2]. They are the smallest lipoprotein within the circulating lipoproteins, which include very low-density lipoproteins (VLDL) and low-density lipoproteins (LDL). The most established functional properties associated with HDL are its atheroprotective activities, such as its antioxidant [3] and anti-inflammatory capabilities [4], endothelial cell maintenance functions [1], and its role in mediating cholesterol efflux. Its role in the promotion of reverse cholesterol transport (RCT) and cellular cholesterol efflux is commonly considered to be HDL's most crucial anti-atherogenic property, leading the research community to investigate whether direct infusion of reconstituted apolipoprotein A-I (ApoA-I), the major protein component of HDL, can reduce coronary events in humans with CVD [5]. The infusion of recombinant/synthetic high-density lipoproteins (rHDL/sHDL) in animals and early clinical imaging trials reported evidence of plaque regression [2,6]. A series of major ApoA-I-derived rHDL mimetics, including ETC-216/MDCO-216 (ApoA-I Milano) [7], CER-001 (recombinant, wild-type ApoA-I) [8,9], and CSL111/CSL112 (native ApoA-I isolated from human plasma) [10], have completed human clinical trials with discrete clinical performance and/or are still under investigation.

1.2 HDL structure and composition

HDL's composition is very heterogenous but mainly consists of phospholipids and amphipathic alpha-helical apolipoprotein A-I (ApoA-I). Along with ApoA-I, more than 50 other proteins have been isolated from human HDL, including other apolipoproteins, enzymes, lipid transfer proteins and other major proteins. HDL also contain many different molecular species of lipids, up to 200, as found by lipidomic analysis, including cholesterol, cholesteryl esters and triglycerides, and phospholipids. These lipids make up the surface monolayer of HDL [11].

1.2.1 Apolipoprotein A-1

ApoA-I, the primary structural protein of HDL, is secreted predominantly by the liver and the small intestine [12,13]. ApoA-I accounts for about 70% of total HDL protein. The gene responsible for ApoA-I encoding belongs to the apolipoprotein multigene superfamily, including apoA-II and apoE apolipoproteins. Mature ApoA-I contains 243 amino acid residues and is 28 kDa in atomic weight. This amphipathic protein consists of 11 and 22-mer repeats, which form the 8 alpha-helical amphipathic domains [14]. These domains allow the protein to bind to lipids and move between different lipoprotein particles, such as chylomicrons and, less frequently, very low-density lipoproteins (VLDL). Once bound, the percent of alpha-helical content shifts from 40-50% to around 75%, depending on the type of lipid or lipoprotein complex formed [14].

On a cellular level, ApoA-I interacts with cellular receptors, activates lecithin:cholesterol acyltransferase (LCAT), and facilitates many anti-atherogenic activities of HDL [11]. More specifically, ApoA-I plays a crucial role in reverse cholesterol transport, where free cholesterol is taken from peripheral tissues, esterified by LCAT, and eliminated through the liver. It has also been shown to play a role in autoimmune disease, possess anti-clotting effects on platelets due to

its structural homology with prostacyclin (PGI2), function as an anti-inflammatory molecule, and have anti-tumor activity [15–17].

1.2.2 Phospholipids

Phospholipids comprise around 50% of the HDL lipidome by weight, followed by cholesteryl esters (30-40%) and free cholesterol (5-10%). Phosphatidylcholine and sphingomyelin are the major classes of phospholipids in HDL, where around 70% of phospholipids are phosphatidylcholine species [11]. Minorly, other phospholipids in the HDL lipidome include lysophosphatidylcholine, phosphatidylethanolamine, and phosphatidylinositol [18]. Depending on the structure and subclass of HDL, phospholipid content in percent by weight can vary, and percentages of each phospholipid type are in dynamic equilibrium between HDL subpopulations. Structurally, these phospholipids make up the HDL surface lipid monolayer.

The antiatherogenic activity of HDL is highly dependent on the lipid composition of HDL. Phospholipid composition can impact cholesterol efflux through differences in physical state, which can affect the ability of HDL to accept cholesterol from peripheral tissues [18]. In disease states, the phospholipid content in HDL can also be modified by reducing some phospholipid populations and elevation in others. For example, the content of lysophosphatidylcholine was shown to be reduced in patients with low HDL-C levels, while patients with isolated arterial hypertension had reduced phosphatidylcholine content [19,20].

1.2.3 Subclasses and biosynthesis

HDL is an endogenous lipoprotein particle with a density between 1.063 and 1.21 g/ml and a size ranging from 5 to 17 nm in diameter. The heterogeneity of HDL can be attributed to ApoA-

I, which is uniquely flexible in binding differing amounts of phospholipids to create stable particles of various sizes and conformations. Depending on the state of maturation or synthesis, HDL takes on many forms *in vivo*. In terms of density, HDL can be broken up into 3 major subpopulations, HDL1, HDL2 and HDL3, listed in increasing densities and decreasing size. In terms of size and composition, it can exist as lipid-poor small discoidal particles or larger spherical particles rich in cholesterol esters and other hydrophobic cargo [21]. Pre-beta HDL, which exists in a discoidal confirmation, contains the least amount of lipids compared to other confirmations. HDL3, usually ranging from 8-9 nm in diameter, is lipid-poor with a density around 1.125-1.21 g/mL. HDL2, the large and lipid-rich HDL, has a density ranging from 1.063-1.126 g/mL with a mean size of 9-10 nm. Furthermore, the composition of different HDL subpopulations may vary in both major and minor protein and lipid components. For example, HDL can contain only ApoA-I (LpA-I) or both ApoA-I and ApoA-II (LpA-I:A-II). For HDL only containing ApoA-I, particles can increase in size as ApoA-I molecules in the particle increase from two to three to four. For LpA-I:A-II, only two ApoA-I molecules can be present in each particle, while ApoA-II can vary from one to three molecules present. In terms of lipids, the amount of different molecular species of lipids can vary, where the total content of these lipids decreases with an increase in HDL density. Moreover, the percentage of total lipid compared to sphingomyelin in HDL decreases with a decreased density of HDL.

The catabolism of HDL starts with the secretion of ApoA-I from the liver as a lipid-free apolipoprotein. The nascent form of HDL, preβ-HDL, is formed when 2 molecules of ApoA-I combine with a few molecules of lipid, such as phospholipids and cholesterol [22]. Phospholipids and free cholesterol transported via ATP-binding cassette (ABC) transporter A1 (ABCA1) rapidly lipidate the protein. The stability of ApoA-I and the formation of nascent HDL particles (discoidal

form) is dependent on this initial lipidation. The primary function of nascent HDL is to remove cholesterol and phospholipids from peripheral tissues. More specifically, nascent HDL particles enter circulation and efflux cellular cholesterol from atherosclerotic plaque-associated lipid-laden macrophages via ABCA1 to form cholesterol-rich HDL [23]. HDL matures when cholesterol is esterified to cholesterol ester (CE) by lecithin-cholesterol acyltransferase (LCAT). The hydrophobic CE sequesters into the core of HDL particles, forming a spherical mature HDL and reducing free cholesterol levels on the particle surface [24]. This reduction of free cholesterol levels is critical for maintaining the concentration gradient of free cholesterol between cells and plasma to prevent the net efflux of cholesterol from reaching equilibrium. Mature HDL can internalize more excess cholesterol effluxed by ATP-binding cassette transporter G1 (ABCG1) to become larger and more mature.

1.3 HDL transformations and plasma stability in circulation

Table 1.1 Breakdown of endogenous lipoprotein populations found in blood circulation. Derived from Ginsberg et.al. [25].

Lipoprotein	Density (g/L)	Diameter (nm)	Lipid composition of %		
			TG	Chol	PL
Chylomicrons	0.95	75-100	80-90	2-7	3-9
VLDL	0.95-1.006	30-80	55-80	5-15	10-20
IDL	1.006-1.019	25-35	20-50	20-40	15-25
LDL	1.019-1.063	18-25	5-15	40-50	20-25
HDL	1.063-1.21	5-12	5-10	15-25	20-30

HDL can be remodeled by enzymes and proteins such as hepatic lipase, phospholipid transfer protein, and endothelial lipase [26]. Hepatic lipase (HL) can hydrolyze phospholipids and triglycerides on HDL, converting lipid-rich spherical HDL (HDL_2) to smaller spherical HDL particles (HDL_3). It is also believed that HL plays a role in the catabolism of HDL, in which lipids detach from mature HDL to gradually produce smaller particles until ApoA-I is either cleared by the kidney or returns to begin the RCT pathway once again [27]. Phospholipid transfer protein (PLTP) can transfer phospholipids between HDL and other lipoproteins and participate in HDL conversion, in which there are alterations to the size and composition of HDL. Two different proposed theories explain the method by which HDL conversion occurs when PLTP binds. The first proposed method is that multiple small lipid-poor ApoA-I/phospholipid complexes dissociate from mature HDL particles and form a new, HDL particle. The second proposition is the fusion of two HDL particles, creating an unstable intermediate, in which excess phospholipids dissociate and fuse with ApoA-I to form a nascent HDL particle, while the rest of the HDL particle stabilizes, resulting in a new, mature HDL particle [28]. Lastly, endothelial lipase (EL) can bind to HDL, its preferred substrate, and hydrolyze phosphatidylcholine lipids, which can then be used in the biosynthesis of lipids when taken up by cells [29]. All these processes contribute to the existence of different forms of HDL particles in vivo.

Along with the remodeling of endogenous HDL within its own subpopulation, HDLs can exchange lipids with other lipoproteins, such as VLDL, LDL, and chylomicrons. As LCAT esterifies cholesterol, it will migrate to the core of the HDL, allowing HDL to accept more cholesterol from other lipoproteins. Cholesteryl esters in HDL can then be exchanged by cholesteryl ester transfer protein (CETP) for triglycerides from VLDL and chylomicrons, producing TG-rich HDL and cholesteryl-rich VLDL [26]. In addition, PLTP plays a significant

role in transferring phosphatidylcholine between different lipoproteins classes, sphingomyelin and diacylglycerol. PLTP facilitates the formation of mature HDL and smaller lipoproteins, like LDL, by transferring excess surface lipids from lipoproteins to HDL [28,30].

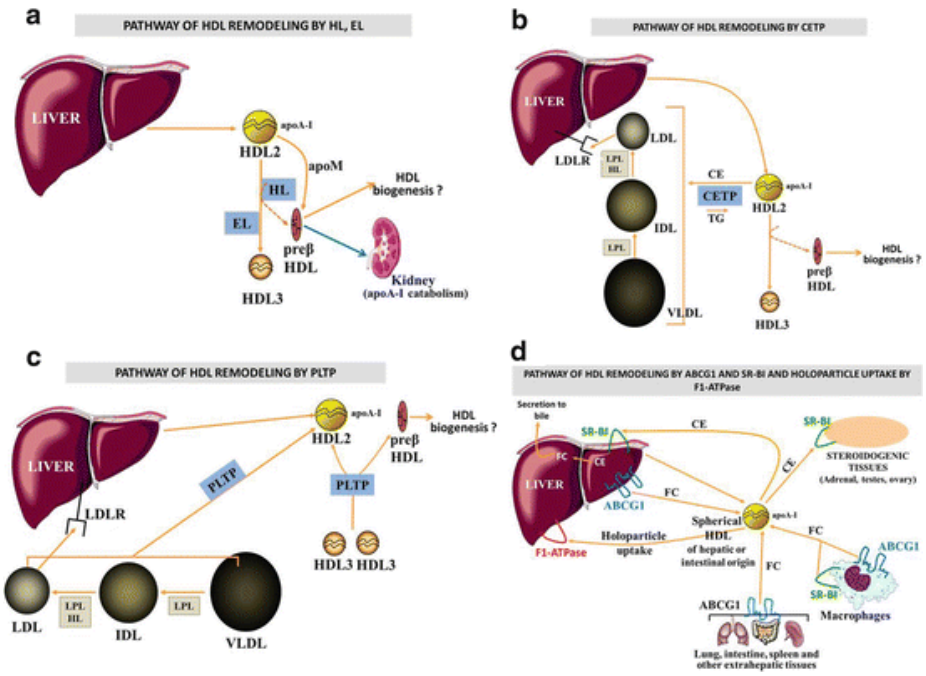

Figure 1.1 HDL remodeling by HL, CETP, PLTP and SR-BI [30].

1.4 HDL biological functions

HDL possesses several biological functions that make it a natural cardioprotective particle. One of HDL's major activities is reverse cholesterol transport, where excess cholesterol from peripheral cells is carried by HDL and delivered to the liver for elimination. HDL has anti-inflammatory activities through the reduction of cytokine and adhesion molecule expression. Lastly, HDL has been shown to positively affect endothelial function through various pathways,

including increasing nitric oxide levels, increasing endothelial nitric oxide synthase activity or abundance, and reducing endothelial cell apoptosis.

1.4.1 Reverse cholesterol transport

HDL's ability to remove excess cholesterol from atherosclerotic plaque-associated lipid-laden macrophages has been recognized as its primary mechanism of action for protecting against atherosclerosis and reducing CVD risks [7,21,31,32]. Cholesterol efflux is a process in which HDL removes excess cholesterol from peripheral tissues and delivers it to the liver for elimination or redistribution. Briefly, lipid poor ApoA-I is transcytosed through endothelial cells and is lipidated by ABCA1, where phospholipids and cholesterol combine with ApoA-I to form nascent discoidal HDL. Once cholesterol is transferred to nascent HDL particles, cholesterol is esterified by LCAT to form cholesteryl ester (CE), which then migrates to the core of HDL, forming mature, spherical HDL. Mature HDL can then mediate the removal of more cholesterol, promoting RCT, via two different methods. In the plasma compartment, mature HDL can transfer CE to low-density lipoproteins (LDL) in exchange for triglycerides (TG), a process favored by cholesteryl ester transfer protein (CETP). Hepatocytes then take up cholesterol-loaded LDL through the LDL receptor. Secondly, HDL can interact with scavenger receptor-B1 (SR-B1), which uptakes CE and other lipids from mature HDL. The CE is hydrolyzed to free cholesterol and is excreted through the feces for elimination [33].

1.4.2 Anti-inflammatory function

HDL show anti-inflammatory activity through a multitude of mechanisms. HDL’s anti-inflammatory activity may arise from the removal of oxidized lipids. Low-density lipoprotein

(LDL) oxidation can damage the artery wall cells and promote atherosclerotic plaque formation and arterial wall inflammation. HDL can play a role in slowing down LDL oxidation through enzymes that it carries, such as paraoxonase (PON), platelet-activating factor acetylhydrolase (PAFAH), and lecithin-cholesterol acyltransferase (LCAT) [11,34].

HDL has also been shown to affect lipopolysaccharide (LPS) and toll-like receptor 4 (TLR4) stimulation and activation in inflamed macrophages. LPS is an important outer-membrane component of gram-negative bacteria and is a potent TLR4 agonist. When LPS binds to TLR4, downstream signaling pathways activate NF-KB and other transcription factors, leading to the production of cytokines [35]. Numerous studies have shown that HDL can bind and neutralize LPS, leading to reductions in TLR4 activation and downstream inflammatory effects, such as the release of IL-6 and TNF- α cytokines. HDL and ApoA-I are also suggested to reduce membrane cholesterol and lipid raft contents, reducing TLR4 recruitment to the cell membrane for downstream signaling [11]. Moreover, HDL decreases the expression of VCAM-1, ICAM-1 and E-Selectin adhesion molecules, in which the synthesis is induced by the presence of cytokines [36].

1.4.3 Endothelial function

The endothelium is a network of endothelial cells that lines the inner part of blood vessels, including the arteries, veins, capillaries, and venules. It creates a selectively permeable barrier that separates the tissue from blood circulation, where molecules, cells, and pathogens are circulating. The endothelium helps maintain vascular homeostasis by promoting vasodilation, suppressing smooth muscle cell growth, and inhibiting inflammatory response. Nitric oxide (NO) is the most potent vasodilator that helps balance vasodilation and vasoconstriction of the blood vessels. It also

serves as an anti-inflammatory agent and anti-aggregant for platelets. NO is generated by endothelial NO synthase (eNOS) as a product of L-arginine conversion to L-citruline [37].

HDL has a direct role in protecting the endothelium and promoting proper function. HDL can impact endothelial nitric oxide synthase (eNOS) localization and function. For example, oxidized LDL (OxLDL) and cholesterol can cause uncoupling of eNOS and redistribution intracellularly, limiting its ability to be activated. HDL reduces the uncoupling of eNOS through its ability to prevent oxLDL formation. It has also been found that the addition of HDL can prevent eNOS displacement from the lipid plasma membrane microdomains of caveolae by preserving the lipid microenvironment. HDL can also serve as an agonist of eNOS through mediation by SR-BI [38]. Moreover, high-density lipoprotein increases the abundance of eNOS protein in human vascular endothelial cells by increasing its half-life [39].

HDL also affects endothelial cell apoptosis as well as cell proliferation and migration. Cell apoptosis can occur due to circulating inflammatory molecules disrupting endothelial cell wall integrity. These inflammatory molecules include tumor necrosis factor-α (TNF-α) and oxLDL [40]. HDL can reverse the increase in intracellular Ca^{2+} in endothelial cells by oxLDL, which prevents apoptosis. HDL can also prevent endothelial cell apoptosis induced by TNF-α by reducing the induction of caspase 3. [41]. Moreover, HDL can promote Ca+ dependent endothelial cell proliferation [42]. Lastly, endothelial cell migration is stimulated by HDL via SR-BI-initiated signaling, which promotes integrity of the endothelial monolayer [43].

1.5 Disease implications: endothelial dysfunction and atherosclerosis

Cardiovascular disease is the leading cause of death globally. Two major players in cardiovascular disease are endothelial dysfunction and atherosclerosis. Endothelial dysfunction

occurs in the early process of atherosclerosis and can contribute to the progression of the disease. In advanced atherosclerosis, plaque can rupture, leading to thrombosis and the formation of blood clots. Clots may break apart and hinder the flow of blood to the heart or brain, leading to heart attack and stroke, which accounts for almost 80% of cardiovascular deaths each year.

1.5.1 Endothelial dysfunction and implications on cardiovascular-related diseases

Endothelial dysfunction is a disease characterized by a decrease in vasodilation, production of NO, and a shift towards a pro-inflammatory state. It is associated with the development of many types of cardiovascular-related diseases, such as atherosclerosis, coronary artery disease, and diabetes. Endothelial dysfunction leads to increased vasoconstriction of the vessel wall, leukocyte adhesion, lipid infiltration, oxidative stress, and many other physiological responses that are detrimental to the cardiovascular system [37].

One of the first early events of atherosclerosis disease progression is endothelial dysfunction, where mechanical forces on the artery wall can lead to a damaged barrier and accumulation of LDL in the subendothelial space [37]. VCAM-1 binds to monocytes at the vessel wall, transforming into lipid-loaded foam cells. Uptake of oxidized LDL by LOX-1 reduces eNOS expression, leading to a diminished NO availability. Moreover, low levels of NO can weaken the atherosclerosis fibrous cap, leading to plaque rupture and thrombus formation, which can result in occlusion of the artery, causing heart attack and stroke [44]. NO deficiency also enhances smooth muscle cell proliferation and platelet aggregation and adhesion. Overall, endothelial dysfunction can initiate atherosclerosis progression, and contribute to the advancement of the disease.

A reduction in NO availability is usually linked with endothelial dysfunction. NO availability depends on (i) the bioavailability of NO, where NO can be quenched by reactive

oxygen species (ROS), and (ii) eNOS activity, which can be affected by endogenous inhibitors or substrates, such as L-arginine. The quenching of NO by ROS can lead to the uncoupling of eNOS. ROS and oxidative stress can also lead to an increased inflammatory state at the vessel wall, where adhesion molecules, such as VCAM-1 and ICAM-1, are upregulated. Production of pro-inflammatory cytokines, like TNF-α and IL-6, synthesis of adhesion molecules, and activation of NF- kB can also lead to decreased NO bioavailability [44,45].

When HDL functionality decreases, also known as dysfunctional HDL, its endothelial protective properties are also impaired. Its ability to increase NO levels, modulate eNOS activity and expression, suppress inflammatory state, and reduce endothelial cell apoptosis is greatly reduced. Thus, creating a therapeutic that can improve HDL functionality or assist/substitute for HDL would be beneficial to minimize endothelial dysfunction development and progression.

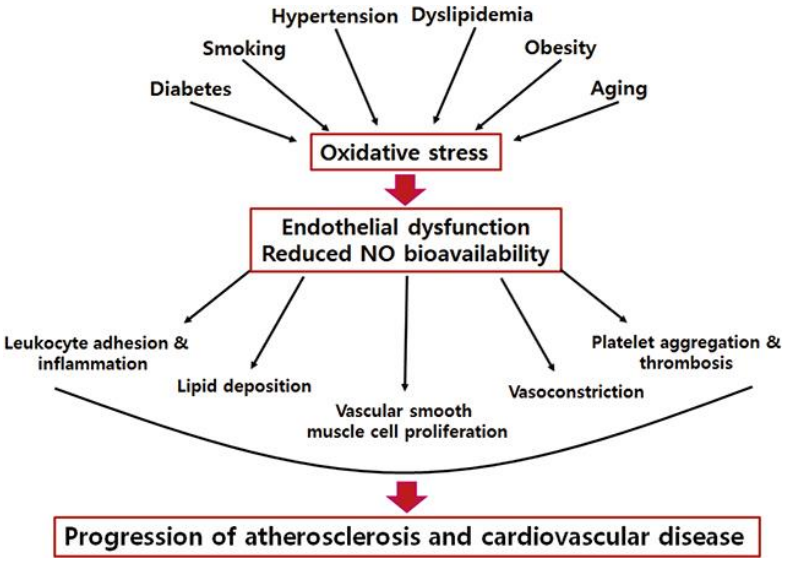

Figure 1.2 Endothelial dysfunction is the first step of atherosclerosis development [46].

1.5.2 Atherosclerosis disease progression

Atherosclerosis is a chronic inflammatory disease that is characterized by plaque buildup in the arterial lumen. Atherosclerosis is initiated when the endothelial barrier is compromised due to oxidative stress or fluid stress. This allows for an increased permeability of macromolecules, such as LDL, to pass through the endothelium layer and start accumulating in the subendothelial matrix. This accumulation of LDL stimulates pro-inflammatory molecule production by endothelial cells and recruitment of monocytes and leukocytes to the artery wall, bind to VCAM-1 and ICAM-I on endothelial cells and migration into the intima space [47]. Through differentiation, foamy macrophages are formed. These macrophages, along with endothelial cells, produce reactive oxygen species (ROS), which modify LDL to make oxidized LDL. The production of ROS also further propagates the inflammatory responses occurring from the activated endothelial cells [48]. Finally, foam cells are produced when the oxLDL bind to scavenger receptors on macrophages or are internalized by vascular smooth muscle cells through different scavenger receptors, such as CD36 and LOX-1 [49,50]. The accumulation of smooth muscles cells, cholesterol and extracellular lipids creates fibrous plaque, where the necrotic core, lipid rich and cell-free, is stabilized by fibers [51]. The migration and proliferation of vascular smooth muscle cells leads to the production of extracellular matrix component such as collagen, elastin and proteoglycans, which cover the atherosclerotic plaque and prevents it from rupture [52,53]. Once vascular smooth muscle cells start to die, the production of extracellular matrix components is reduced, which leads to a weakened fibrous cap. Inflammation can also affect production of collagen from these cells and increases expression of metalloproteinases, which makes the fibrous cap weaker [54]. Upon the rupture of the plaque, the subendothelial space is exposed to blood, leading to platelets aggregation at the site injury and form a thrombus, which can lead to arterial thrombosis [55] . Heart attack and stroke can result when the thrombus detaches

from the artery wall, circulates as an embolus clot, and obstructs blood flow to the heart or brain [37].

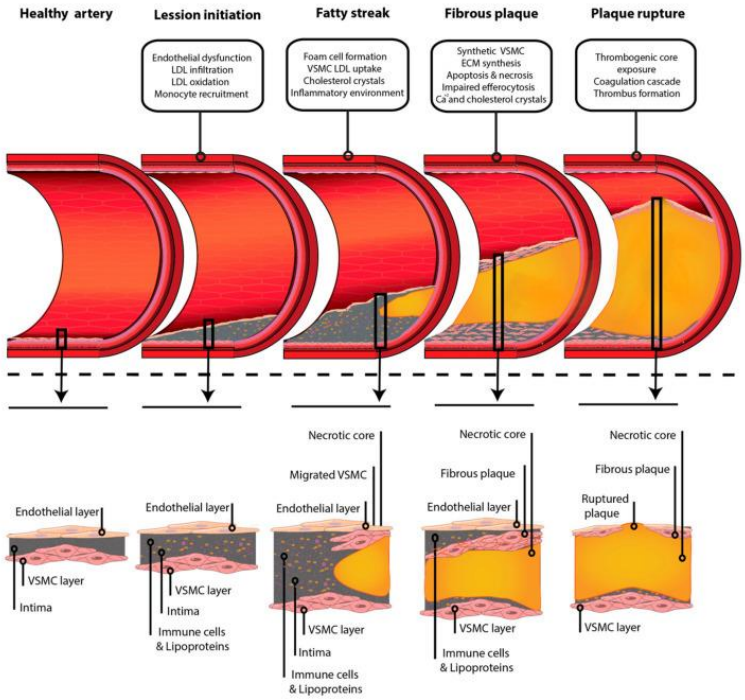

Figure 1.3 Schematic representation of atheroma plaque formation from a healthy artery to plaque rupture underlying the most important vents that contribute to its development in each stage [37].

1.5.3 Current therapies and limitations

Current therapies for endothelial dysfunction aim to preserve or restore endothelial function and to slow down possible progression of atherosclerosis. Lifestyle changes such as exercise and weight and diet control are often suggested for patients who may be able to prevent cardiovascular risk factors before they become significantly detrimental. Secondarily, pharmacological treatments can be used for patients with an already injured endothelium, in which the delay of atherosclerosis progression is the goal. These treatments include lipid-lower therapy, angiotensin receptor blockers, renin inhibitors, beta blockers, and estrogens. Many statins have been shown to improve and correct endothelial dysfunction. For example, simvastatin was shown

to reduce inflammation, oxidative stress, and endothelial apoptosis stress [56]. Angiotensin-converting enzyme inhibitors and renin inhibitors have led to an increase in NO release through increasing the activation of bradykinin [57]. Lastly, estrogens have been shown to improve endothelial function through antioxidant properties that reduce ROS production and increase NO expression [58].

In addition to the therapies used to target endothelial function, atherosclerosis therapies include fibrates, cholesterol absorption inhibitors, and PCSK9 inhibitors [59]. Statins are the first-line therapy options for atherosclerosis. Statins function by inhibiting 3-hydroxy-3-methylglutaryl coenzyme A (HMG-CoA) reductase, which in turn causes the upregulation of LDL receptors on the hepatocyte, leading to increased elimination of LDL from circulation [60]. They have also been shown to improve endothelial function, stabilize plaque, and inhibit inflammatory responses. Alternatively, for patients who do not respond positively to statins, fibrates can promote ApoA-I synthesis and reduce cholesterol ester transfer protein activity, leading to increases in HDL-C. Cholesterol absorption inhibitors, such as ezetimibe, inhibit the absorption of cholesterol in the brush border lining of the intestines. This action leads to the upregulation of LDL receptors in the liver and increased clearance of LDL from circulation. PCSK9 inhibitors prevent binding of PCSK9 to LDL-receptors at the cell surface, which usually causes internalization and degradation of the LDL receptors. By inhibiting this activity, LDL receptor expression would be greater, increasing LDL-C clearance from circulation. Overall, there are limitations to these current therapies. Improving the lipid profile can be beneficial, but patients can still fail to meet recommended LDL-C levels. Some patients cannot tolerate statins who also do not respond to other alternative lipid-lowering therapies. Moreover, it has been found in a large clinical trial that

statins only decrease the risk of a cardiovascular event by only 34% [61]. Therefore, there is room to improve treatment options for patients suffering from atherosclerosis [59].

1.6 Synthetic high-density lipoproteins (sHDL) and clinical trials

Recombinant or synthetic high-density lipoproteins (rHDL or sHDL) have been developed utilizing various ApoA-I constituents, such as purified ApoA-I from plasma, recombinant ApoA-I, or mimetic peptides, and various phospholipids, such as soy PC, sphingomyelin and other phosphatidylcholine (PC) lipids.

1.6.1 sHDL tested in clinical trials

Several ApoA-I-based reconstituted HDL therapies have been developed for intravenous administration in humans, which include three major ApoA-I–based approaches (ETC-216/MDCO-216, CER-001, and CSL111/CSL112). It is important to note that these three approaches differ considerably in composition (Table 1.2). Regarding the protein composition, ETC-216/MDCO-216 contains recombinant ApoA-I Milano, CER-001 contains recombinant wild-type human ApoA-I, and CSL111/CSL112 contains native ApoA-I isolated from human plasma. The differences in phospholipids used to reconstitute ApoA-I are also significant among these rHDL products (Table 1.2). The type and amount of ApoA-I and phospholipids influence the ability of HDL to enhance cellular cholesterol efflux. Thus, differences in composition may considerably impact the relative functionality and efficacy of these products in humans [6,31,62].

Table 1.2 Characteristics and clinical updates of apolipoprotein A-I-based rHDL infusion therapeutics.

rHDL product	ApoA-I source	Phospholipid	Protein to phospholipid ratio	Clinical trials	Patients enrolled	Status	Change in percent atheroma volume (PAV, %) from baseline	Cholesterol efflux capacity (%)
ETC-216	Recombinant ApoA-I Milano	DPPC	1:2.7 weight ratio	Milano, Phase 2	57	Completed	-1.06% (treatment) versus 0.14% (placebo), p=0.02	NA
MDCO-216		POPC	1:1.1 weight ratio	MILANO-PILOT, Phase 3, NCT02678923	126	Completed	-0.21% (treatment) versus -0.94% (placebo), p=0.07	80.4% increase
CER-001	Recombinant wild type ApoA-I	SPM and DPPG at molar ratio of 32:1	1:2.7 weight ratio	CHI SQUARE, Phase 2, NCT01201837	507	Completed	-0.02% (treatment) versus 0.02% (placebo), p=0.86	NA
				CARAT, Phase 2, NCT2484378	293	Completed	-0.09% (treatment) versus -0.41% (placebo), p=0.15	44% increase
CSL111	Native ApoA-I isolated from human plasma	Mixed PC isolated from soy	1:150 molar ratio	ERASE Phase 2, NCT00225719	183	Completed	-3.4% (treatment) versus -1.6% (placebo), p=0.48	15% increase
CSL112			1:55 molar ratio	AEGIS-I, Phase 2, NCT02108262	1258	Completed	NA	300% increase
				AEGIS-II, Phase 3, NCT03473223	17400	Ongoing	NA	NA

Apolipoprotein Milano (ETC-216/MDCO-216), developed by US biopharmaceutical company Esperion Therapeutics, is a recombinant ApoA-I Milano/phospholipid complex synthetic variant of HDL. In 2003, its phase II clinical trial was conducted in 57 patients with acute coronary syndrome (ACS). Patients were randomized to five-weekly infusions of either ETC-216 or placebo (Saline). Intravascular ultrasound (IVUS) was performed to measure the changes in the percentage of atheroma volume within 2 weeks of patients experiencing ACS (baseline) and after each weekly infusion (Nissen et al., 2003). Results showed that 5 weeks of treatment with ETC-216 decreased the atheroma volume by a significant 4.2% ($p < 0.01$). Subsequently, MDCO-216, a refined and purified form of ETC-216, was developed to promote cholesterol efflux capacity without any adverse effects on immune function [63]. However, the phase III trial (MILANO-PILOT) completed in 2018 demonstrated that although MDCO-216 infusion increased cholesterol efflux, it did not yield an incremental benefit to patients with coronary disease. (ClinTrial.gov identifier NCT02678923) [9].

CER-001, bioengineered by US biopharmaceutical company Cerenis Therapeutics, is a bio-engineered complex of recombinant wild-type human ApoA-I and sphingomyelin [64]. In 2014, a phase II trial (CHI-SQUARE trial) was conducted where 504 patients with ACS were randomized to receive 6 weekly infusions of either CER-001 (3, 6, or 12 mg/kg) or placebo (ClinTrial.gov identifier NCT01201837). Although CER-001 failed to produce a significant reduction in coronary atherosclerosis as assessed by IVUS [65], reanalysis in anatomically matched arterial segments revealed plaque regression achieved at the lowest dose arm (3 mg/kg), especially in patients with high plaque burden at baseline [66]. In 2018, a phase II CARAT trial was conducted to evaluate the effect of CER-001 infusions (3 mg/kg) in patients with ACS and a high coronary plaque burden (ClinTrial.gov identifier NCT2484378). The CARAT trial showed no benefit after 10 weekly infusions of CER-001 compared with placebo. In patients with high coronary plaque burden, no regression of atherosclerosis was noted [7,64].

CSL111, developed by global biotherapeutics leader CSL Behring, is a reconstituted HDL-particle comprised of soybean phosphatidylcholine and human ApoA-1 [67]. In 2007, a phase II ERASE trial was conducted in which 183 patients were randomly assigned to 4 weekly infusions of placebo, 40 mg/kg of CSL-111 or 80 mg/kg of CSL-111 [65]. A high incidence of transaminase elevations with the 80 mg/kg treatment led to a premature discontinuation of this arm. There was a significant change from baseline in atheroma volume (−3.4%; $p > 0.001$) in the 40 mg/kg group, but this difference did not reach statistical significance ($p = 0.48$) compared with placebo (ClinTrial.gov identifier NCT00225719). CSL-112, a second-generation derived from CSL-111, was then developed to further increase the tolerant dose in humans and is still in clinical development today [68,69]. In a phase IIa clinical trial, no patients developed anti-CSL-112 or apoA-I antibodies, suggesting that CSL-112 does not cause an immunogenic response [69].

Furthermore, CSL-112 has also completed a large phase II safety study in 1200 patients receiving four weekly infusions of either 2 or 6 g of ApoA-I protein reconstituted to form HDL. In this study, CSL-112 was found to be well tolerated in patients, lacking any signs of hepatic or renal toxicity or any other safety concerns. A phase 3 AEGIS-II trial was initiated in 2017, in which more than 17,000 subjects were enrolled from approximately 1000 sites around the world to evaluate whether CSL-112 reduces cardiovascular events in high-risk patients [10].

1.7 sHDL As a drug delivery vehicle

Though sHDLs can be used as therapeutics alone, the use of sHDLs as delivery systems has also been investigated due to their biocompatibility, small size and amphipathicity. Generally, hydrophobic drugs are difficult to develop as pharmaceutical agents because of their low water solubility. sHDLs become an attractive delivery system for these drugs because the phospholipid bilayer of sHDLs allows for the incorporation of hydrophobic drugs. Another mode of functionalizing sHDL can be done by inserting molecules containing hydrophobic moieties into the phospholipid bilayer.

As previously discussed, the ApoA-I component of HDLs can bind to many cellular receptors, such as SR-BI, which is highly expressed in hepatocytes, macrophages, and cancer cells, which makes it an attractive delivery system for therapeutics that target and accumulate in these areas. For cancer therapy, HDL can be taken up by tumor cells due to its small size and binding to SR-BI, which is overexpressed in some cancer cells and malignant tumors [70]. Subsequence release of its cargo in the cancer cell and tumors can lead to higher therapeutic efficiency than free drug alone. For tumor cells that do not express SR-BI, sHDLs can be modified with other targeting ligands to enhance tumor uptake. sHDLs have also been modified

for glioblastoma and other brain diseases to help the particles efficiently penetrate the BBB and aggregate in target sites [70,71].

For cardiovascular applications, sHDLs have been used to deliver drugs to atherosclerotic plaque due to high accumulation in plaque lesions. For example, Tanshinone IIA loaded sHDL was able to target atherosclerotic plaque in a foam cell model and show promising pharmacokinetics and safety profiles in rabbits, proving it to be a potentially useful drug carrier for cardiovascular drugs [72]. sHDLs have also been used to encapsulate liver X receptor (LXR) agonist, T0901317, for atherosclerosis treatment. sHDL-T1317 was able to upregulate Abca1 and Abcg1 expression in macrophages and cholesterol-loaded foam cells [73]. Moreover, sHDL-T1317 was able to accumulate in atherosclerotic plaques in ApoE-deficient mice. Due to sHDL's cardioprotective effects, they can work synergistically with the payload to target atherosclerosis plaque, cholesterol accumulation, and inflammation.

1.8 sHDL mimetic nanoparticles

In addition to conventional recombinant HDL (rHDL) or synthetic HDL (sHDL), various HDL-mimicking nanoparticles [21] have been developed for CVD, including liposomes, inorganic or polymeric nanoparticles, cyclodextrins, micelles, metal nanoparticles, and lipid-conjugated core scaffold nanoparticles. These HDL-mimicking nanoparticles have exhibited similar biofunctions to native HDL, including RCT, antioxidant, and anti-thrombotic effects [59,74]. Moreover, HDL-mimicking nanoplatforms have been shown to provide several advantages over the traditional rHDL strategy [75]. Foremost, the surface of nanoparticles can be decorated with ligands specific to disease sites or targets, allowing for improvement of therapeutic efficacy without a notable change in cytotoxicity to normal tissue [76]. Furthermore,

the preparation process of rHDL requires expensive raw materials like apolipoproteins, challenging the wide availability of the final product. Meanwhile, advances in chemical synthesis have made HDL-mimicking nanoparticles simpler and more efficient nanoplatforms to sufficiently fulfill the functionality of native HDL.

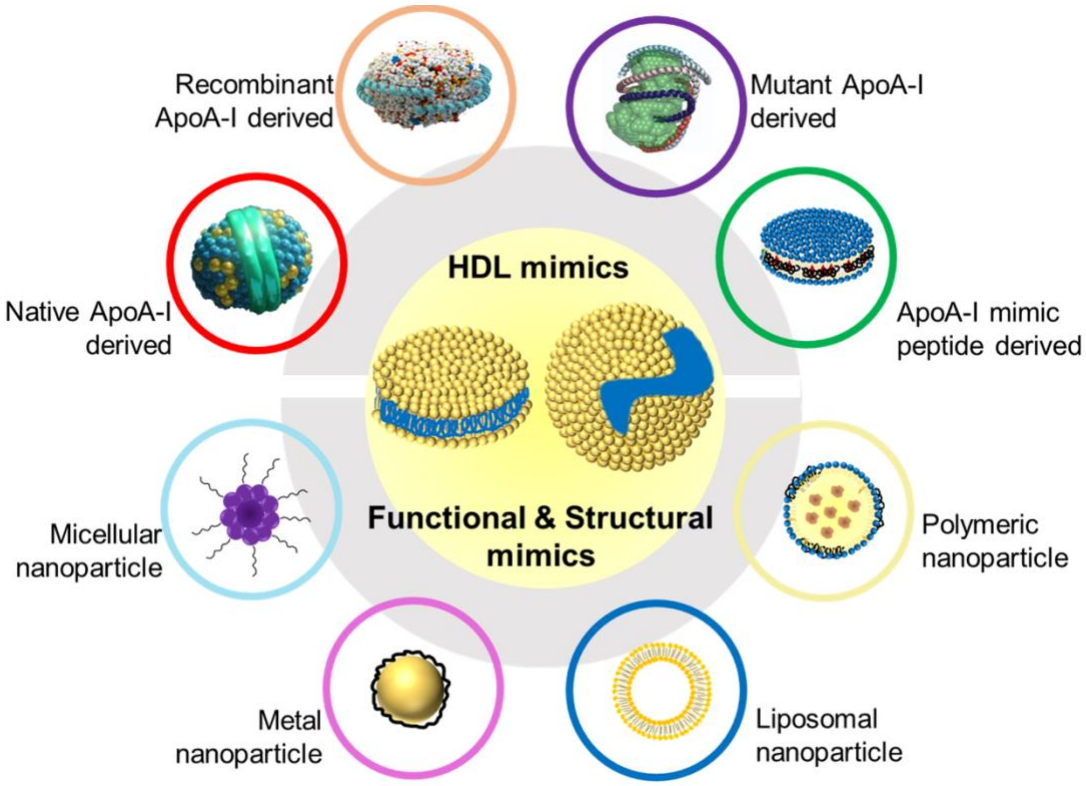

Figure 1.4 Types of HDL mimics and HDL-mimicking nanoparticles.

1.8.1 Challenges associated with ApoA-I based products

ApoA-I-based rHDL products present serious challenges, such as expansive and complex manufacturing processes and the need to produce a high quantity of pure protein due to the relatively high ApoA-I doses required to achieve therapeutic benefit. The current dose of ApoA-I

in CSL-112, the ApoA-I-based rHDL product undergoing phase 3 clinical trial, is 6 g per infusion administered four times in weekly intervals [10]. Thus, the course of therapy will require 24 g of ApoA-I protein. When considering the number of patients worldwide who currently suffer from a cardiovascular-related disease, the feasibility of acquiring this high amount of protein greatly diminishes. Treating just a million patients will require 24 tons of protein. For plasma purified ApoA-I, it will be difficult to secure sufficient volumes of human plasma. For ApoA-I produced by recombinant technologies, the cost of manufacturing and manufacturing process complexity remains high due to the hydrophobic nature of ApoA-I, relatively low expression levels, and high endotoxin binding tendencies. Because of the levels of endotoxin, host cell protein and host cell DNA impurities are limited for each protein infusion by the WHO and FDA guidelines. Thus, large doses of ApoA-I necessitates the production of highly pure protein. The hydrophobic nature of ApoA-I leads to relatively low expression titers in recombinant processes and a need for an extensive purification process to remove impurities, resulting in an expansive protein product. Ultimately, rHDL will be challenging to produce in a scalable and economically feasible manner.

1.8.2 Poly(lactic-co-glycolic acid)-based high-density lipoproteins-mimicking nanoparticles

Polymer-based nanoparticles, such as those composed of poly(lactic-*co*-glycolic acid) (PLGA), have been advantageous in therapeutic applications due to their biodegradability, long circulation half-life, and ability to modify the surface for targeted activity. These properties are favorable as a decrease in the rapid clearance from the site of action increases the ability to achieve a rise in localized therapeutic concentration at the target site. In recent years, polymer-based nanoparticles have become of high interest for drug delivery purposes and have been utilized as imaging and diagnostics tools in the cardiovascular space [74,77]. Here, we will discuss the use of

PLGA nanoparticles and cyclodextrin as targeted therapies and imaging tools for atherosclerosis and CVD.

PLGA is a polymer commonly used in nanoparticles to achieve an extended release of a drug over time due to the slow degradation of PLGA into glycolic and lactic acid. PLGA can be incorporated into HDL's hydrophobic core, allowing drug encapsulation and slow release. For example, Sanchez-Gaytan et al. formulated PLGA–HDL that was shown to mimic HDL activity, including uptake by macrophages and cholesterol efflux capabilities in vitro and colocalization with macrophages in atherosclerotic plaque in the aorta of $ApoE^{-/-}$ mice [77]. PLGA–HDL contains a hydrophobic PLGA core coated with phospholipids and ApoA-I protein at a lipid-to-protein ratio similar to endogenous HDL. The particle size ranges from 60 to 120 nm, determined by the flow rate of the microfluidics technology during production (Figure 1.5(a)). In the drug release experiment using Nile Red hydrophobic dye as a model drug, it was found that within 24 hours, 60% of the dye had been released. Within 5 days, 90% of the dye had been released, confirming the slow-release capabilities of the nanoparticle. Moreover, cholesterol was effluxed to a similar extent to native HDL at concentrations of 20 and 50 µg/ml PLGA-HDL in human macrophage-like THP-1 cells (Figure 1.5b,c). DiR dye was used to label PLGA-HDL, and the particle was administered via tail vein injection to $ApoE^{-/-}$ mice at a concentration of 10 mg/ml. PLGA-HDL was shown to colocalize with macrophages in the aortas of the $ApoE^{-/-}$ mice, showing preferential targeting of the atherosclerotic plaque. Altogether, the slow-release profile, cholesterol efflux, and ability of the particle to localize in atherosclerotic plaque areas show promising potential for PLGA-HDL to be an effective therapeutic for atherosclerosis (Figure 1.5d, e).

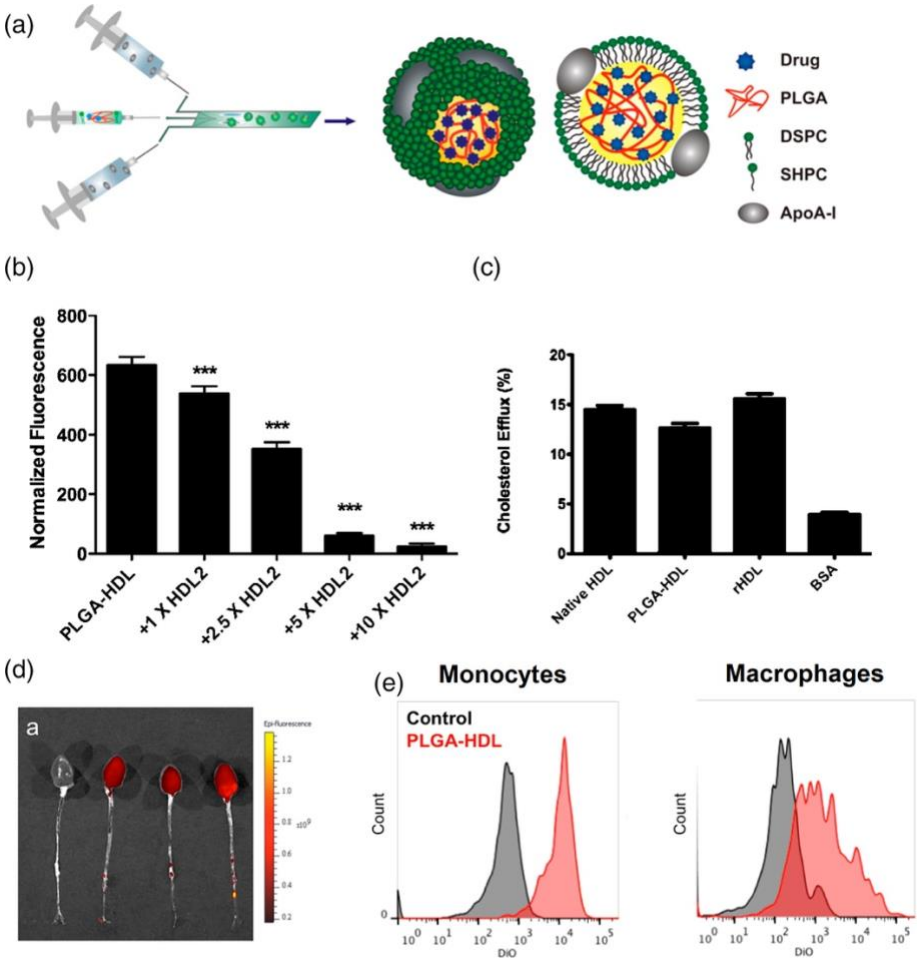

Figure 1.5 PLGA HDL-like nanoparticles. (a)"Schematic depiction of the synthesis of PLGA–HDL by microfluidic technology. PLGA–HDL nanoparticles target atherosclerotic plaques. (b) The preferential interaction of PLGA–HDL with macrophages was confirmed with flow cytometry analysis. Fluorescence of macrophages, pancreatic endothelial cells, smooth muscle cells, and hepatocytes incubated with PEG–PLGA NP (white) and PLGA–HDL (black). (c) Cholesterol efflux assay of native-HDL, PLGA–HDL, and microfluidic-synthesized HDL on human macrophage-like THP-1 cells at 50 μg/ml. (d) Fluorescence imaging of excised aortas of ApoE-/- mice injected with placebo or PLGA–HDL nanoparticles. (e) Fluorescent activated cell sorting of digested aortas injected with PLGA–HDL; the label DiR is mainly associated with monocytes and macrophages in the aorta." Figures combined and reprinted with permission from Sanchez-Gaytan et al. (2015). Copyright 2015. American Chemical Society.

Macrophage apoptosis is a major contributor to atherosclerotic plaque instability. These unstable or vulnerable plaques can then rupture, leading to thrombosis. In order to detect macrophage apoptosis and identify vulnerable plaque early on, Marrache et al. synthesized TPP-HDL-ApoA-I-QD NPs. This nanoparticle is composed of a PLGA and cholesteryl oleate biodegradable core lined with quantum dots, decorated with a phospholipid bilayer coat containing

ApoA-I mimetic peptide, 4F, and triphenylphosphine (TPP) cations, which are used to detect mitochondrial membrane potential collapse, the initiating phase of macrophage apoptosis [78]. The average particle size was 123 nm, roughly 10 times the size of HDL. In RAW macrophage cells, confocal microscopy showed that TPP-HDL-ApoA-I-QD NPs accumulated in healthy cells but were undetected in apoptotic cells due to the lack of electrochemical proton gradient across the membrane present in healthy cells. Using flow cytometry, they confirmed that TPP-HDL-ApoA-I-QD NPs could differentiate between apoptotic and healthy cells. TPP-HDL-ApoA-I-QD NPs also had cholesterol-binding properties in vitro, and the particle reduced total cholesterol levels by 30% and triglyceride levels by 24% in vivo. All in all, these activities indicate the therapeutic and imaging capabilities of TPP-HDL-ApoA-I-QD NPs on vulnerable plaque in atherosclerosis.

Early detection of vulnerable plaque could enhance the outcomes for atherosclerosis patients by allowing for the adjustment of the therapeutic approach and acquiring the right treatment plan for the patient. In a more recent study, Banik et al. optimized TPP-HDL-ApoA-I-QD NPs by modifying the cholesteryl oleate and PLGA composition to target both intracellular cholesterol metabolism pathways and extracellular cholesterol removal (Banik et al., **2017**). The resulting nanoparticle was optimized based on size and cholesterol binding kinetics. It contains 40% cholesteryl oleate and is named T-CO_{40}-HDP-NP. DSPE-PEG serves as the phospholipid component, while L-4F serves as the ApoA-I mimetic protein in T-CO_{40}-HDP-NP, which differs from TPP-HDL-ApoA-I-QD NP. T-CO_{40}-HDP-NP was able to localize in the mitochondria of macrophages and remove cholesterol from RAW 267.4 macrophage cells and smooth muscle cells in a cholesterol efflux assay. Furthermore, T-CO_{40}-HDP-NP was reported to accumulate primarily in the aorta and liver tissues and significantly reduced triglycerides and cholesterol levels in Balb/c albino mice. After a twice/week treatment of 10 mg/kg T-CO_{40}-HDP-NP for 7 weeks in ApoE−/−

mice, there was a reduction in triglycerides, total cholesterol, and LDL compared with controls, little foam cell presence along the endothelium and decreased TNF-α cytokine levels. Due to its mitochondrial targeting and HDL mimetic activities, T-CO_{40}-HDP-NP helped maintain cholesterol balance intracellularly and extracellularly, having potential as a therapeutic to reduce atherosclerotic plaque formation.

1.8.3 Gold/metal-based high-density lipoprotein-mimicking nanoparticles

Metal-based nanoparticles act as drug delivery carriers, diagnostic tools, and radiation-based anticancer therapies [79]. They became of interest in the medical and therapeutic space due to their high biocompatibility, stability, and customizability. These properties make metal-based nanoparticles ideal for mimicking endogenous HDL and allow for the possibility of achieving the 5–17 nm in diameter in size and discoidal or spherical shape of the particle. In the cardiovascular space, metal-based nanoparticles, especially gold nanoparticles (Au-NP), have been utilized as both therapy-based and imaging tools to enhance RCT pathways and analyze atherosclerotic plaque.

Au-NPs can be used to enhance RCT activity, leading to the reduction of atherosclerotic plaque formation. For example, Thaxton et al. formulated an HDL mimetic gold-based nanoparticle (HDL-Au NP) that can bind cholesterol in an in vitro assay, titrating NBD-cholesterol in a 5 nM HDL-Au NP solution to create a binding isotherm from the fluorescent signal [80]. HDL-Au NP consists of a 5 nm gold core scaffold, surrounded by 1,2-dipalmitoyl-sn-glycero-3-phosphoethanolamine-*N*-[3-(2-pyridyldithio) propionate] (PDP-PE), and amine-functionalized lipid, 1-2-dipalmitoyl-sn-glycero-3-phosphocholine (DPPC) phospholipids, and ApoA-I protein (Figure 1.6a). The resulting HDL-Au NP was determined to be 17.9 nm in size. The average

number of proteins and phospholipids per particle, 3 and 83, respectively, corresponded well to amounts found in endogenous HDL. The Kd of binding was determined to be 3.8 nM. The ability of HDL-Au NP to bind cholesterol shows the early potential of this nanoparticle to be of use in enhancing RCT and improving atherosclerosis outcomes.

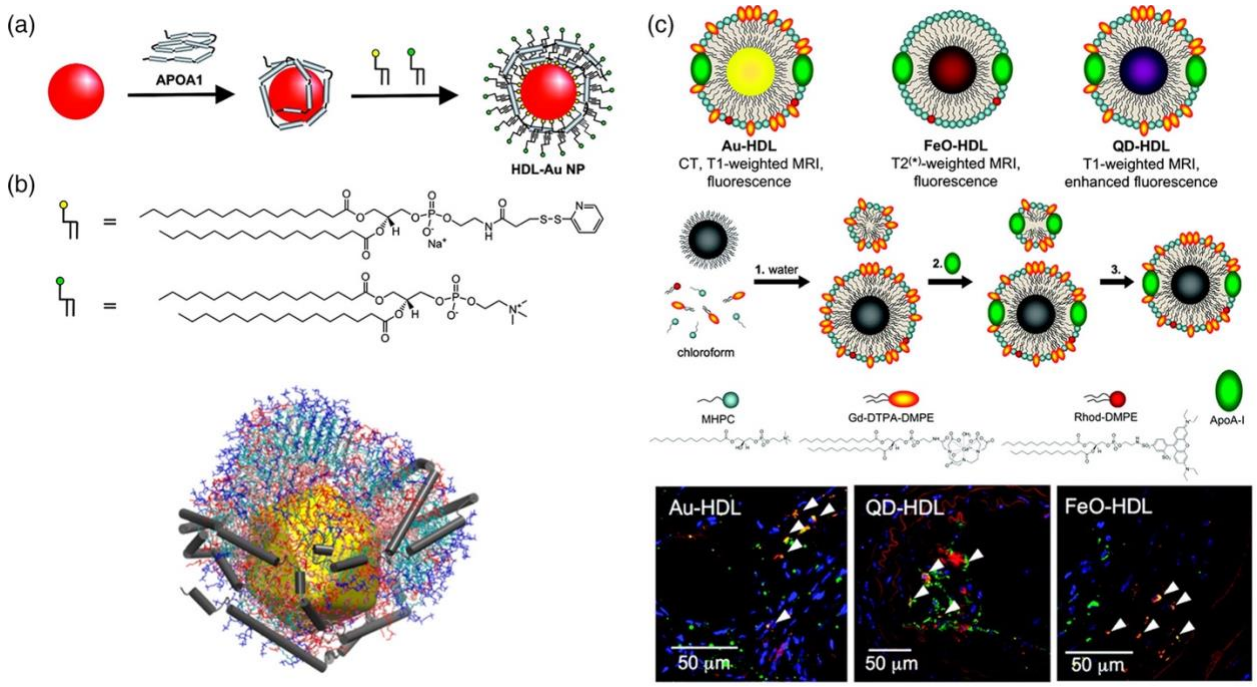

Figure 1.6 (a) "Synthesis of biomimetic HDL using an Au NP core for use as a therapeutic. Au NPs of 5 nm in diameter were surface-functionalized with ApoA-I and then with two phospholipids, 1,2-dipalmitoyl-sn-glycero-3-phosphoethanolamine-N-[3-(2-pyridyldithio) propionate (yellow) and 1-2-dipalmitoyl-sn-glycero-3-phosphocholine (green)." Reprinted with permission from Thaxton et al. (2009). Copyright 2009. American Chemical Society. (b) "Self-assembly of a mixture of DPPC/MPDP PE/2-MPT (175:175:175) on three apoA-I loaded AuNPs." Reprinted with permission from Lai et al. (2017). Copyright 2017. American Chemical Society. (c) "Representative synthesis of the three nanocrystal HDLs for imaging atherosclerotic plaque and their imaging of atherosclerosis. Confocal microscopy images of aortic sections of mice injected with nanocrystal HDL. Red is nanocrystal HDL, macrophages are green, and nuclei are blue. Yellow indicates colocalization of nanocrystal HDL with macrophages and is indicated by arrowheads." Reprinted with permission from Cormode et al. (2008). Copyright 2008. American Chemical Society.

Moreover, in an experiment designed to examine how different lipids and the addition of ApoA-I affect the self-assembly interactions of Au with these components, Lai et al. showed that

their Au-NP was able to activate LCAT and form CE. This Au-NP consists of a gold core functionalized with DPPC/MPDP Pe/2-MPT at a 175:175:175 ratio and 3 ApoA-I proteins. It was found that CE distributed near the core of the Au-NP, mimicking endogenous HDL [81]. This is important because the packaging of CE near the core maintains a concentration gradient that allows more cholesterol to bind at the nanoparticle's surface during RCT (Figure 1.6b). They confirmed that ApoA-I incorporation in the Au-NP was necessary to activate LCAT and form CE, highlighting the importance of HDL's primary protein in the functional activity of gold nanoparticles.

Metal-based nanoparticles have various uses that span beyond enhancing HDL's RCT capabilities, such as acting as contrast agents for medical imaging and targeting atherosclerotic plaque areas, providing insight into atherosclerosis progression and vulnerability. In a series of imaging experiments, Cormode et al. were able to show the utility of gold particles (Au), iron oxides (FeO), and quantum dots (QD) in molecular imaging [82]. These inorganic nanocrystals served as the hydrophobic core of HDL in the nanocrystal-core HDL particles. Along with ApoA-I, phospholipids, including fluorescent and paramagnetic lipids, were incorporated onto the hydrophobic core to create an HDL mimetic nanoparticle. The sizes of Au-HDL, FeO-HDL, and QD-HDL were 9.7, 11.9, and 12.0 nm, respectively. To induce atherosclerotic plaque formation, $ApoE^{-/-}$ mice were fed a high-fat diet for 10 weeks (Figure 1.6c). Following nanocrystal-core HDL particle administration, MRI imaging of the abdominal aorta detected particles in the aortic wall, and confocal microscopy showed the particles colocalized with macrophages. In a CT scan, Au-HDL showed a lower signal-to-noise ratio in the images of the aortas of mice when compared with saline and Au-PEG, which was used as a non-specific particle lacking ApoA-I. Moreover, the image showed two hotspots where Au-HDL accumulated, both areas of plaque with high

macrophage content. This shows the potential for Au-NP to be useful in CT imaging to provide insight into a plaque with high macrophage content.

In a separate experimental study, Cormode et al. used the Au-HDL particle in combination with multicolor CT to identify macrophage burden, calcification, and stenosis of atherosclerotic plaques from a single scan [83]. They discovered that distinction of Au-HDL, gold-based contrast agent, iodinated contrast agent, and calcium-rich matter was achievable using spectral CT, and concentrations of these agents could be determined with high accuracy. As previously shown, TEM and confocal microscopy confirmed the ability of Au-HDL to accumulate in the aortas of $ApoE^{-/-}$ mice, primarily in the macrophage-rich areas. Due to the ability of spectral CT to distinguish between the Au-HDL in the macrophages, iodinated contrast agents, and calcified structures, this technique could allow for a detailed analysis of atherosclerotic plaque composition, stenosis of the artery, calcification, and inflammation. This information can help diagnose and monitor atherosclerosis disease progression, potentially leading to improved patient therapeutic outcomes.

1.9 Research scope

This introduction discusses the composition, structure, and function of high-density lipoproteins, and their implications on cardiovascular-related diseases, such as endothelial dysfunction and atherosclerosis. Synthetic HDLs have been developed and tested in clinical trials to reduce overall atherosclerotic plaque formation and promote reverse cholesterol transport. sHDLs are composed of phospholipids and ApoA-I or ApoA-I mimetic peptides. The lipid composition of HDL and HDL-mimicking nanoparticles could potentially impact its size, rigidity, biological activity, pharmacokinetics, stability, and overall therapeutic potential.

Therefore, this work presented here will highlight the potential usage of sHDL and HDL-mimetic micelle nanoparticles for modulating endothelial function and atherosclerosis, respectively, and the importance of considering lipid composition when developing sHDL and HDL-mimetic nanoparticles. We will also show the impacts of lipid composition on the stability and remodeling of sHDL in human serum over time.

1.10 Dissertation overview

The dissertation aims to investigate the therapeutic potential of sHDL and HDL mimetic micelle nanoparticles for treating cardiovascular-related diseases and understand how phospholipid composition affects its overall therapeutic activity and stability. These studies support for further optimization and exploration of sHDLs and HDL-mimicking micelles as cardiovascular therapies.

In chapter 2 of this dissertation, we studied how the lipid composition of HDL-mimicking micelles influenced the protective mechanisms against atherosclerosis. HDL-mimicking micelles were designed to be ApoA-I free, which makes them more scalable and cost-friendly than sHDLs. We created a library of micelles composed of (i) different phosphatidylcholine (PC) lipids with a fixed ratio of PC lipid to PEGylated lipid and (ii) a single PC lipid with varying ratios of PC to PEGylated lipid, and tested these micelles in cholesterol efflux, cholesterol crystal dissolution and pro-inflammatory cytokine reduction in vitro and evaluated the pharmacokinetic/pharmacodynamic activity and cholesterol mobilization in vivo to understand how the activity of these micelles changed with varying lipid composition.

In chapter 3, we investigated the impact of sHDL on processes that influence endothelial function. Previous studies have shown that endogenous HDL has positive effects on the

endothelium. Therefore, we designed multiple formulations of sHDLs consisting of different phospholipids and tested these sHDLs' ability to impact adhesion molecule expression and promote eNOS expression in inflamed endothelial cells, NO levels in endothelial cells, and endothelial blood-brain barrier integrity in a murine traumatic brain injury model.

In chapter 4, we sought to understand how the lipid composition of sHDLs affects its stability and remodeling in human serum. Endogenous HDL are dynamic systems that constantly exchange components with other HDL and larger lipoproteins, such as LDL and VLDL. In this study, we investigated how lipid composition affects sHDL remodeling by monitoring sHDL component movement to larger lipoproteins over time after incubation with human plasma.

Lastly, in chapter 5, we draw final conclusions of this dissertation work and discuss future plans and potential for this work to continue the investigation and optimization of sHDLs and HDL-mimicking micelles to treat cardiovascular disease. Each chapter is written in manuscript format. Chapter 2 is published in *Pharmaceutics*, and Chapter 4 will be submitted for publication shortly after the dissertation defense.

1.11 References

1. Lüscher TF, Landmesser U, Von Eckardstein A, Fogelman AM. High-density lipoprotein: Vascular protective effects, dysfunction, and potential as therapeutic target. *Circ Res*. 2014;114(1):171-182. doi:10.1161/CIRCRESAHA.114.300935

2. Rader DJ, Tall AR. The not-so-simple HDL story: Is it time to revise the hdl cholesterol hypothesis? *Nat Med*. 2012;18(9):1344-1346. doi:10.1038/nm.2937

3. Brites F, Martin M, Guillas I, Kontush A. Antioxidative activity of high-density lipoprotein (HDL): Mechanistic insights into potential clinical benefit. *BBA Clin*. 2017;8:66-77. doi:10.1016/j.bbacli.2017.07.002

4. Fotakis P, Kothari V, Thomas DG, et al. Anti-Inflammatory Effects of HDL (High-Density Lipoprotein) in Macrophages Predominate over Proinflammatory Effects in Atherosclerotic Plaques. *Arterioscler Thromb Vasc Biol*. 2019;39(12):E253-E272. doi:10.1161/ATVBAHA.119.313253

5. Khera A V., Demler O V., Adelman SJ, et al. Cholesterol Efflux Capacity, High-Density Lipoprotein Particle Number, and Incident Cardiovascular Events: An Analysis from the JUPITER Trial (Justification for the Use of Statins in Prevention: An Intervention Trial Evaluating Rosuvastatin). *Circulation*. 2017;135(25):2494-2504. doi:10.1161/CIRCULATIONAHA.116.025678

6. Rader DJ. Apolipoprotein A-I infusion therapies for coronary disease: Two outs in the ninth inning and swinging for the fences. *JAMA Cardiol*. 2018;3(9):799-801. doi:10.1001/jamacardio.2018.2168

7. Nicholls SJ, Andrews J, Kastelein JJP, et al. Effect of serial infusions of CER-001, a pre-β High-density lipoprotein mimetic, on coronary atherosclerosis in patients following acute coronary syndromes in the CER-001 atherosclerosis regression acute coronary syndrome trial: A randomized clinical trial. *JAMA Cardiol*. 2018;3(9):815-822. doi:10.1001/jamacardio.2018.2121

8. Andrews J, Janssan A, Nguyen T, et al. Effect of serial infusions of reconstituted high-density lipoprotein (CER-001) on coronary atherosclerosis: Rationale and design of the CARAT study. *Cardiovasc Diagn Ther*. 2017;7(1):45-51. doi:10.21037/cdt.2017.01.01

9. Nicholls SJ, Puri R, Ballantyne CM, et al. Effect of infusion of high-density lipoprotein mimetic containing recombinant apolipoprotein A-I Milano on coronary disease in patients with an acute coronary syndrome in the MILANO-PILOT trial: A randomized clinical trial. *JAMA Cardiol*. 2018;3(9):806-814. doi:10.1001/jamacardio.2018.2112

10. Gibson CM, Kastelein JJP, Phillips AT, et al. Rationale and design of ApoA-I Event Reducing in Ischemic Syndromes II (AEGIS-II): A phase 3, multicenter, double-blind, randomized, placebo-controlled, parallel-group study to investigate the efficacy and

safety of CSL112 in subjects after acute myocardial infarction. *Am Heart J*. 2021;231:121-127. doi:10.1016/j.ahj.2020.10.052

11. Kontush Anatol, Chapman MJ. *High-Density Lipoproteins : Structure, Metabolism, Function, and Therapeutics*. John Wiley & Sons, Inc; 2012.

12. Fisher EA, Feig JE, Hewing B, Hazen SL, Smith JD. High-density lipoprotein function, dysfunction, and reverse cholesterol transport. *Arterioscler Thromb Vasc Biol*. 2012;32(12):2813-2820. doi:10.1161/ATVBAHA.112.300133

13. Ikonen E. Cellular cholesterol trafficking and compartmentalization. *Nat Rev Mol Cell Biol*. 2008;9:125-138. doi:https://doi.org/10/1038/nrm2336

14. Frank PG, Marcel YL. Apolipoprotein A-I: Structure-function relationships. *J Lipid Res*. 2000;41(6):853-872. doi:10.1016/s0022-2275(20)32028-9

15. Mangaraj M, Nanda R, Panda S. Apolipoprotein A-I: A Molecule of Diverse Function. *Indian Journal of Clinical Biochemistry*. 2016;31(3):253-259. doi:10.1007/s12291-015-0513-1

16. Wilhelm AJ, Zabalawi M, Owen JS, et al. Apolipoprotein A-I modulates regulatory T cells in autoimmune LDLr -/-, ApoA-I-/- mice. *Journal of Biological Chemistry*. 2010;285(46):36158-36169. doi:10.1074/jbc.M110.134130

17. Hyka N, Dayer JM, Modoux C, et al. *Apolipoprotein A-I Inhibits the Production of Interleukin-1 and Tumor Necrosis Factor-by Blocking Contact-Mediated Activation of Monocytes by T Lymphocytes*.; 2001. http://ashpublications.org/blood/article-pdf/97/8/2381/1672948/h8080102381.pdf

18. Kontush A, Lhomme M, Chapman MJ. Thematic review series: High density lipoprotein structure, function, and metabolism: Unraveling the complexities of the HDL lipidome. *J Lipid Res*. 2013;54(11):2950-2963. doi:10.1194/jlr.R036095

19. Yetukuri L, Söderlund S, Koivuniemi A, et al. Composition and lipid spatial distribution of HDL particles in subjects with low and high HDL-cholesterol. *J Lipid Res*. 2010;51(8):2341-2351. doi:10.1194/jlr.M006494

20. Ozerova IN, Perova N V, Shchel'tsyna N V, Mamedov MN. *Parameters of High-Density Lipoproteins in Patients with Arterial Hypertension in Combination with Other Components of Metabolic Syndrome*. Vol 143.; 2007.

21. Chen J, Zhang X, Millican R, Creutzmann JE, Martin S, Jun HW. High density lipoprotein mimicking nanoparticles for atherosclerosis. *Nano Converg*. 2020;7(1). doi:10.1186/s40580-019-0214-1

22. Segrest JP, Li L, Anantharamaiah GM, Harvey SC, Liadaki KN, Zannis V. *Structure and Function of Apolipoprotein A-I and High-Density Lipoprotein*. Vol 11. Lippincott Williams & Wilkins; 2000. http://journals.lww.com/co-lipidology

23. Navdaev A V., Sborgi L, Wright SD, Didichenko SA. Nascent HDL (High-Density Lipoprotein) Discs Carry Cholesterol to HDL Spheres: Effects of HDL Particle Remodeling on Cholesterol Efflux. *Arterioscler Thromb Vasc Biol*. 2020;40(5):1182-1194. doi:10.1161/ATVBAHA.120.313906

24. Waksman R, Torguson R, Kent KM, et al. A First-in-Man, Randomized, Placebo-Controlled Study to Evaluate the Safety and Feasibility of Autologous Delipidated High-Density Lipoprotein Plasma Infusions in Patients With Acute Coronary Syndrome. *J Am Coll Cardiol*. 2010;55(24):2727-2735. doi:10.1016/j.jacc.2009.12.067

25. Ginsberg HN. *LIPOPROTEIN PHYSIOLOGY*.

26. Trajkovska KT, Topuzovska S. High-density lipoprotein metabolism and reverse cholesterol transport: Strategies for raising HDL cholesterol. *Anatol J Cardiol*. 2017;18(2):149-154. doi:10.14744/AnatolJCardiol.2017.7608

27. Deeb SS, Zambon A, Carr MC, Ayyobi AF, Brunzell JD. Hepatic lipase and dyslipidemia: Interactions among genetic variants, obesity, gender, and diet. *J Lipid Res*. 2003;44(7):1279-1286. doi:10.1194/jlr.R200017-JLR200

28. Albers JJ, Vuletic S, Cheung MC. Role of plasma phospholipid transfer protein in lipid and lipoprotein metabolism. *Biochim Biophys Acta Mol Cell Biol Lipids*. 2012;1821(3):345-357. doi:10.1016/j.bbalip.2011.06.013

29. Yu JE, Han SY, Wolfson B, Zhou Q. The role of endothelial lipase in lipid metabolism, inflammation and cancer. *Histol Histopathol*. 2018;33(1):1-10. doi:10.14670/HH-11-905

30. Von Eckardstein A, Kardassis D. *High Density Lipoproteins From Biological Understanding to Clinical Exploitation*.; 2015. http://www.springer.com/series/164

31. Singh IM, Shishehbor MH, Ansell BJ. *High-Density Lipoprotein as a Therapeutic Target A Systematic Review*. www.jama.com

32. Sacks FM, Jensen MK. From high-density lipoprotein cholesterol to measurements of function: Prospects for the development of tests for high-density lipoprotein functionality in cardiovascular disease. *Arterioscler Thromb Vasc Biol*. 2018;38(3):487-499. doi:10.1161/ATVBAHA.117.307025

33. Ouimet M, Barrett TJ, Fisher EA. HDL and reverse cholesterol transport: Basic mechanisms and their roles in vascular health and disease. *Circ Res*. 2019;124(10):1505-1518. doi:10.1161/CIRCRESAHA.119.312617

34. Barter PJ, Nicholls S, Rye KA, Anantharamaiah GM, Navab M, Fogelman AM. Antiinflammatory properties of HDL. *Circ Res*. 2004;95(8):764-772. doi:10.1161/01.RES.0000146094.59640.13

35. Suzuki M, Pritchard DK, Becker L, et al. High-density lipoprotein suppresses the type i interferon response, a family of potent antiviral immunoregulators, in macrophages

challenged with lipopolysaccharide. *Circulation*. 2010;122(19):1919-1927. doi:10.1161/CIRCULATIONAHA.110.961193

36. Cockerill GW, Rye KA, Gamble JR, Vadas MA, Barter PJ. *High-Density Lipoproteins Inhibit Cytokine-Induced Expression of Endothelial Cell Adhesion Molecules*.; 1995. http://ahajournals.org

37. Jebari-Benslaiman S, Galicia-García U, Larrea-Sebal A, et al. Pathophysiology of Atherosclerosis. *Int J Mol Sci*. 2022;23(6). doi:10.3390/ijms23063346

38. Mineo C, Deguchi H, Griffin JH, Shaul PW. Endothelial and antithrombotic actions of HDL. *Circ Res*. 2006;98(11):1352-1364. doi:10.1161/01.RES.0000225982.01988.93

39. Rämet ME, Rämet M, Lu Q, et al. High-density lipoprotein increases the abundance of eNOS protein in human vascular endothelial cells by increasing its half-life. *J Am Coll Cardiol*. 2003;41(12):2288-2297. doi:10.1016/S0735-1097(03)00481-9

40. Sugano M, Tsuchida K, Makino N. High-density lipoproteins protect endothelial cells from tumor necrosis factor-α-induced apoptosis. *Biochem Biophys Res Commun*. 2000;272(3):872-876. doi:10.1006/bbrc.2000.2877

41. Dimmeler S, Haendeler J, Zeiher AM. Regulation of endothelial cell apoptosis in atherothrombosis. *Curr Opin Lipodol*. 2002;13(5):531-536. http://journals.lww.com/co-lipidology

42. Tauber JP, Cheng J, Gospodarowicz D. *Effect of High and Low Density Lipoproteins on Proliferation of Cultured Bovine Vascular Endothelial Cells*.

43. Seetharam D, Mineo C, Gormley AK, et al. High-density lipoprotein promotes endothelial cell migration and reendothelialization via scavenger receptor-B type I. *Circ Res*. 2006;98(1):63-72. doi:10.1161/01.RES.0000199272.59432.5b

44. Endemann DH, Schiffrin EL. Endothelial dysfunction. *Journal of the American Society of Nephrology*. 2004;15(8):1983-1992. doi:10.1097/01.ASN.0000132474.50966.DA

45. Esper RJ, Nordaby RA, Vilariño JO, Paragano A, Cacharrón JL, Machado RA. Endothelial dysfunction: A comprehensive appraisal. *Cardiovasc Diabetol*. 2006;5. doi:10.1186/1475-2840-5-4

46. Park KH, Park WJ. Endothelial dysfunction: Clinical implications in cardiovascular disease and therapeutic approaches. *J Korean Med Sci*. 2015;30(9):1213-1225. doi:10.3346/jkms.2015.30.9.1213

47. Ley K, Laudanna C, Cybulsky MI, Nourshargh S. Getting to the site of inflammation: The leukocyte adhesion cascade updated. *Nat Rev Immunol*. 2007;7(9):678-689. doi:10.1038/nri2156

48. De Paoli F, Staels B, Chinetti-Gbaguidi G. Macrophage phenotypes and their modulation in atherosclerosis. *Circulation Journal*. 2014;78(8):1775-1781. doi:10.1253/circj.CJ-14-0621

49. Ricciarelli R, Zingg JM, Azzi A. *Vitamin E Reduces the Uptake of Oxidized LDL by Inhibiting CD36 Scavenger Receptor Expression in Cultured Aortic Smooth Muscle Cells*.; 2000. http://www.circulationaha.org

50. Aoyama T, Chen M, Fujiwara H, Masaki T, Sawamura T. LOX-1 mediates lysophosphatidylcholine-induced oxidized LDL uptake in smooth muscle cells. *FEBS Lett*. 2000;467(2-3):217-220. doi:10.1016/S0014-5793(00)01154-6

51. Lusis AJ. *Atherosclerosis*.; 2000. www.nature.com

52. Shen CM, Mao SJT, Huang GS, Yang PC, Chu RM. *Stimulation of Smooth Muscle Cell Proliferation by Ox-LDL-and Acetyl LDL-Induced Macrophage-Derived Foam Cells*. Vol 70.; 2001.

53. Bentzon JF, Otsuka F, Virmani R, Falk E. Mechanisms of plaque formation and rupture. *Circ Res*. 2014;114(12):1852-1866. doi:10.1161/CIRCRESAHA.114.302721

54. Kovanen PT, Kaartinen M, Pavonen T. Infiltrates of Activated Mast Cells at the Site of Coronary Atheromatous Erosion or Ruption in Myocardial Infarction. *Circulation*. 1995;92(5):1084-1088.

55. Mackman N, Tilley RE, Key NS. Role of the extrinsic pathway of blood coagulation in hemostasis and thrombosis. *Arterioscler Thromb Vasc Biol*. 2007;27(8):1687-1693. doi:10.1161/ATVBAHA.107.141911

56. Kirmizis D, Papagianni A, Dogrammatzi F, et al. *Effects of Simvastatin on Markers of Inflammation, Oxidative Stress and Endothelial Cell Apoptosis in Patients on Chronic Hemodialysis*. Vol 17.; 2010.

57. Ferrari R, Guardigli G, Ceconi C. Secondary prevention of CAD with ACE inhibitors: A struggle between life and death of the endothelium. In: *Cardiovascular Drugs and Therapy*. Vol 24. ; 2010:331-339. doi:10.1007/s10557-010-6244-x

58. Somani YB, Pawelczyk JA, De Souza MJ, et al. Aging women and their endothelium: probing the relative role of estrogen on vasodilator function. *REVIEW Sex Differences in Cardiovascular and Cerebrovascular Physiology, Disease, and Signaling Mechanisms Am J Physiol Heart Circ Physiol*. 2019;317:395-404. doi:10.1152/ajpheart.00430.2018.-Despite

59. Kumar K, Shair G, Ranjodh A, Sanghera S. Pharmacological Options in Atherosclerosis: A Review of the Existing Evidence. *Cardiol Ther*. 2019;8:5-20. doi:https://doi.org/10.1007/s40119-018-0123-0

60. Formanowicz D, Krawczyk JB. Controlling the thickness of the atherosclerotic plaque by statin medication. *PLoS One*. 2020;15(10 October). doi:10.1371/journal.pone.0239953

61. Larosa JC, He J, Vupputuri S. Effect of Statins on Risk of Coronary Disease A Meta-analysis of Randomized Controlled Trials. *JAMA*. 1999;282(24). www.jama.com

62. Karalis I, Jukema JW. HDL Mimetics Infusion and Regression of Atherosclerosis: Is It Still Considered a Valid Therapeutic Option? *Curr Cardiol Rep*. 2018;20(8). doi:10.1007/s11886-018-1004-9

63. Nissen SE, Tsunoda T, Murat Tuzcu E, et al. Effect of Recombinant ApoA-I Milano on Coronary Atherosclerosis in Patients With Acute Coronary Syndromes A Randomized Controlled Trial. *JAMA*. 2003;290:2292-2300. www.jama.com

64. Zheng KH, Kaiser Y, van Olden CC, et al. No benefit of HDL mimetic CER-001 on carotid atherosclerosis in patients with genetically determined very low HDL levels. *Atherosclerosis*. 2020;311:13-19. doi:10.1016/j.atherosclerosis.2020.08.004

65. Tardif JC, Ballantyne CM, Barter P, et al. Effects of the high-density lipoprotein mimetic agent CER-001 on coronary atherosclerosis in patients with acute coronary syndromes: a randomized trial. *Eur Heart J*. 2014;35:3277-3286. doi:10.1093/eurheartj/ehu194

66. Kootte RS, Smits LP, Van Der Valk FM, et al. Effect of open-label infusion of an apoA-I-containing particle (CER-001) on RCT and artery wall thickness in patients with FHA. *J Lipid Res*. 2015;56(3):703-712. doi:10.1194/jlr.M055665

67. Shaw JA, Bobik A, Murphy A, et al. Infusion of reconstituted high-density lipoprotein leads to acute changes in human atherosclerotic plaque. *Circ Res*. 2008;103(10):1084-1091. doi:10.1161/CIRCRESAHA.108.182063

68. Gille A, D'Andrea D, Tortorici MA, Hartel G, Wright SD. CSL112 (Apolipoprotein A-I [Human]) Enhances Cholesterol Efflux Similarly in Healthy Individuals and Stable Atherosclerotic Disease Patients. *Arterioscler Thromb Vasc Biol*. 2018;38(4):953-963.

69. Tricoci P, D'Andrea DM, Gurbel PA, et al. Infusion of Reconstituted High-Density Lipoprotein, CSL112, in Patients With Atherosclerosis: Safety and Pharmacokinetic Results From a Phase 2a Randomized Clinical Trial. *J Am Heart Assoc*. 2015;4(8):e002171. doi:10.1161/JAHA.115.002171

70. Lacko AG, Nair M, Paranjape S, Johnson S, Mcconathy WJ. High Density Lipoprotein Complexes as Delivery Vehicles for Anticancer Drugs. *Anticancer Res*. 2002;22:2045-2049.

71. Ma X, Song Q, Gao X. Reconstituted high-density lipoproteins: novel biomimetic nanocarriers for drug delivery. *Acta Pharm Sin B*. 2018;8(1):51-63. doi:10.1016/j.apsb.2017.11.006

72. Zhang X, Kang X, Du L, et al. Tanshinone IIA loaded chitosan nanoparticles decrease toxicity of β-amyloid peptide in a Caenorhabditis elegans model of Alzheimer's disease. *Free Radic Biol Med*. 2022;193:81-94. doi:10.1016/j.freeradbiomed.2022.09.030

73. Guo Y, Yuan W, Yu B, et al. Synthetic High-Density Lipoprotein-Mediated Targeted Delivery of Liver X Receptors Agonist Promotes Atherosclerosis Regression. *EBioMedicine*. 2018;28:225-233. doi:10.1016/j.ebiom.2017.12.021

74. Kuai R, Li D, Chen YE, Moon JJ, Schwendeman A. High-Density Lipoproteins: Nature's Multifunctional Nanoparticles. *ACS Nano*. 2016;10(3):3015-3041. doi:10.1021/acsnano.5b07522

75. Kornmueller K, Vidakovic I, Prassl R. Artificial high density lipoprotein nanoparticles in cardiovascular research. *Molecules*. 2019;24(15). doi:10.3390/molecules24152829

76. Chuang ST, Cruz S, Narayanaswami V. Reconfiguring nature's cholesterol accepting lipoproteins as nanoparticle platforms for transport and delivery of therapeutic and imaging agents. *Nanomaterials*. 2020;10(5). doi:10.3390/nano10050906

77. Sanchez-Gaytan BL, Fay F, Lobatto ME, et al. HDL-Mimetic PLGA Nanoparticle To Target Atherosclerosis Plaque Macrophages. *Bioconjug Chem*. 2015;26(3):443-451. doi:10.1021/bc500517k

78. Marrache S, Dhar S. Biodegradable synthetic high-density lipoprotein nanoparticles for atherosclerosis. *Proc Natl Acad Sci U S A*. 2013;110(23):9445-9450. doi:10.1073/pnas.1301929110

79. Klębowski B, Depciuch J, Parlińska-Wojtan M, Baran J. Applications of noble metal-based nanoparticles in medicine. *Int J Mol Sci*. 2018;19(12). doi:10.3390/ijms19124031

80. Thaxton CS, Daniel WL, Giljohann DA, Thomas AD, Mirkin CA. Templated spherical high density lipoprotein nanoparticles. *J Am Chem Soc*. 2009;131(4):1384-1385. doi:10.1021/ja808856z

81. Lai CT, Sun W, Palekar RU, Shad Thaxton C, Schatz GC. Molecular dynamics simulation and experimental studies of gold nanoparticle templated HDL-like nanoparticles for cholesterol metabolism therapeutics. *ACS Appl Mater Interfaces*. 2017;9(2):1247-1254. doi:10.1021/acsami.6b12249

82. Cormode DP, Skajaa T, Van Schooneveld MM, et al. Nanocrystal core high-density lipoproteins: A multimodality contrast agent platform. *Nano Lett*. 2008;8(11):3715-3723. doi:10.1021/nl801958b

83. Cormode DP, Roessl E, Thran A, et al. Atherosclerotic Plaque Composition: Analysis with Multicolor CT and Targeted Gold Nanoparticles 1. 2010;256(3). doi:10.1148/radiol.10092473/-/DC1

Chapter 2 Effect of Lipid Composition of the Atheroprotective Properties of HDL-Mimicking Micelles

2.1 Abstract

Atherosclerosis progression is driven by an imbalance of cholesterol and unresolved local inflammation in the arteries. The administration of recombinant apolipoprotein A-I (ApoA-I)-based high-density lipoprotein (HDL) nanoparticles has been used to reduce the size of atheroma and rescue inflammatory response in clinical studies. Because of the difficulty in producing large quantities of recombinant ApoA-I, here, we describe the preparation of phospholipid-based, ApoA-I-free micelles that structurally and functionally resemble HDL nanoparticles. Micelles were prepared using various phosphatidylcholine (PC) lipids combined with 1,2-distearoyl-*sn*-glycero-3-phosphoethanolamine- N-[azido(polyethylene glycol)-2000] (DSPE-PEG2k) to form nanoparticles of 15–30 nm in diameter. The impacts of PC composition and PEGylation on the anti-inflammatory activity, cholesterol efflux capacity, and cholesterol crystal dissolution potential of micelles were investigated in vitro. The effects of micelle composition on pharmacokinetics and cholesterol mobilization ability were evaluated in vivo in Sprague Dawley rats. The study shows that the composition of HDL-mimicking micelles impacts their overall atheroprotective properties and supports further investigation of micelles as a therapeutic for the treatment of atherosclerosis.

2.2 Introduction

Atherosclerosis is a main pathologic process that causes atherosclerotic cardiovascular diseases (ASCVD), including coronary heart disease (CHD), stroke and peripheral vascular disease [1]. Atherosclerotic plaques, made up of cholesterol, phospholipids, inflammatory cells, and calcium deposition, lead to the narrowing of the arteries and cause limitations of blood flow to vital organs and tissues in the body [1–3]. Although statins and other cholesterol-lowering drugs have been demonstrated as the most effective intervention to reduce mortality and cardiovascular events in patients with established ASCVD, statin therapy only shows a 34% decrease in the risk of major coronary events [1,4,5].

Dysregulated cholesterol metabolism and unresolved endothelial inflammation are pivotal pathogenic factors for atherosclerosis. In the early stages of atherosclerosis, the arterial endothelium gets activated by low-density lipoprotein cholesterol (LDL-C), and macrophages are recruited to the activated endothelium [6]. Phagocytizing LDL-C causes excessive intracellular cholesterol deposition in macrophages. The cholesterol-laden macrophages are converted into foam cells, causing unresolved inflammation on the artery walls through pro-inflammatory cytokines [7]. Crystallized cholesterol, which resides both intracellularly and extracellularly, also plays a detrimental role by inducing inflammation and destabilizing plaques [8–10]. Promoting reverse cholesterol transport, removing cholesterol crystals, and resolving endothelial inflammation would be promising treatment strategies for atherosclerosis.

In the past decade, synthetic high-density lipoprotein (sHDL) has been one of the most promising drug candidates in enhancing cholesterol efflux and resolving vascular inflammation. Typically composed of phospholipids and apolipoprotein A-I (ApoA-I) or its mimetics, sHDL mimics functions of endogenous HDLs, including mediating cholesterol efflux and resolving

endothelial inflammation [11]. sHDL candidates such as CER-001 and CSL112 have entered clinical trials, where a significantly increased cholesterol efflux was observed following sHDL infusion [12,13]. In addition to sHDLs, other HDL-mimetic nanoparticles such as ApoA-I coated PLGA particles and ApoA-I functionalized gold nanoparticles are also in preclinical development [14,15]. However, the technical difficulties in the production and purification of ApoA-I have made the bench-to-bedside transition of sHDL and other HDL mimetics particularly challenging and costly [16–20].

Protein-free, phospholipid-based nanoparticles have long been suggested as potential anti-atherosclerotic agents due to their ability to facilitate cholesterol efflux and reduce plaque burden in animal models [21,22]. Previous research in our lab has found that a series of micelles, which are phospholipid-based nanoparticles composed of phosphatidylcholine and a pegylated phosphatidylethanolamine, showed cholesterol mobilization and plaque reduction capacities in atherosclerosis animal models with no induction of anti-PEG anti- bodies after IV injection [23]. To further understand the composition–activity relationship of micelles, in the present study, a series of micelles composed of different phospholipid compositions and PEGylation extents were prepared. The cholesterol crystal dissolution capacity, cholesterol efflux capacity, anti-inflammatory effects, as well as the in vivo PK/PD profiles of the micelles were evaluated, based on which the structure-activity relationship was analyzed.

2.3 Material and methods

2.3.1 Materials

The compounds 1-palmitoyl-2-oleoyl-glycero-3phosphocholine (POPC), 1,2-dimyristoyl-*sn*-glycero-3-phosphocholine (DMPC), 1,2-dipalmitoyl-*sn*-glycero-3-phosphocholine (DPPC)

and 1,2-distearoyl-*sn*-glycero-3-phosphocholine (DSPC) were purchased from NOF corporation (White Plains, NY, USA). The compound 1,2-distearoyl-*sn*-glycero-3-phosphoethanolamine- N-[azido(polyethylene glycol)-2000] (DSPE-PEG2k) was purchased from Avanti Polar Lipids (Alabaster, AL, USA). Lipopolysaccharide (LPS) (*E. coli* O111:B4) was purchased from Sigma Aldrich (St. Louis, MO, USA). Cholesterol was purchased from Sigma Aldrich (Milwaukee, WI, USA). Wako Cholesterol E Kit was purchased from Fujifilm (Richmond, VA, USA). IL-6 and TNF-α ELISA kits were purchased from Invitrogen (Ann Arbor, MI, USA).

2.3.2 Preparation of micelle library

All micelles were prepared using the co-lyophilization method as described previously [23–25]. Phosphatidylcholine (PC) lipids (POPC, DMPC, DPPC, or DSPC) and DSPE-PEG2k were dissolved in acetic acid and mixed at specified molar ratios as shown in Table 2.1. The resulting mixture was flash-frozen in liquid nitrogen and lyophilized overnight to remove the organic solvent. The lyophilized powder was then rehydrated with phosphate-buffered saline (PBS, pH 7.4)) and heated above and cooled below the transition temperature of each phospholipid for 10 min. This thermocycle process was repeated three times. All micelle concentrations are expressed in terms of total lipid concentration. The final micelle lipid concentration was 20 mM after preparation.

2.3.3 Characterization of micelles

The particle size of micelles was determined using dynamic light scattering (DLS) on Malvern Zetasizer Nano ZSP (Westborough, MA) at a concentration of 2 mM in PBS.

Transmission electron microscopy was used to assess the morphology of micelles. At a diluted concentration of 20 μM in PBS, the samples were deposited on a carbon film-coated 400 mesh copper grid (Electron Microscopy Sciences) and negatively stained with 1% (w/v) uranyl formate. The grid was dried before TEM observation. All specimens were imaged on a 100kV Morgagni TEM equipped with a Gatan Orius CCD.

2.3.4 Cholesterol crystal dissolution

Cholesterol (Sigma-Aldrich) was dissolved in pure ethanol to obtain a concentration 105 of 2 mg/mL cholesterol solution. 100 μL of cholesterol solution was transferred to each 106 well of the 96-well plate, and then 150 uL of sterile water was added to form cholesterol 107 crystals. After drying, cholesterol crystals were incubated with 200 μl of PBS containing 108 indicated micelles at a concentration of 1 mM for 7 days. The supernatant was collected 109 and cholesterol content was measured using Wako Cholesterol E Kit from Fujifilm (Rich- 110 mond, VA) [23].

2.3.5 Cholesterol efflux

J774A.1 cells were cultured in DMEM supplemented with 10% FBS and 1% Penicillin-Streptomycin (10,000 U/mL). Cells were seeded in a 24-well plate at a density of 1×10^5 cells/well and allowed to grow for 2 days. Cells were then labeled with 1 μCi/mL [^{3}H] cholesterol (Perkin Elmer) in DMEM containing 3% fatty acid-free bovine serum albumin (BSA) (Sigma, A8806) and 5 μg/mL ACAT inhibitor Sandoz 58-035 (Sigma, S9318) and incubated overnight. The next day, cells were washed twice with PBS and equilibrated for 24 h in fresh DMEM media containing 0.3% BSA and 5 μg/mL ACAT inhibitor as described above. Cells

were then incubated with DMEM containing 0.1% BSA in the presence of indicated micelles at 20 μM for 4 h at 37 °C. At the end of the incubation, the media was collected. The cells were lysed in 0.5 mL of 0.1% SDS and 0.1 N NaOH, and cell lysate was also collected. The [^{3}H] cholesterol content of medium and cells was measured by liquid scintillation counting using Perkin Elmer Tri-Carb 2910TR (Waltham, MA, USA). Cholesterol efflux was presented as a percentage calculated by media counts divided by the sum of media counts and cell counts as described in previous studies [23,26].

2.3.6 Anti-inflammatory effects of micelles

RAW 264.7 macrophages were obtained from ATCC and cultured in DMEM media supplemented with 10% fetal bovine serum (FBS) and 1% Penicillin-Streptomycin (10,000 U/mL) and grown in a 37 °C incubator with 5% CO_2. Cells were seeded in a 96-well plate at 5 × 10^4 cells/well and grown for 2–3 h. The cells were incubated with micelles (20 μM) and LPS (2 ng/mL) for 18 h. The levels of TNF-α and IL-6 pro-inflammatory cytokines in the culture media were measured using ELISA kits (Thermofisher Scientific, Ann Arbor, MI, USA).

2.3.7 Pharmacokinetic/pharmacodynamic evaluation in rats

All animal experiments in the present study were approved by the Institutional Animal Care and Use Committee (IACUC) of the University of Michigan. Male Sprague-Dawley rats (7–8 weeks old) were obtained from Charles River Laboratory (Mattawan, MI, USA). Rats were randomly assigned to each treatment group, with 4 rats in each group. Rats were fasted 8 h before dosing. Rats were given PBS or different micelle formulations at 136 μmol/kg total lipid dose via tail vein injection. Blood was collected from the jugular vein in BD centrifuge tubes

(BD, Franklin Lakes, NJ, USA) at predetermined time points, 0, 0.25, 1, 2, 4, 8, 24, 36, and 48 h, after dosing. Serum samples were separated by centrifugation at 10,000 rpm for 10 min at 4 °C and stored at −80 °C until further analysis [**26**]. At the study termination, rats were euthanized with carbon dioxide and sacrificed according to IACUC guidelines (Policy on Human Care and Use of Laboratory Animals Approved Animal Welfare Assurance Number, D16–00072 (A3114–01)).

2.3.8 Quantification of serum phospholipids and cholesterol

Phospholipid, total cholesterol, and free cholesterol levels in the serum were analyzed using commercially available kits as instructed by the manufacturer (Wako Chemicals, Richmond, VA, USA). The cholesterol ester levels were calculated by subtracting the free cholesterol levels from total cholesterol levels at each time point.

2.3.9 Pharmacokinetic/pharmacodynamic analysis

Phoenix© WinNonlin® Version 8.2 (Pharsight Corporation, Mountain View, CA, USA) was used to analyze serum concentrations of phospholipids and cholesterol vs. time profiles of each micelle formulation. A non-compartmental model was used to obtain pharmacokinetic and pharmacodynamic parameters. The pharmacokinetic parameters obtained from the plot of concentration of phospholipid versus time include the maximum plasma concentration of phospholipid (C_{max}), area under the curve (AUC), elimination rate constant (K_{10}), half-life of elimination ($T_{1/2}$), total clearance of phospholipid (CL), and volume of distribution at steady state (V_{ss}). The mean and coefficient of variation within each group are presented in the table. The pharmacodynamic parameters derived from total and free cholesterol, and cholesterol ester

concentration versus time profiles include the area under the effect curve (AUEC), the maximum plasma concentration (E_{max}) and the time at which Emax is observed (T_{max}). The mean and coefficient of variation was calculated for each of the above parameters.

2.3.10 Statistical analysis

All data are presented as mean ± SD. Significance between different micelle formulations and formulations vs. control was assessed by ordinary one-way ANOVA with Dunnett's multiple comparisons test. Statistical difference was considered at $p < 0.05$.

2.4 Results

2.4.1 Preparation and characterization of micelles

Particle size and morphology of micelles composed of different phospholipids and with different PEGylation percentages were analyzed by DLS and TEM. As seen in Table 2.1 and Figure 2.1, with a fixed lipid:DSPE-PEG2k ratio of 1:2.09, micelles composed of different PC lipids all showed a uniform size distribution with an average diameter ranging from 15–18 nm. For micelles composed of DMPC and DSPE-PEG2k, on the other hand, increasing the DSPE-PEG2k percentage generally led to a reduction of particle size.

Table 2.1 Average particle size of different micelles measured by DLS (n = 3, mean ± SD). Micelles were diluted to a 2mM concentration with PBS and size was determined using Malvern Zetasizer Nano ZSP.

Formulation (molar ratio)	Size (nm)	PDI
POPC:DSPE-PEG2k (1:2.09)	15.97 ± 0.20	0.162 ± 0.047
DMPC:DSPE-PEG2k (1:2.09)	17.12 ± 1.09	0.298 ± 0.030
DPPC:DSPE-PEG2k (1:2.09)	18.29 ± 1.39	0.196 ± 0.028
DSPC:DSPE-PEG2k (1:2.09)	17.32 ± 0.30	0.061 ± 0.016
DMPC:DSPE-PEG2k (1:0.5)	29.74 ± 2.02	0.306 ± 0.002
DMPC:DSPE-PEG2k (1:1)	17.14 ± 0.51	0.190 ± 0.048
DMPC:DSPE-PEG2k (1:1.5)	18.88 ± 1.45	0.333 ± 0.033
DMPC:DSPE-PEG2k (1:2)	15.51 ± 0.41	0.260 ± 0.030
DMPC:DSPE-PEG2k (1:2.5)	17.69 ± 0.69	0.559 ± 0.028
DMPC:DSPE-PEG2k (1:3)	15.86 ± 0.88	0.344 ± 0.050

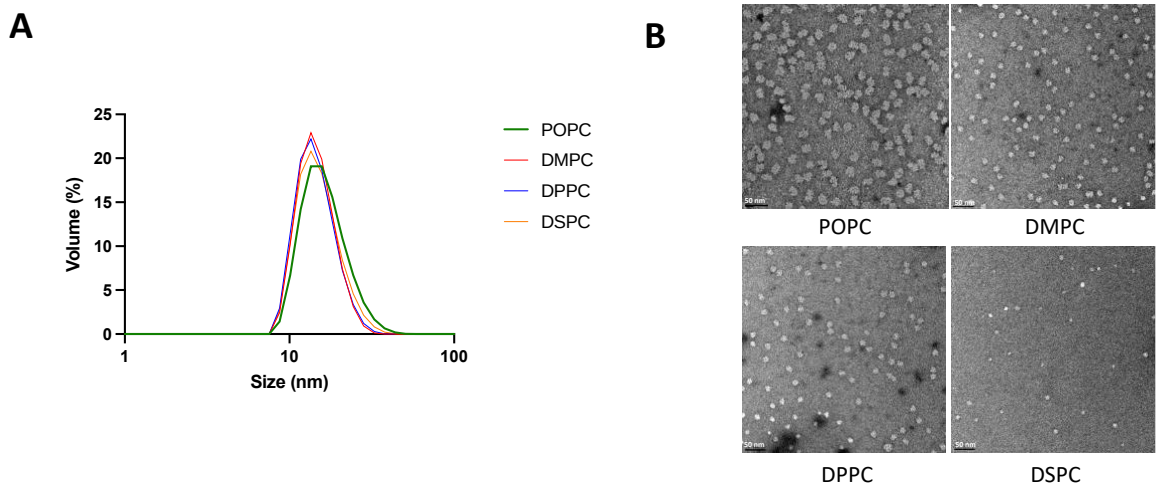

Figure 2.1 Micelle size and morphology analyzed by DLS (A) and TEM (B). Malvern Zetasizer Nano ZSP was used to determine the size of micelles diluted with PBS to a 2mM concentration. Micelles were diluted to 10 μM in PBS and TEM images were taken on a 100kV Morgagni TEM equipped with a Gatan Orius CCD.

2.4.2 Cholesterol crystal dissolution and cholesterol efflux capacity of micelles

To examine the effect of micelle composition on cholesterol crystal dissolution capacities, micelles were incubated with cholesterol crystals at physiological temperature for 1 week. All micelles with different lipid compositions and PEGylation resulted in significant cholesterol crystal dissolution, with at least a 10-fold increase in cholesterol crystal dissolution. DMPC micelles showed more potent cholesterol crystal dissolution capacity compared to POPC,

DPPC, and DSPC micelles (**Figure 2.2A**). Micelles composed of 1:1.5 and 1:2 ratios of DMPC:DSPE-PEG2k dissolved the largest concentration of cholesterol from the cholesterol crystals (**Figure 2.2C**).

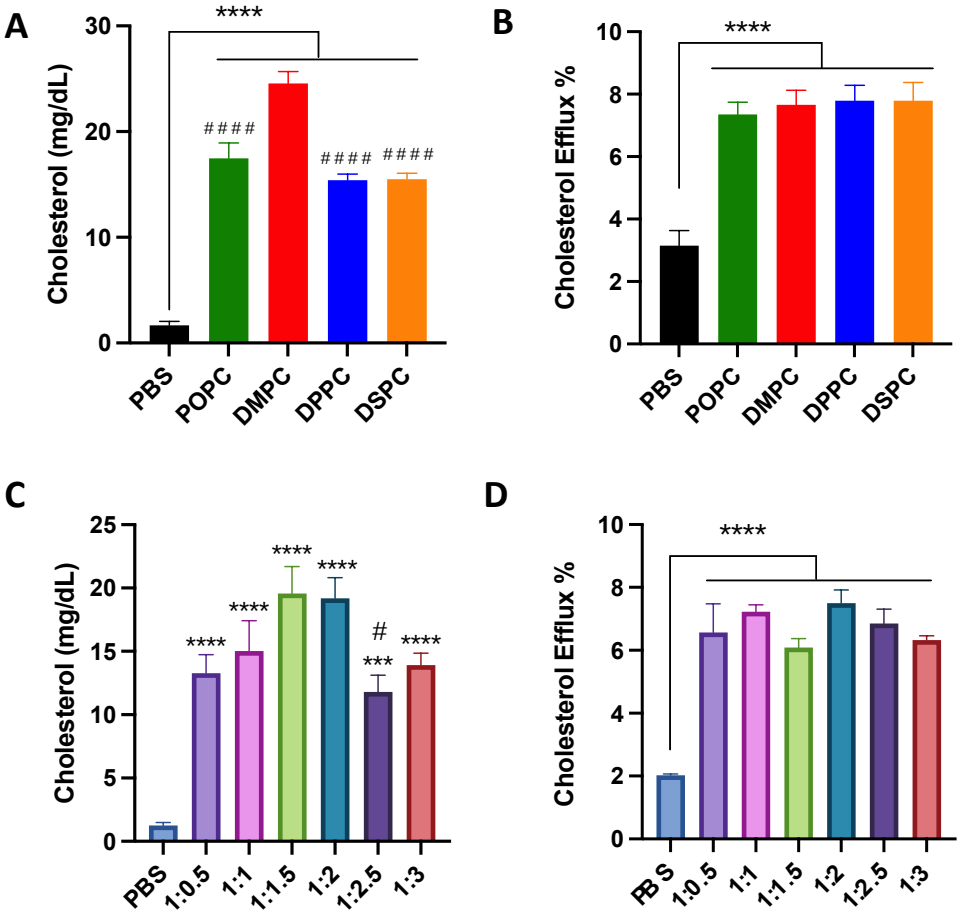

Figure 2.2 Cholesterol crystal dissolution after 7 days of incubation with different PC lipids (A) and different ratios of DMPC:DSPE-PEG2k (C). Effect of 4 hour incubation of different PC lipids (B) and different ratios of DMPC:DSPE-PEG2k (D) on the cholesterol efflux of J774A.1 macrophage cells containing radiolabeled cholesterol. ***P < 0.001, ****P < 0.0001 when compared to untreated PBS group. (n = 3, mean ± SD. $^{\#}$P < 0.05, $^{\#\#\#\#}$P < 0.0001 when compared to DMPC or 1:2 group).

Next, the cholesterol efflux capacity of micelles was tested in J774A.1 macrophages. Micelles composed of different PC lipids were able to promote cholesterol efflux, showing a 2.5 to 3-fold increase in cholesterol efflux as compared to PBS control, but there was no significant

difference in the cholesterol efflux capacity of all four micelles (**Figure 2.2B**). Micelles with different ratios of DMPC:DSPE-PEG2k also showed an ability to promote cholesterol efflux, with a three-fold increase in cholesterol effluxed as compared to PBS control, though no statistical difference was observed among micelles composed of different DMPC:DSPE-PEG2k ratios (**Figure 2.2D**). Overall, the composition of micelles does not seem to substantially affect the cholesterol efflux capabilities of the nanoparticle.

2.4.3 Anti-inflammatory effects of micelles

The effect of composition on the anti-inflammatory properties of micelles was evaluated in LPS-treated macrophage cells. Micelles composed of different PC lipids reduced TNF-α levels significantly compared to the LPS-only group. DMPC micelles were able to reduce TNF-α levels to the largest extent (70% reduction compared to LPS-only group), followed by POPC, DPPC and DSPC micelles (**Figure 2.3A**). A similar pattern was also observed in IL-6 levels (**Figure 2.3B**). POPC and DMPC micelles displayed a greater ability to reduce IL-6 levels than DPPC and DSPC, and showed a 90% reduction in IL-6 levels as compared to LPS-only group. As for the effects of PEGylation, micelles with less PEGylation showed stronger abilities to reduce TNF-α levels (**Figure 2.3C**). Micelles with a 1:3 DMPC:DSPE-PEG ratio performed the worst out of all formulations. At the same time, all PEGylated micelles strongly inhibited the secretion of IL-6, with a 70% reduction as compared to LPS-only group (**Figure 2.3D**). Overall, the impact of PEGylation on the anti-inflammatory activity of micelles is less significant than that of PC species.

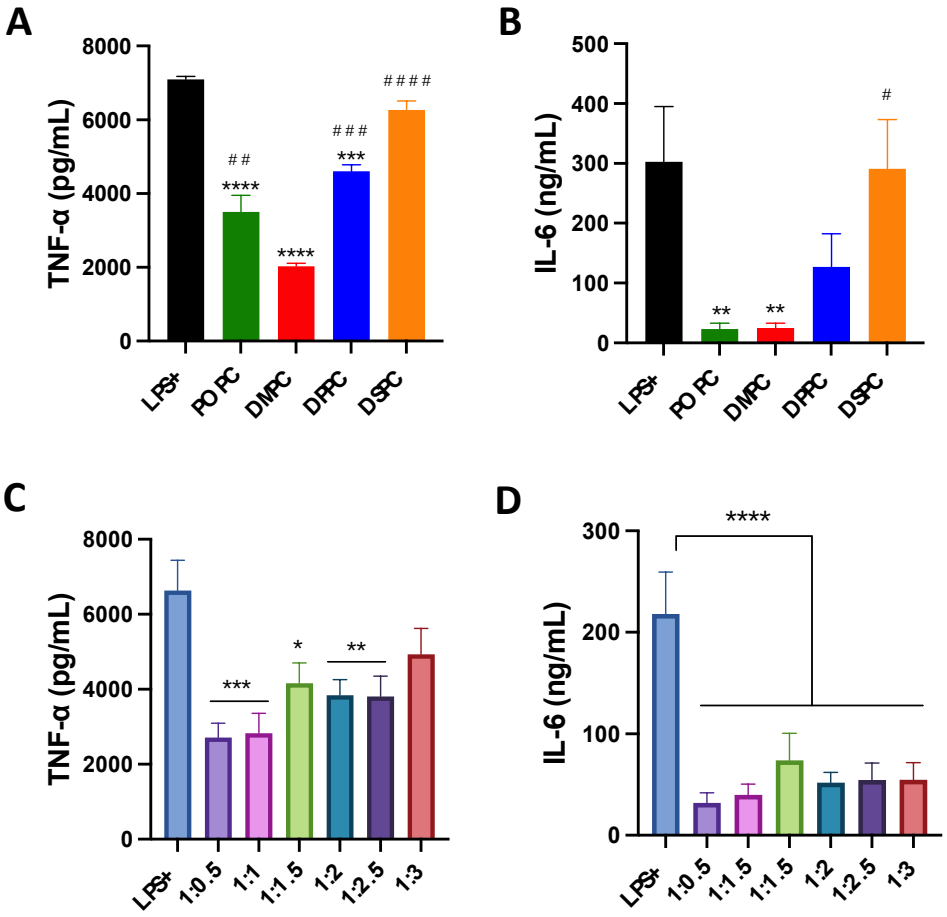

Figure 2.3 TNF-α and IL-6 pro-inflammatory cytokine release was measured after induction of inflammation with LPS endotoxin in Raw 264.7 macrophage cells with simultaneous addition of micelles composed of different PC lipids (A,B) and micelles composed of different ratios of DMPC:DSPE-PEG2k lipid (C,D). *P < 0.05; **P < 0.01; ***P < 0.001: ****P < 0.0001 when compared to untreated LPS+ group. $^{\#}$P < 0.05; $^{\#\#}$P < 0.01; $^{\#\#\#}$P < 0.001: $^{\#\#\#\#}$P < 0.0001 when compared to DMPC group (n = 3, mean ± SD).

2.4.4 Effects of PC lipid composition on the PK/PD profiles

Micelles composed of different PC lipids were tested in a pharmacokinetic study using Sprague Dawley rats to investigate whether PC composition affects the pharmacokinetic and pharmacodynamic parameters of the particle. The pharmacokinetic parameters were obtained by performing a non-compartmental model (NCA) analysis on the phospholipid concentration vs. time plot (**Figure 2.4A**). As shown in **Table 2.2**, when comparing the micelles composed of different PC lipids, there were slight differences in the pharmacokinetic parameters. While the

differences were not significant, DSPC had the largest phospholipid AUC, followed by DPPC, DMPC and POPC, suggesting that DSPC micelles had the greatest drug exposure over 48 h. Though small differences were found in the AUC and C_{max}, other pharmacokinetic parameters calculated from the NCA, T_{max}, CL, and V_{ss}, $T_{1/2}$ and K_{10}, were all similar between micelle groups (**Table 2.2**).

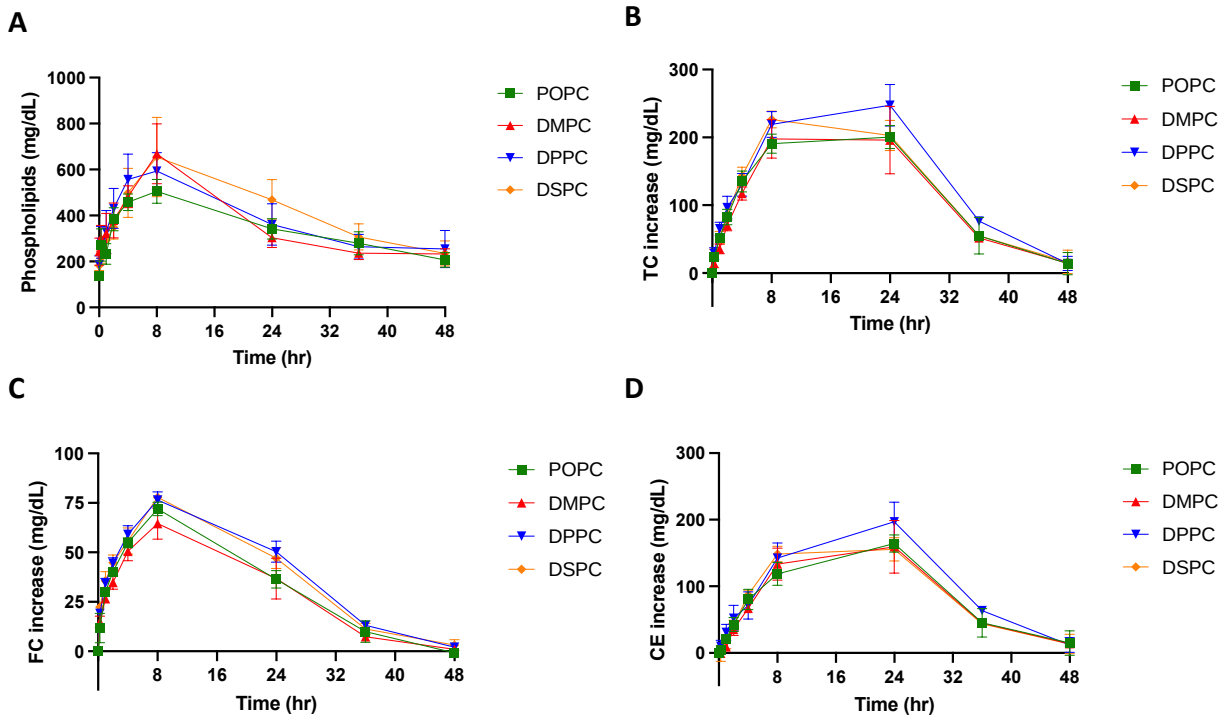

Figure 2.4 A pharmacokinetic/pharmacodynamic study was completed using Sprague Dawley Rats. Micelles were injected via tail vein injection and blood was collected from the jugular vein at various time points between 0 and 48 hours post-injection. The concentration of a) phospholipid, b) total cholesterol (TC), c) free cholesterol (FC), and d) cholesterol ester (CE), over a 48-hour time frame were measured using commercially available kits. Profiles of concentration vs. time are displayed over a 48 hour time period (n = 4, mean ± SD).

Table 2.2 Pharmacokinetic parameters (% CV) of phospholipids after a 136 μmol/kg dose of micelles containing different PC lipids.

Parameters	POPC	DMPC	DPPC	DSPC
C_{max} (mg/dL)	507.4 (20.1)	723.7 (24.1)	613.5 (25.1)	678.1 (48.5)
T_{max} (h)	7.0 (28.6)	7.0 (28.6)	6.7 (34.6)	7.0 (28.6)
AUC (mg*h/dL)	16732.8 (21.4)	17654.4 (18.2)	188482.0 (32.2)	20607.5 (37.4)
K_{10} (h^{-1})	0.022 (33.6)	0.027 (17.1)	0.025 (36.0)	0.026 (44.9)
$T_{1/2}$ (h)	35.0 (46.5)	31.0 (41.8)	29.9 (34.5)	33.5 (81.7)
CL (dL/h)	0.001 (32.9)	0.001(5.4)	0.001(56.7)	0.001 (57.1)
V_{SS} (dL)	0.051 (20.2)	0.047 (37.9)	0.044 (20.7)	0.043 (49.4)

C_{max}: the maximum plasma concentration of phospholipid; AUC: the area under the curve in a plot of concentration of phospholipid against time; K_{10}: elimination rate constant; $T_{1/2}$: the half-life of elimination; CL: total clearance for phospholipid; V_{ss}: volume of distribution for phospholipid at steady state.

To examine if the PC composition of micelles affects its ability to mobilize cholesterol in vivo, the total cholesterol (TC), free cholesterol (FC), and cholesterol ester (CE) concentrations in serum were determined and plotted on a concentration vs. time plot (**Figure 2.4B–D**). As shown in **Table 2.3**, the T_{max} of FC occurs at 8 h and the T_{max} of CE occurs at 20 or 24 h. This follows the typical pattern of response that has been seen after sHDL IV infusion, where free cholesterol is mobilized and picked up by HDL, then esterified by LCAT in the reverse cholesterol transport process, and finally eliminated through the liver. When comparing TC AUEC values, DPPC had the largest TC AUEC, followed by DSPC, POPC, and DMPC. The AUC, E_{max}, and T_{max} values were not significantly different between micelle groups. All cholesterol levels returned back to baseline 48 h post-micelle injection.

Table 2.3 Pharmacodynamic parameters (% CV) of total cholesterol (TC), free cholesterol (FC) and cholesterol ester (CE) after 136 μmol/kg doses of micelles containing different PC lipids.

	Parameters	POPC	DMPC	DPPC	DSPC
TC	T_{max} **(h)**	20.0 (40.0)	12.0 (66.7)	18.6 (49.5)	8.0 (0.0)
	E_{max} **(mg/dL)**	201.9 (16.8)	234.7 (33.6)	251.4 (20.6)	226.2 (11.0)
	***AUEC* (mg*h/dL)**	6043.8 (23.9)	5925.7 (28.4)	7266.0 (16.5)	6472.5 (12.4)
FC	T_{max} **(h)**	8.0 (0.0)	8.0 (0.0)	8.0 (0.0)	8.0 (0.0)
	E_{max} **(mg/dL)**	72.0 (9.4)	64.5 (24.7)	76.5 (9.5)	77.9 (1.5)
	***AUEC* (mg*h/dL)**	1600.0 (8.1)	1488.0 (32.1)	1923.6 (11.6)	1868.6 (9.5)
CE	$T_{max,}$ **(h)**	24.0 (0.0)	20.0 (4.0)	24.0 (0.0)	20.0 (4.0)
	E_{max} **(mg/dL)**	164.1 (15.9)	180.1 (37.9)	197.0 (25.9)	159.0 (18.8)
	***AUEC* (mg*h/dL)**	4382.4 (30.7)	4437.7 (27.2)	5189.1 (25.3)	4492.7 (16.0)

T_{max}: time at which the E_{max} is observed. E_{max}: the maximum concentration of different cholesterol species. AUEC: the area under the effect curve. Data was shown as mean with CV%.

2.4.5 Effects of PEGylation on the PK/PD profiles

To examine how the lipid ratio of DMPC:DSPE-PEG2k influences the pharmacokinetics of micelles, four out of the six different ratio micelles were chosen to test in the Sprague Dawley rats. The DMPC:DSPE-PEG2k ratio had an effect on the pharmacokinetics of micelles as seen in the phospholipid concentration vs. time plot **(Figure 2.5A**). As shown in **Table 2.4,** the C_{max} and AUC grew larger as the amount of DSPE-PEG2k increased in the micelle formulation. Micelles composed of a 1:3 ratio of DMPC:DSPE-PEG2k had a significantly larger AUC and C_{max} than 1:0.5 DMPC:DSPE-PEG2k ratio micelles, suggesting larger overall exposure and maximum serum concentration of micelles with higher PEGylation ratios. The $T_{1/2}$ of the 1:0.5 ratio micelles was also significantly different from both 1:2 and 1:3 ratio micelles.

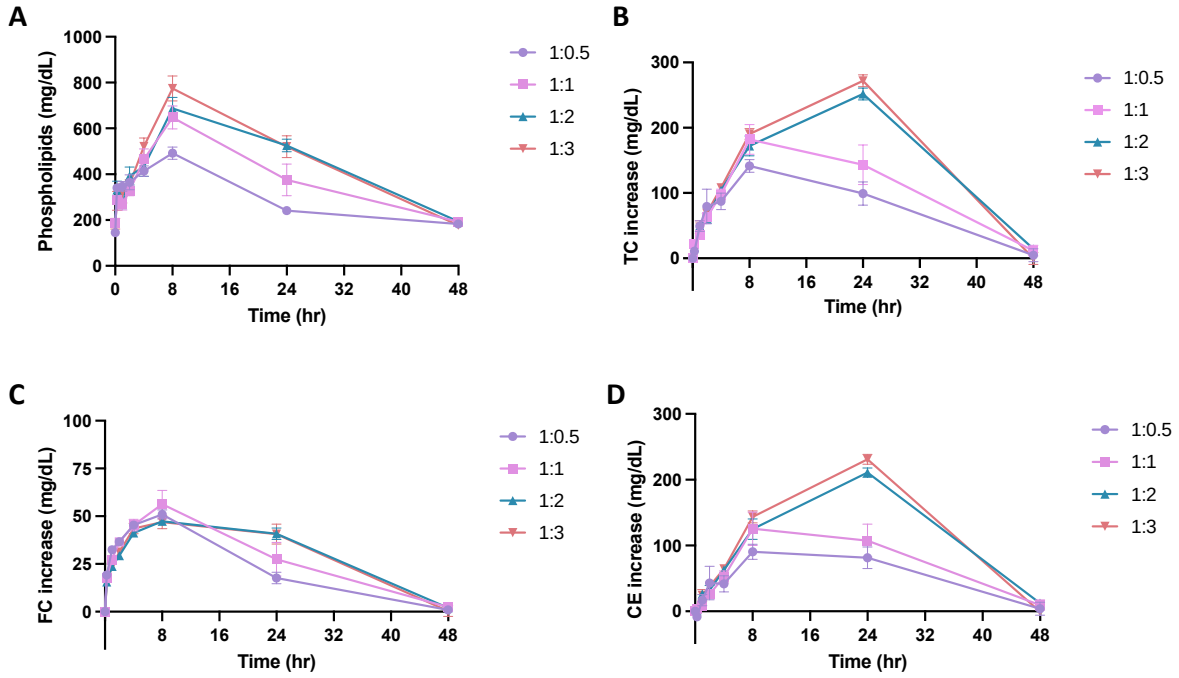

Figure 2.5 A pharmacokinetic/pharmacodynamic study was completed using Sprague Dawley Rats. Micelles were injected via tail vein injection and blood was collected from the jugular vein. The concentration of a) phospholipid, b) total cholesterol (TC), c) free cholesterol (FC), and d) cholesterol ester (CE), over a 48-hour time frame were measured using commercially available kits. Profiles of concentration vs. time are displayed over a 48 hour time period to examine the effect of DMPC:DSPE-PEG2k ratio on the phospholipid pharmacokinetics and cholesterol mobilization ability of the micelles (n = 4, mean ± SD).

Table 2.4 Pharmacokinetic parameters (% CV) of phospholipids for micelles containing different ratios of DMPC:DSPE-PEG2k lipid dosed at 136 μmol/kg.

Parameters	**1:0.5**	**1:1**	**1:2**	**1:3**
C_{max} [a] **(mg/dL)**	523.2 (18.0)	648.0 (15.6)	686.7 (14.2)	775.0 (14.1)
T_{max} [b] **(h)**	6.0 (63.9)	8.0 (0.0)	8.0 (0.0)	8.0 (0.0)
AUC[c] **(mg*h/dL)**	14266.1 (7.0)	18595.4 (19.7)	22019.4 (10.1)	22815.2 (13.5)
K_{10} [d] **(h^{-1})**	0.023 (23.3)	0.030 (20.2)	0.032 (10.8)	0.038 (9.6)
$T_{1/2}$ [e] **(h)**	31.2 (20.3)	24.0 (21.3)	21.6 (10.8)	18.58 (9.3)
CL[f] **(dL/h)**	0.006 (11.6)	0.005 (18.3)	0.005 (9.2)	0.005 (13.0)
V_{SS} [g] **(dL)**	0.277 (12.8)	0.196 (22.7)	0.158 (13.0)	0.142 (17.4)

C_{max}: the maximum plasma concentration of phospholipid; AUC: the area under the curve in plot of concentration of phospholipid against time; K_{10}: elimination rate constant; $T_{1/2}$: the half-life of elimination; CL: total clearance for phospholipid; V_{ss}: volume of distribution for phospholipid at steady state.

The ability of micelles composed of different DMPC:DSPE-PEG2k ratios to promote cholesterol mobilization was evaluated by analyzing the TC, FC and CE concentration vs. time profiles over 48 h (**Figure 2.5B–D**). Using an NCA model on WinNonlin, the T_{max}, E_{max}, and AUEC were determined for each cholesterol population **(Table 2.5).** As previously seen with the different PC lipid micelles, the maximum FC mobilization occurred first, followed by the peak CE mobilization, showing the subsequent elimination of cholesterol. All mobilized cholesterol was eliminated 48 h post-injection. The AUEC for TC and CE grew larger with increasing amounts of DSPE-PEG2k in the formulation, where micelles with a 1:3 ratio had a two-fold increase in AUEC as compared to the 1:0.5 micelles. For TC and CE profiles, the E_{max} was also significantly higher for 1:2 and 1:3 ratio micelles as compared to 1:0.5 ratio micelles. Overall, more cholesterol was mobilized and eliminated from the body as the amount of PEG increased in the micelles.

Table 2.5 Pharmacodynamic parameters (% CV) of total cholesterol (TC), free cholesterol (FC) and cholesterol ester (CE) for DMPC micelles containing different ratios of PC:DSPE-PEG lipid dosed at 136 μmo/kg.

	Parameters	**1:0.5**	**1:1**	**1:2**	**1:3**
TC	$T_{max,E}$[a] **(h)**	8.0 (0.0)	8.0 (0.0)	24.0 (0.0)	24.0 (0.0)
	E_{max}[b] **(mg/dL)**	141.5 (13.7)	181.9 (25.2)	251.7 (7.2)	271.7 (6.7)
	AUEC **(mg*h/dL)**	3883.3 (17.9)	5252.1 (33.8)	7383.8 (8.7)	7813.3 (8.0)
FC	$T_{max,E}$ **(h)**	8.0 (0.0)	12.0 (66.7)	8.0 (0.0)	6.0 (38.5)
	E_{max} **(mg/dL)**	50.9 (9.5)	58.4 (24.5)	47.3 (4.7)	47.3 (14.8)
	AUEC **(mg*h/dL)**	1102.7 (14.6)	1529.6 (30.0)	1511.5 (10.0)	1492.6 (23.3)
CE	$T_{max,E}$ **(h)**	15.0 (70.10	12.0 (66.7)	24.0 (0.0)	24.0 (0.0)
	E_{max} **(mg/dL)**	96.9 (19.6)	129.6 (38.1)	210.8 (6.8)	231.0 (6.6)
	AUEC **(mg*h/dL)**	2780.5 (24.9)	3722.5 (44.0)	5872.2 (10.1)	6320.7 (6.1)

Tmax: time at which the Emax is observed. Emax: the maximum plasma concentration of different cholesterol species. AUEC: the area under the effect curve. Data was shown as mean with CV%.

2.5 Discussion

The anti-atherosclerotic potential of phospholipid-based nanoparticles has long been studied due to their ability to promote cholesterol efflux, decrease inflammation, and reduce plaque burden [22,23,27]. Due to this fact, our group developed a series of phospholipid-based, HDL mimetic micelles composed of a PC lipid and DSPE-PEG2k. Recently, our group showed that a micelle composed of DPPC and DSPE-PEGk, named MiNano, was able to bind and dissolve cholesterol crystals, enhance cholesterol efflux, and suppress inflammatory responses in macrophages [23]. In this current study, we manipulate the lipid composition of micelles and we show that the lipid composition can affect micelles' anti-inflammatory activity, cholesterol crystal dissolution abilities, cholesterol efflux capacity and in vivo PK/PD profiles.

A series of micelles composed of different phospholipids was first compared to determine the effects of PC on the therapeutic effects of micelles. PC with varying degrees of saturation and lipid tail chain lengths present different transition temperatures (T_m) at which the lipids change phases [28,29]. Lipids with lower transition temperatures and shorter fatty acid chains, such as POPC (1-palmitoyl-2-oleoyl-glycero-3-phosphocholine) and DMPC (1,2-dimyristoyl-*sn*-glycero-3-phosphocholine), form a liquid crystalline phase at physiological temperature, where the lipids are fluid and randomly oriented. Lipids with higher transition temperatures and longer fatty acid chains and saturation, such as DPPC (1,2-dipalmitoyl-*sn*-glycero-3-phosphocholine) and DSPC (1,2-distearoyl-*sn*-glycero-3-phosphocholine), exist at a gel-ordered phase at physiological temperature, where the lipids are tightly packed and fully extended [28,30]. The phase in which the PC lipids exist may affect the ability of the lipids to interact with their molecular targets, leading to a significant pharmacological effect. Several other groups have observed differences in nanoparticle activity due to PC lipid composition changes [24,25,31,32].

Phospholipid composition has been found to significantly affect the cholesterol efflux capacity, anti-inflammatory effects, and PK/PD profiles in our previous studies on sHDL composed of ApoA-I mimetics and phospholipids. sHDLs composed of lipids with lower phase transition temperature such as DMPC and POPC have been found to have greater anti-inflammatory effects due to higher endotoxin neutralization capacity and TLR-4 displacing effects [33]. sHDL prepared with POPC and DMPC also showed a greater ability to efflux cholesterol in vitro compared to that with DPPC and DSPC [**24**]. However, DSPC-sHDL induced more significant cholesterol mobilization in vivo, possibly due to its longer circulation time.

Compared to previous results on peptide-containing sHDLs, there are some similarities and differences concerning the effects of phospholipids on cholesterol efflux capacities, anti-inflammatory effects, and PK/PD profiles of micelles. Similar to previous results, micelles composed of POPC and DMPC showed a greater ability to reduce pro-inflammatory cytokine levels induced by LPS (**Figure 2.3**), which may be attributed to higher LPS neutralization and/or TLR-4 displacement effects. POPC and DMPC micelles also presented better capacities in dissolving cholesterol crystals (**Figure 2.2**) as compared to micelles composed of DPPC and DSPC. However, when tested using cholesterol-loaded macrophages, no statistically significant difference was observed in cholesterol efflux among micelles composed of different phospholipids. In vivo studies suggested that changing the PC lipid of micelles did not significantly affect the PK parameters and cholesterol mobilization abilities of the micelles. Overall, the results suggested that phospholipid composition mainly affects the anti-inflammatory effects but not the cholesterol efflux capacities of micelles.

The effects of PEGylation on micelle activity and stability were also investigated. PEGylation is an extensively used strategy to extend the circulation time of nanomedicine by

shielding the NPs from aggregation, phagocytosis and opsonization [**26**,**34**,**35**,**36**]. On the other hand, the shielding effects of PEG can limit the interaction between nanoparticles and target tissues, reducing the therapeutic effects of nanoparticles. In relevance to HDL-mimicking nanoparticles, Li et al. found that the addition of PEG to sHDL increased circulation time and cholesterol mobilization in rats [**26**]. Similarly, it was shown in this study that while micelles with different PEGylation presented comparable cholesterol efflux capacity in vitro (**Figure 2.2**), more PEGylated micelles induced a greater drug exposure and cholesterol mobilization in vivo (**Table 2.3** and **Table 2.4**). On the other hand, PEGylation might reduce the anti-inflammatory effects of micelles (**Figure 2.3**), which could be attributed to the fact that a large amount of PEG may hinder the lipids from interacting with LPS itself or disrupt the lipid raft microenvironment which affects toll-like receptor (TLR4) recruitment. Such results suggested that the amount of PEGylation in micelles should be carefully adjusted to balance the PK profile and anti-atherogenic effects.

2.6 Conclusion

The present study highlights that the lipid composition can affect the size, anti-inflammatory activity, cholesterol crystal dissolution, cholesterol mobilization capacity and PK/PD profiles of micelles. Micelles composed of different PCs presented comparable cholesterol efflux capacity in vitro and in vivo, while micelles composed of DMPC and POPC presented more potent anti-inflammatory effects in vitro. PEGylation was found to increase the circulation time of micelles, leading to greater cholesterol mobilization when administered in vivo. The results obtained in this study may provide useful information to optimize the design of peptide-free micellar HDL mimetics for atherosclerosis therapy.

2.7 References

1. Pahwa R, Jialal I. Atherosclerosis - StatPearls - NCBI Bookshelf. *StatPearls [Internet]*. 2021. https://www.ncbi.nlm.nih.gov/books/NBK507799/.

2. NIH. Atherosclerosis |NHLBI, NIH. *Natl Heat, Lung, Blood Institutre*. 2020. https://www.nhlbi.nih.gov/health-topics/atherosclerosis.

3. Spagnoli LG, Mauriello A, Sangiorgi G, et al. Extracranial thrombotically active carotid plaque as a risk factor for ischemic stroke. *J Am Med Assoc*. 2004;292(15):1845-1852. doi:10.1001/jama.292.15.1845

4. Formanowicz D, Krawczyk JB. Controlling the thickness of the atherosclerotic plaque by statin medication. *PLoS One*. 2020;15(10 October):1-20. doi:10.1371/journal.pone.0239953

5. LaRosa JC, He J, Vupputuri S. Effect of statins on risk of coronary disease. A meta-analysis of randomized controlled trials. *J Am Med Assoc*. 1999;282(24):2340-2346. doi:10.1001/jama.282.24.2340

6. Yurdagul Jr. A, Finney A, Woolard MD, Orr AW. The Arterial Microenvironment: The Where and Why of Atherosclerosis. *Biochem J*. 2016;473(10):1281-1295. doi:10.1042/BJ20150844

7. Chistiakov DA, Melnichenko AA, Myasoedova VA, Grechko A V., Orekhov AN. Mechanisms of foam cell formation in atherosclerosis. *J Mol Med*. 2017;95(11):1153-1165. doi:10.1007/s00109-017-1575-8

8. Janoudi A, Shamoun FE, Kalavakunta JK, Abela GS. Cholesterol crystal induced arterial inflammation and destabilization of atherosclerotic plaque. *Eur Heart J*. 2016;37(25):1959-1967. doi:10.1093/eurheartj/ehv653

9. Abela GS. Cholesterol crystals piercing the arterial plaque and intima trigger local and systemic inflammation. *J Clin Lipidol*. 2010;4(3):156-164. doi:10.1016/j.jacl.2010.03.003

10. Elvind O. Samstad, Niyonzima N, Nymo S, Aune MH, Ryan L. Cholesterol crystals induce complement-dependent inflammasome activation and cytokine release. *J Immunol*. 2014;192(6):2837-2845. doi:10.4049/jimmunol.1302484.

11. Kuai R, Li D, Chen YE, Moon JJ, Schwendeman A. High-Density Lipoproteins: Nature's Multifunctional Nanoparticles. *ACS Nano*. 2016;10(3):3015-3041. doi:10.1021/acsnano.5b07522

12. Tricoci P, D'Andrea DM, Gurbel PA, et al. Infusion of Reconstituted High-Density Lipoprotein, CSL112, in Patients With Atherosclerosis: Safety and Pharmacokinetic Results From a Phase 2a Randomized Clinical Trial. *J Am Heart Assoc*. 2015;4(8):e002171. doi:10.1161/JAHA.115.002171

13. Keyserling CH, Barbaras R, Benghozi R, Dasseux JL. Development of CER-001: Preclinical Dose Selection Through to Phase I Clinical Findings. *Clin Drug Investig*. 2017;37(5):483-491. doi:10.1007/s40261-017-0506-3

14. Sanchez-Gaytan BL, Fay F, Lobatto ME, et al. HDL-mimetic PLGA nanoparticle to target atherosclerosis plaque macrophages. *Bioconjug Chem*. 2015;26(3):443-451. doi:10.1021/bc500517k

15. Lai CT, Sun WQ, Palekar RU, Thaxton CS, Schatz GC. Molecular Dynamics Simulation and Experimental Studies of Gold Nanoparticle Templated HDL-like Nanoparticles for Cholesterol Metabolism Therapeutics. *ACS Appl Mater Interfaces*. 2017;9(2):1247-1254. doi:10.1021/acsami.6b12249

16. Brace RJ, Sorrenson B, Sviridov D, McCormick SPA. A gel-based method for purification of apolipoprotein A-I from small volumes of plasma. *J Lipid Res*. 2010;51(11):3370-3376. doi:10.1194/jlr.D008300

17. Feng MQ, Cai QS, Song DX, Dong J Bin, Zhou P. High yield and secretion of recombinant human apolipoprotein AI in Pichia pastoris. *Protein Expr Purif*. 2006;46(2):337-342. doi:10.1016/j.pep.2005.11.009

18. Pyle LE, Fidge NH, Barton PA, Luong A, Sviridov D. Production of mature human apolipoprotein A-I in a baculovirus-insect cell system: Propeptide is not essential for intracellular processing but may assist rapid secretion. *Anal Biochem*. 1997;253(2):253-258. doi:10.1006/abio.1997.2371

19. McGuire KA, Davidson WS, Jonas A. High yield overexpression and characterization of human recombinant proapolipoprotein A-I. *J Lipid Res*. 1996;37(7):1519-1528. doi:10.1016/s0022-2275(20)39136-7

20. Brissette L, Cahuzac-Bec N, Desforges M, Bec JL, Marcel YL, Rassart E. Expression of recombinant human apolipoprotein A-I in Chinese hamster ovary cells and Escherichia coli. *Protein Expr Purif*. 1991;2(4):296-303. doi:10.1016/1046-5928(91)90086-X

21. Damen J, Regts J, Scherphof G. Transfer and exchange of phospholipid between small unilamellar liposomes and rat plasma high density lipoproteins Dependence on cholesterol content and phospholipid composition. *Biochim Biophys Acta (BBA)/Lipids Lipid Metab*. 1981;665(3):538-545. doi:10.1016/0005-2760(81)90268-X

22. Dass CR, Jessup W. Apolipoprotein A-I, Cyclodextrins and Liposomes as Potential Drugs for the Reversal of Atherosclerosis. A Review. *J Pharm Pharmacol*. 2010;52(7):731-761. doi:10.1211/0022357001774606

23. Luo Y, Guo Y, Wang H, et al. Phospholipid nanoparticles: Therapeutic potentials against atherosclerosis via reducing cholesterol crystals and inhibiting inflammation. *EBioMedicine*. 2021;74:103725. doi:10.1016/j.ebiom.2021.103725

24. Fawaz M V., Kim SY, Li D, et al. Phospholipid component defines pharmacokinetic and

pharmacodynamic properties of synthetic high-density lipoproteins. *J Pharmacol Exp Ther*. 2020;372(2):193-204. doi:10.1124/JPET.119.257568

25. Schwendeman A, Sviridov DO, Yuan W, et al. The effect of phospholipid composition of reconstituted HDL on its cholesterol efflux and anti-inflammatory properties. *J Lipid Res*. 2015;56(9):1727-1737. doi:10.1194/jlr.M060285

26. Li D, Fawas M, Morin E, et al. The effect of synthetic high density lipoproteins modification with polyethylene glycol on pharmacokinetics and pharmacodynamics. *Mol Pharm*. 2018;15(1):83-96. doi:10.1021/acs.molpharmaceut.7b00734.The

27. Prilepskii AY, Serov NS, Kladko D V., Vinogradov V V. Nanoparticle-based approaches towards the treatment of atherosclerosis. *Pharmaceutics*. 2020;12(11):1-31. doi:10.3390/pharmaceutics12111056

28. Thewalt JL, Bloom M. Phosphatidylcholine: cholesterol phase diagrams. *Biophys J*. 1992;63(4):1176-1181. doi:10.1016/S0006-3495(92)81681-8

29. Koynova R, Caffrey M. Phases and phase transitions of the phosphatidylcholines. *Biochim Biophys Acta - Rev Biomembr*. 1998;1376(1):91-145. doi:10.1016/S0304-4157(98)00006-9

30. Wang M, Zander T, Liu X, et al. The effect of temperature on supported dipalmitoylphosphatidylcholine (DPPC) bilayers: Structure and lubrication performance. *J Colloid Interface Sci*. 2015;445:84-92. doi:10.1016/j.jcis.2014.12.042

31. Chen J, Cheng D, Li J, et al. Influence of lipid composition on the phase transition temperature of liposomes composed of both DPPC and HSPC. *Drug Dev Ind Pharm*. 2013;39(2):197-204. doi:10.3109/03639045.2012.668912

32. Abumanhal-Masarweh H, da Silva D, Poley M, et al. Tailoring the lipid composition of nanoparticles modulates their cellular uptake and affects the viability of triple negative breast cancer cells. *J Control Release*. 2019;307(February):331-341. doi:10.1016/j.jconrel.2019.06.025

33. Kim SY. Optimization of Syntheic High-Density Lipoprotein Nanostructures for Treatment of Inflammatory Diseases. 2019.

34. Matthew T H, Huang Le. Maximizing the Supported Bilayer Phenomenon: Liposomes Comprised Exclusively of PEGylated Phospholipids for Enhanced Systemic and Lymphatic Delivery. *Physiol Behav*. 2017;176(3):139-148. doi:10.1021/acsami.6b05534.Maximizing

35. Yang C, Gao S, Dagnæs-Hansen F, Jakobsen M, Kjems J. Impact of PEG Chain Length on the Physical Properties and Bioactivity of PEGylated Chitosan/siRNA Nanoparticles in Vitro and in Vivo. *ACS Appl Mater Interfaces*. 2017;9(14):12203-12216. doi:10.1021/acsami.6b16556

36. Parveen S, Sahoo SK. Long circulating chitosan/PEG blended PLGA nanoparticle for tumor drug delivery. *Eur J Pharmacol*. 2011;670(2-3):372-383. doi:10.1016/j.ejphar.2011.09.023

Chapter 3 – Evaluation of Synthetic High-Density Lipoproteins for the Protection of Endothelial Function

3.1 Abstract

Endothelial dysfunction is implicated in the development of many types of cardiovascular-related diseases. Previous studies have shown that endogenous high-density lipoproteins (HDL) display a variety of protective properties on the vascular endothelium, including modulating vascular tone and enhancing endothelial monolayer integrity. To mimic the natural cardioprotective behaviors of endogenous HDL, synthetic high-density lipoproteins (sHDLs) have been developed in the present study. sHDLs were prepared by combining an ApoA-1 mimetic peptide, 22A, with various phosphatidylcholine (PC) phospholipids, resulting in homogenous nanoparticles ranging from 9-13 nm in size. In lipopolysaccharide (LPS) and tumor necrosis factor alpha (TNF-α) activated human umbilical vein endothelial cells (HUVECs), sHDL composed of different PC lipids decreased the expression of adhesion molecules *VCAM1*, *ICAM1*, and *SELE* to varying extents. DMPC-sHDL was also able to partially restore the expression of *NOS3*. DMPC-sHDLs showed the ability to increase nitric oxide (NO) release after incubation with HUVEC. In a traumatic brain injury model, treatment with DMPC-sHDLs lead to a slight reduction in Evans blue dye leakiness though the blood brain barrier. This study shows that sHDLs can increase NO levels, reduce inflammatory adhesion

molecules, and may have a positive impact on endothelial integrity, which supports further optimization and investigation of sHDLs for improving endothelial function.

3.2 Introduction

The endothelium is made up of endothelial cells that line the blood vessels and create a selectively permeable barrier which modulates the passage of molecules, cells, and other materials from blood circulation into the tissue [1–3]. In a healthy state, the endothelium helps maintain vascular homeostasis, where a balance of vasodilation and vasoconstriction is observed, smooth muscle cell growth is suppressed, and inflammatory responses are inhibited [3,4]. Damage to the endothelium and disruptions in endothelial cell signaling can lead to endothelial dysfunction. Endothelial dysfunction is characterized by a decrease in vasodilation, reduction of NO production, and an elevated pro-inflammatory and prothrombotic state [5–7]. Endothelial dysfunction can lead to the development of many types of cardiovascular-related diseases, such as hypertension, atherosclerosis, chronic heart failure and diabetes [8,9]. Current therapies, which include lifestyle changes [10], lipid-lowering therapies [11,12], and antioxidant agents [13] , aim to preserve endothelial function to slow down the progression of disease.

Endothelial dysfunction can be caused by a reduction in nitric oxide (NO) bioavailability, which can occur through quenching by reactive oxygen species or changes in endothelial nitric oxide synthase (eNOS) abundance and activity [1,6]. Quenching of NO with ROS can lead to the formation of peroxynitrite, which can cause the uncoupling of eNOS, further reducing NO production [14] Oxidative stress can also promote a shift toward a pro-inflammatory state at the vessel wall, where expression of adhesion molecules, such as VCAM-1 and ICAM-I, are upregulated [15]. Therefore, treatment strategies for targeting endothelial dysfunction could

include increasing NO production, increasing eNOS expression/activity, as well as reducing adhesion molecule expression in the endothelial cell layer.

High-density lipoproteins (HDL) are endogenous nanoparticles that mediate reverse cholesterol transport (RCT), a process in which cholesterol is effluxed from peripheral calls and transferred to the liver for elimination [16,17]. In addition to its RCT activity, HDL have been shown to have protective effects on the endothelium and promote proper endothelial function [18,19]. For example, HDL can help preserve the lipid microenvironment of caveolae, preventing eNOS displacement from the cell membrane [20]. It has also been suggested that HDL are eNOS agonists and promote eNOS activity through mediation by SR-BI, which could lead to an increase in NO production, promoting healthy endothelial function [21,22]. Endothelial cell apoptosis can be prevented by HDL though modulation of pro-inflammatory molecules, such as tumor necrosis factor-α (TNF-α) and oxidized low-density lipoproteins (oxLDL) [23]. HDL can also promote endothelial cell proliferation and cell migration, which promotes the integrity of the endothelial cell monolayer [24]. Therefore, in the present study, we evaluate the potential benefit of synthetic high-density lipoproteins (sHDL) on endothelial function.

sHDL have been designed to mimic the structure and function of endogenous HDL. sHDLs consist of phospholipids complexed with apolipoprotein (ApoA-I) or ApoA-I mimetics, which create discoidal particles that are 9-12 nm in size. Several sHDL candidates, such as CSL-112 and CER-001, have been developed and tested in clinical trials, and were safe and tolerable in patients [25–27]. Here, we propose to develop and optimize sHDLs to promote healthy endothelial function. We hypothesized that sHDLs may possess activities that mimic endogenous HDL, which include the ability to improve endothelial cell function and barrier integrity, as well

as reduce inflammatory responses. Previous studies from our lab have shown that the lipid composition of sHDLs can impact activity and stability of the particle [28,29], thus, the effect of phospholipid composition on the ability of sHDL to improve endothelial function was also investigated. To test this hypothesis, we examined if sHDLs could restore expression of eNOS and reduce expression adhesion molecules, VCAM-1, ICAM-I and E-selectin, in activated human umbilical vein endothelial cells (HUVECs) and if this activity differed between sHDLs composed of different phosphatidylcholine (PC) lipids. We also evaluated the potential of sHDL to increase NO levels after incubation with HUVECs. Lasty, In a proof-of-concept experiment, a traumatic brain injury (TBI) murine model was used to evaluate the effect of sHDLs on endothelial barrier integrity in vivo.

3.3 Materials and methods

3.3.1 Materials

The compounds 1-palmitoyl-2-oleoyl-glycero-3phosphocholine (POPC), 1,2-dimyristoyl-*sn*-glycero-3-phosphocholine (DMPC), 1,2-dipalmitoyl-*sn*-glycero-3-phosphocholine (DPPC) and 1,2-distearoyl-*sn*-glycero-3-phosphocholine (DSPC) were purchased from NOF corporation (White Plains, NY, USA). 22A (PVLDLFRELLNELLEALKQKLK) peptide was synthesized by GenScript (Piscataway, NJ) and purity was approximately 80% as determined by HPLC. The compound Nω-Nitro-L-arginine methyl ester hydrochloride (L-NAME) was purchased from Sigma Aldrich (Milwaukee, WI, USA). Lipopolysaccharide (LPS) (*E. coli* O111:B4) was purchased from Sigma Aldrich (St. Louis, MO, USA). Human TNF-alpha (TNF-α) recombinant protein was purchased from Gibco (Grand Island, NY, USA).

3.3.2 Cell culture

Human umbilical vein endothelial cells (HUVEC) were purchased from Lonza (Walkersville, MD). HUVECs were maintained in EGM-2 complete media (Lonza) and used between passage 3-6 for all experiments. Cells were maintained at 37°C and 5% CO_2.

3.3.3 Preparation of sHDL library

All sHDLs were prepared using the co-lyophilization method. Phosphatidylcholine (PC) lipids (POPC, DMPC, DPPC, or DSPC) and 22A were dissolved in acetic acid and mixed at a weight ratio of 2:1. The resulting mixture was flash-frozen in liquid nitrogen and lyophilized overnight to remove the organic solvent. The lyophilized powder was rehydrated with phosphate-buffered saline (PBS, pH 7.4)) and heated above and cooled below the transition temperature for 5 minutes, 3 times repeatedly. All sHDL concentrations are expressed in terms of 22A peptide concentration. The final sHDL concentration was 12 mg/mL after preparation.

3.3.4 Characterization of sHDL

The particle size of all sHDL were determined using dynamic light scattering (DLS) on Malvern Zetasizer Nano ZSP (Westborough, MA) at a concentration of 1mg/mL in PBS. Gel permeation chromatography (GPC) was used to determine the purity of the sHDL. At a diluted concentration of 1 mg/mL in PBS, the samples were run on a Waters HPLC equipt with Tosoh TSKgel G3000SWxl column (Tosoh Bioscience**,** King of Prussia, PA), with UV detection at 220 nm.

3.3.5 qPCR for eNOS and adhesion molecule expression

HUVECS were seeded in a 6-well plate at a density of $3x10^5$ cells/well and incubated overnight. The next day, the cells were treated with PBS or sHDL (0.2 mg/mL) for 18 hours. Following pretreatment with PBS or sHDL, cells were incubated with LPS (1 ug/mL) or TNF-α (1 ng/mL) for 6 hours. Cells were washed twice with ice cold PBS and collected with 350 µL lysis buffer. Cell lysates were stored at -80°C until qPCR analysis. StepOnePlus Real-Time PCR System (Applied Biosystems) and TaqMan RNA to Ct 1-Step Kit (Applied Biosystems, Norwalk Connecticut) was used to quantify target RNA. RNA expression levels were determined using Taqman assays for *NOS3* (Hs01574659_m1), *VCAM1* (Hs01003372_m1), *ICAM1* (Hs00164932_m1) and *SELE* (Hs00174057_m1). Expression was calculated using the ddCt method and normalized to PBS-treated, LPS or TNF-α-challenged control.

3.3.6 Nitric oxide release

HUVECs were cultured in EGM-2 media. Cells were seeded in a 6-well plate at a density of 3×10^5 cells/well and allowed to grow for 1.5 days. Cells were then treated with PBS or L-arginine (0.1, 1 or 10 mM) for 15 minutes. In a parallel study, cells were pretreated with L-name (1mM) for 1 hour before treatment with DMPC-sHDL for 1 hour. After pretreatment and treatment, cell media was collected, flash frozen, and stored at -80°C until analysis. Media was assayed for Nitric Oxide (NO) using ozone chemiluminescence with Sievers 280i Nitric Oxide Analyzer (NOA) (GE Analytical Instruments, Boulder, CO, USA) with liquid setup.

3.3.7 Traumatic brain injury murine model

Traumatic brain injury (TBI) model was performed as previously described [30]. Briefly, 10-week-old male C57BL/6J mice were anesthetized with 2% isoflurane. Using an electric drill

(Harvard apparatus), a craniotomy of 3.5 mm was made over the right parietotemporal cortex, and the bone flap was removed. A pneumatic impactor (Precision Systems and Instrumentation, VA) was used for controlled cortical impact (CCI) to the site of bone removal. The impact speed, tissue displacement and impact duration were set at 3.65m/s, 1 mm, and 400 ms respectively. Mice were treated with PBS or sHDL (30 mg/kg) via IV injection 45 min and 4-6 hours after post-injury. 23 hours post injury, 100 µL of 4% Evans blue dye (Sigma-Aldrich) was IV injected to analyze the cerebrovascular permeability after TBI. At 24 hours, the mice were sacrificed, brains were removed, and hemispheres were separated. Brain hemispheres were weighed then homogenized in N, N-dimethylformamide (Sigma-Aldrich) and centrifuged for 45 min at 25,000 rcf. Evans blue leakage levels were determined by the equation: (A620nm −((A500nm+A740nm)/2))/mg wet weight.

3.3.8 Statistical analysis

All data are presented as mean ± SD. Significance between different groups vs. control was assessed by ordinary one-way ANOVA with Dunnett's multiple comparisons test. Statistical difference was considered at $p < 0.05$.

3.4 Results

3.4.1 Preparation and characterization of sHDL

sHDLs were prepared using a co-lyophilization method where 22A, an ApoA-I memetic peptide, and various phosphatidylcholine lipids (POPC, DMPC, DPPC, and DSPC) were mixed at an optimized weight ratio of 1:2 wt/wt peptide to phospholipid. sHDLs composed of different phosphatidylcholine lipids were analyzed by DLS and GPC. As seen in **Figure 3.1A**, sHDLs

showed a uniform size distribution with an average diameter ranging from 9-13 nm: POPC-sHDL (13.4 ± 0.4), DMPC-sHDL (9.8 ± 0.2), DPPC-sHDL (11.3 ± 0.2), and DSPC-sHDL (11.7 ± 0.3). GPC analysis confirmed the purity of all sHDLs, where all sHDLs showed an 8-minute retention time (**Figure 3.1B)**. The broader peak of POPC-sHDL indicates a more heterogenous size distribution. The small peaks appearing at approximately 12 minutes corresponds to free 22A peptide, accounting for less than 2 % of the area, which is negligible for all sHDL formulations.

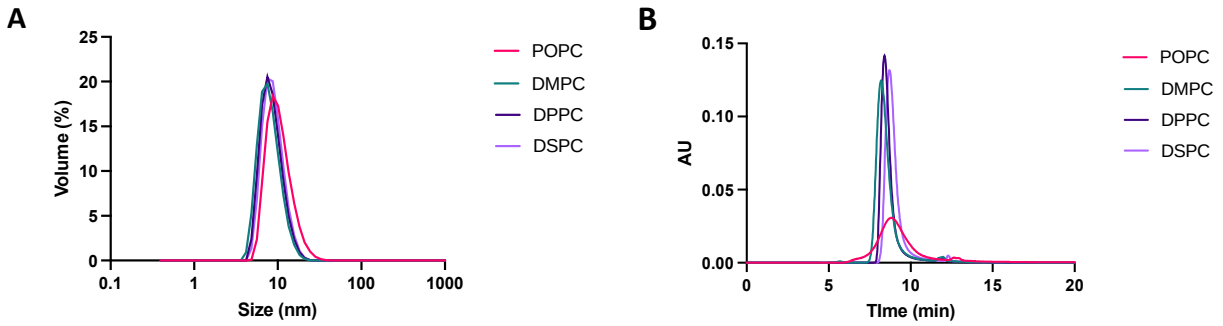

Figure 3.1 Average particle size, size distribution and purity of sHDLs were analyzed by (A) dynamic light scattering (DLS) and (B) gel permeation chromatography (GPC). sHDLs were diluted to a 1 mg/mL concentration of PBS.

3.4.2 Effect of sHDL on eNOS, E-selectin, ICAM1 and VCAM1 expression

To examine if sHDLs would impact the expression of eNOS and various adhesion molecules, E-selectin, ICAM1 and VCAM1, in HUVEC cells in a neutral and inflamed state, we pretreated HUVECs with PBS (control) or different sHDL formulations for 18 hours then incubated cells with plain media (LPS- control) or LPS endotoxin for 4 hours to induce inflammation. For cells lacking addition of LPS, eNOS expression was slightly increased with DMPC-, DPPC- and DSPC-sHDL pretreatment (**Figure 3.2A**). With the addition of LPS endotoxin, we see that eNOS expression is diminished as compared to LPS- cells. With the

pretreatment of DMPC-sHDLs, the expression of eNOS was partially rescued. DMPC-sHDL was the only sHDL that had a positive effect on eNOS expression.

For adhesion molecule expression, all sHDLs were able to significantly reduce expression of ICAM1 (**Figure 3.2C**). and VCAM1 (**Figure 3.2D**) and all sHDLs, excluding DSPC-sHDLs, were able to significantly reduce expression of E-selectin (**Figure 3.2B**) in HUVECs challenged with LPS. Furthermore, POPC-, DMPC- and DPPC-sHDLs showed more potent activity in reducing adhesion molecule expression than DSPC-sHDL in HUVECs challenged with LPS. DPPC-sHDL showed a 25-fold reduction of E-selectin expression, 12-fold reduction expression for ICAM1 and 22-fold reduction in VCAM1 expression. However, in comparison to DPPC-sHDL, POPC- and DMPC-sHDLs had a more potent effect on reducing expression levels, showing a 50-fold reduction in E-selectin expression, 25-fold reduction in ICAM1 expression, and 130-fold reduction in VAM1 expression. These results suggest that sHDL may possess anti-inflammatory activities by reducing expression levels of adhesion molecules in HUVECs challenged with LPS.

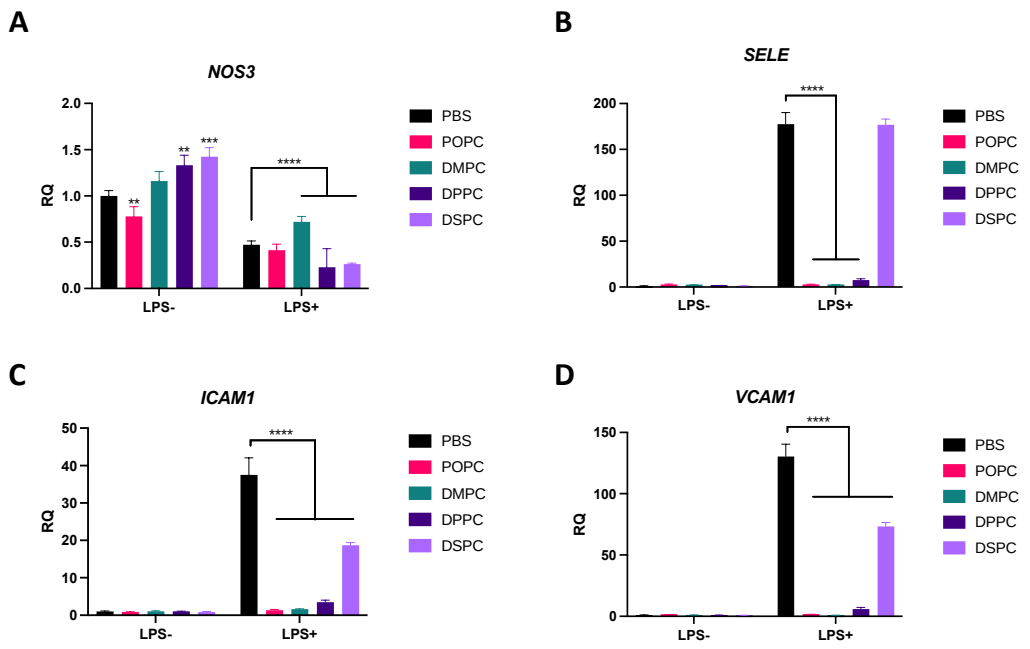

Figure 3.2 Expression levels of eNOS (A), E-selectin (B), ICAM1, (C) and VCAM1 (D) were measured after pretreatment with different sHDLs (0.2 mg/mL) for 18 hours, then with or without LPS endotoxin addition (1 µg/mL) to HUVECs. ****P < 0.0001 when compared to untreated LPS+ group.

We next evaluated whether sHDLs had the same ability to rescue eNOS expression and reduce adhesion molecule expression in HUVECs after induction of inflammation with pro-inflammatory cytokine, TNF-α. Addition of TNF-α reduced eNOS expression. Pretreatment with all sHDL formulations led to an increase in eNOS expression (**Figure 3.3A**). DMPC-sHDL had the greatest ability to partially rescue the expression of eNOS in HUVECs challenged with TNF-α. For adhesion molecule expression, E-selectin and ICAM1 expression were altered by sHDLs in various ways, where some expression was increased or remained unchanged with sHDL pretreatment (**Figure 3.3B, C**). After addition of TNF- α to HUVECs, VCAM1 expression in remained steady with POPC- DPPC- and DSPC-sHDL pretreatment (**Figure 3.3D**). On the contrary, pretreatment with DMPC-sHDL lead to a 2-fold reduction in VCAM1 expression. Due to the partial restoration of eNOS expression and reduction in VCAM1 expression in with the

pretreatment of DMPC-sHDLs in HUVECs challenged by LPS endotoxin and TNF-α, we decided to move forward with DMPC-sHDLs for the remainder of the studies.

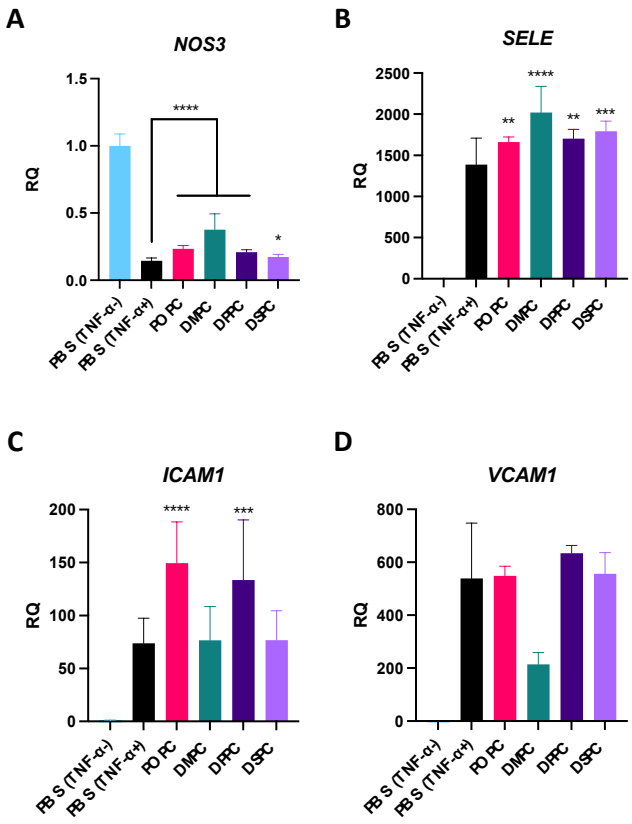

Figure 3.3 Expression levels of eNOS (A), E-selectin (B), ICAM1 (C) and VCAM1 (D) were measured after pretreatment with different sHDLs and addition of TNF- α to HUVECs. **P < 0.01; ***P < 0.001: ****P < 0.0001 when compared to untreated TNF-α + group.

3.4.3 Effect of DMPC-sHDL on nitric oxide levels in HUVECs

Low levels of nitric oxide (NO) are a major contributor of endothelial dysfunction. First, to examine if HUVECs could be activated to produce NO measurable in the cell media, we incubated cells with L-arginine, which is transformed into L-citrulline and NO by eNOS. Increasing the concentration of L-arginine resulted in higher levels of NO detected by the NOA (**Figure 3.4A**). Incubation with 10 mM L-arginine resulted in a 2-fold increase in nitric oxide

production. Next, the effect of sHDLs on NO levels was tested. L-NAME, a potent eNOS inhibitor, was added to a subset of cell as a pretreatment for 1 hour. In the absence of L-NAME pretreatment, addition of DMPC-sHDL to HUVECs for 1 hour led to an increase in NO levels detected in the cell media (**Figure 3.4B**). However, cell pretreated with L-NAME showed no increase in NO levels with the addition of DMPC-sHDL. This data suggests that the increase in NO measured is likely related to an increase in eNOS activity by sHDL treatment. Further studies will need to be completed to understand sHDL's role and interaction with eNOS.

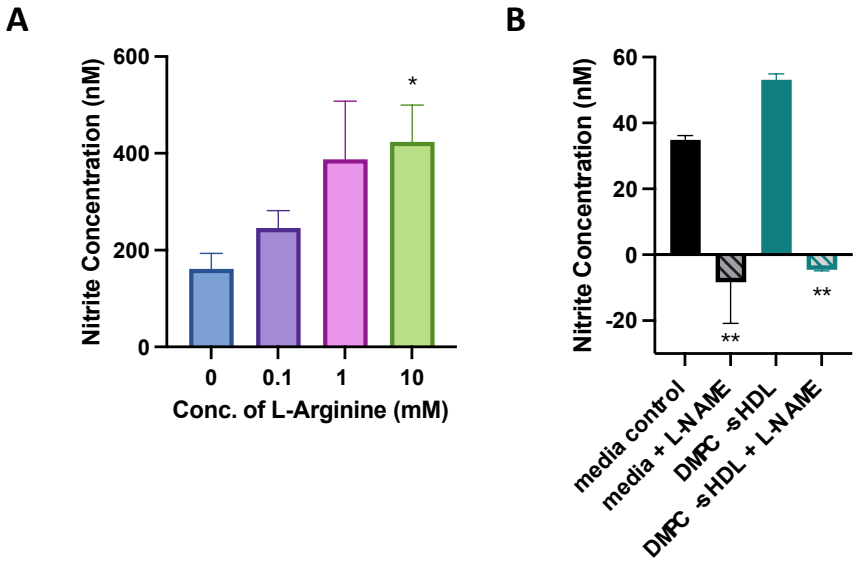

Figure 3.4 Nitrite concentrations measured by NOA in the media of HUVEC cells after incubation with various L-arginine concentrations for 15 minutes (A) and the presence or absence of L-NAME pretreatment (1 hour) and DMPC-sHDL treatment (1hour) (B).*P<0.05 and **P < 0.01 when compared to control group.

3.4.4 Effect of sHDL on blood brain barrier leakiness in mice with traumatic brain injury

The blood brain barrier is made of specialized brain microvascular endothelial cells, which helps monitor which substances can flow into and out of the brain. To test the ability of sHDL to improve endothelial barrier integrity at the blood brain barrier (BBB), mice were given

traumatic brain injury (TBI), then treated with 30 mg/kg DMPC-sHDL 45 minutes and 4-6 hours after injury. Evans blue dye was used to quantify leakiness of the BBB (**Figure 3.5A**). The brain was impacted on the right parietotemporal cortex to induce TBI. The Evans blue dye leakage into the injured hemisphere and non-injured contralateral hemisphere was measured, represented as absorbance normalized by brain weight. With sHDL treatment, Evans blue dye leakiness into the brain was reduced in sHDL treated mice. (**Figure 3.5B**). When comparing only the contralateral hemispheres, the leakiness of the BBB appeared to be unaffected by sHDL treatment (**Figure 3.5C)**. Overall, more studies need to be complete to optimize the dose and dosing schedule of the sHDL treatment to better understand if sHDL can be used to improve endothelial integrity of the BBB after TBI injury in mice.

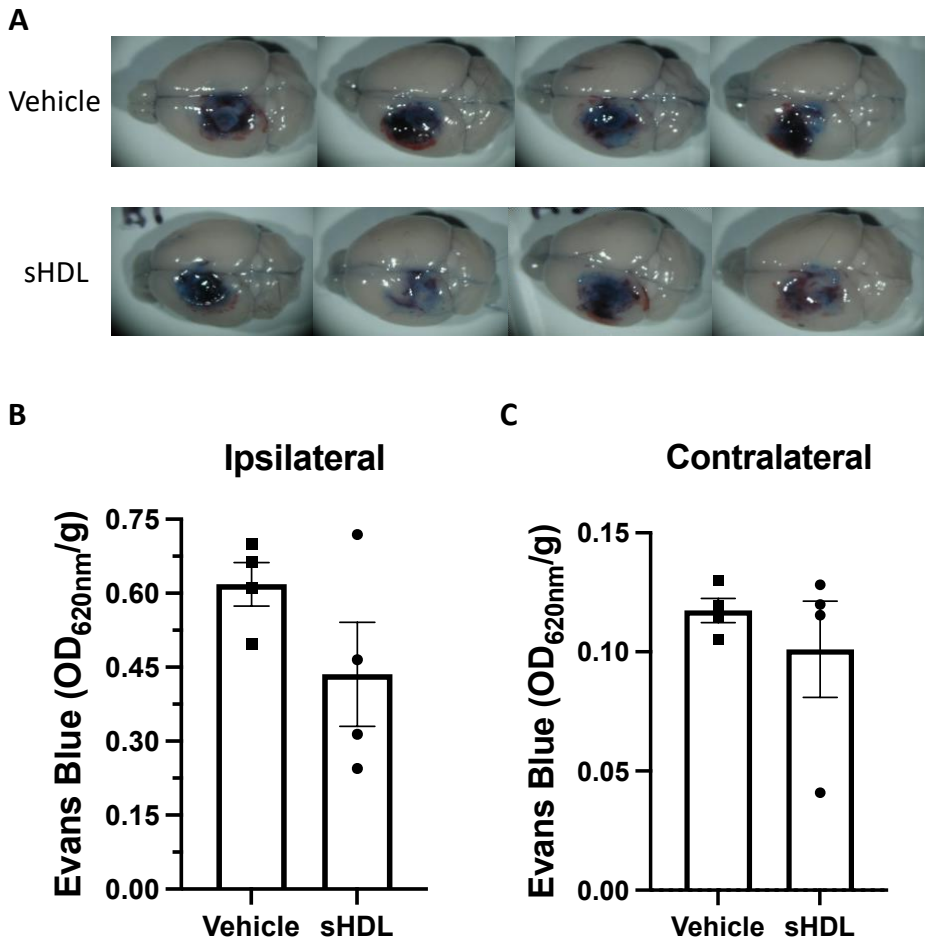

Figure 3.5 Evans blue dye leakage past the blood brain barrier was assessed after no treatment or treatment with DMPC sHDL in mice with induced traumatic brain injury. (A) Photos of full brains after injury, treatment and IV injection of Evans blue dye. (B) Evans blue dye absorbance measured at 620 nm normalized by brain weight of injured hemisphere. (C) Evans blue dye absorbance measured at 620 nm normalized by brain weight for non-injured contralateral hemisphere.

3.5 Discussion

The therapeutic effects of endogenous HDL on endothelial barrier integrity and function have been examined previously, where HDLs have been shown to promote eNOS activity, abundance and activation, promote NO production, improve barrier integrity through reducing cell apoptosis and increasing migration and proliferation, and by reducing expression of pro-inflammatory molecules [19–21]. In our study, we sought to test the therapeutic potential of

sHDLs in treating endothelial dysfunction by investigated its ability to reduce adhesion molecule expression and restore eNOS expression in HUVECs in an inflamed state and increase levels of NO production after incubation with HUVEC cells. As a proof-of-concept-experiment, TBI murine model was used to evaluate the effect of sHDL on endothelial blood brain barrier integrity post injury.

PC lipids with different chain lengths and degrees of saturation exist in different phases, which affects the fluidity of the sHDL bilayer. POPC and DMPC, lipids with lower transition temperatures, exist in a fluid, liquid crystalline phase at physiological temperature, where DPPC and DSPC, PC lipids with higher transition temperatures, exist in a gel-ordered phase at physiological temperature [31]. In our study, we varied PC lipid composition of sHDL to understand how the lipid composition of the sHDL impacted the overall therapeutic activity of the particle in relation to endothelial function. We first analyzed the effect of sHDL on eNOS and adhesion molecule expression after addition of LPS endotoxin or TNF-α to HUVEC cells and evaluated how lipid composition affected the sHDL activity. It was previously found that sHDLs composed of POPC and DMPC, lipids with lower phase transition temperatures, had greater anti-inflammatory effects relating to endotoxin neutralization and TLR-4 displacement, as well as greater cholesterol efflux capabilities [32,33] . Our results were consistent with previous findings, where pretreatment with sHDLs composed of POPC and DMPC were more effective in reducing VCAM1, ICAM1 and E-selectin expression levels in HUVECs challenged with LPS, followed by DPPC-sHDL, then DSPC-sHDL will very minimal effects (**Figure 3.2B-D**). Only pretreatment with DMPC-sHDL had the ability to partially rescue the eNOS expression after addition of LPS and TNF-α to HUVECs (**Figure 3.2A, 3.3A**).

Increasing NO bioavailability and reducing the imbalance of NO production and consumption has been found to reduce progression of endothelial dysfunction [7,34]. In the present study, we found that DMPC-sHDLs could increase NO levels in HUVECs after incubation for 1 hour (**Figure 3.4B**). However, with preincubation with L-NAME, sHDLs ability to increase NO levels were diminished, suggesting that sHDL activation is blocked by L-NAME inhibition of eNOS. Varying theories as to how HDL may promote NO production, such as phosphorylation of eNOS at Ser 1177, binding of SR-BI leading to activation of eNOS, eNOS activation corresponding to a ceramide-dependent pathway, and others have been previously explored [21,35,36]. More mechanistic studies need to be completed to understand sHDLs role in NO production in the present study.

Lastly, in a proof-of-concept study, the therapeutic effects of sHDL were evaluated using a murine model of traumatic brain injury. Though there appeared to be differences in Evans blue dye movement across the BBB of the injured hemisphere for mice treated with sHDLs, no changes were seen when comparing only the contralateral hemispheres between sHDL-treated and vehicle groups (**Figure 3.5A-B**). With minimal differences shown in the contralateral hemispheres of the two groups, it is difficult to conclude that treatment with DMPC-sHDL had a positive therapeutic effect on the endothelial BBB integrity in the mice. It is worth noting that traumatic brain injury has a very complex pathophysiology, where events past initial blunt force to the brain can be prolonged and progressive [37,38]. While the primary injury refers to the mechanical forces that impact the brain leading to disruption of brain cells and tissue, secondary injury can lead to many biomolecular changes such as a modification in cerebral blood flow, oxidative stress, vasospasms, and a multitude of complex inflammatory responses [39,40]. Thus, while the focus in the present animal study was on the initial mechanical damage to the BBB

endothelial cells, other pathways and complications most likely contribute to the overall outcome. Therefore, a more defined animal model may be used to specifically evaluate sHDL therapeutic effect on endothelial barrier integrity.

3.6 Conclusion

The present study highlights the potential therapeutic benefit of sHDL on endothelial function and integrity. sHDLs reduced adhesion molecule expression in HUVECs challenged with LPS endotoxin, and lipid composition influenced the extent of reduction. DMPC-sHDLs showed ability to partially rescue eNOS expression in HUVECs challenged with LPS endotoxin or TNF-α. Furthermore, incubation of DMPC-sHDL with HUVECs lead to an increase in NO levels detected in cell media. Based on our in vivo TBI study, more rigorous studies need to be completed to determine if sHDLs have a positive effect on endothelial barrier integrity. Our results suggest the therapeutic potential of DMPC-sHDL on endothelial function with further optimization.

3.7 References

1. Vanhoutte PM, Shimokawa H, Tang EHC, Feletou M. Endothelial dysfunction and vascular disease. *Acta Physiologica*. 2009;196(2):193-222. doi:10.1111/j.1748-1716.2009.01964.x

2. Godo S, Shimokawa H. Endothelial Functions. *Arterioscler Thromb Vasc Biol*. 2017;37(9):e108-e114. doi:10.1161/ATVBAHA.117.309813

3. Luscher TF, Vanhoutte PM. The Endothelium: Modulators of Cardiovascular Function. 1st ed. CRC press; 1990.

4. Pearson JD. Normal endothelial cell function. *Lupis*. 2000;9(3):159-231. doi:https://doi.org/10.1191/096120300678828299

5. Jebari-Benslaiman S, Galicia-García U, Larrea-Sebal A, et al. Pathophysiology of Atherosclerosis. *Int J Mol Sci*. 2022;23(6). doi:10.3390/ijms23063346

6. Endemann DH, Schiffrin EL. Endothelial dysfunction. *Journal of the American Society of Nephrology*. 2004;15(8):1983-1992. doi:10.1097/01.ASN.0000132474.50966.DA

7. Esper RJ, Nordaby RA, Vilariño JO, Paragano A, Cacharrón JL, Machado RA. Endothelial dysfunction: A comprehensive appraisal. *Cardiovasc Diabetol*. 2006;5. doi:10.1186/1475-2840-5-4

8. Park KH, Park WJ. Endothelial dysfunction: Clinical implications in cardiovascular disease and therapeutic approaches. *J Korean Med Sci*. 2015;30(9):1213-1225. doi:10.3346/jkms.2015.30.9.1213

9. Rajendran P, Rengarajan T, Thangavel J, et al. The vascular endothelium and human diseases. *Int J Biol Sci*. 2013;9(10):1057-1069. doi:10.7150/ijbs.7502

10. Gao J, Pan X, Li G, Chatterjee E, Xiao J. Physical Exercise Protects Against Endothelial Dysfunction in Cardiovascular and Metabolic Diseases. *J Cardiovasc Transl Res*. 2022;15(3):604-620. doi:10.1007/s12265-021-10171-3

11. Martínez-González J, Raposo B, Rodríguez C, Badimon L. 3-Hydroxy-3-Methylglutaryl Coenzyme A Reductase Inhibition Prevents Endothelial NO Synthase Downregulation by Atherogenic Levels of Native LDLs Balance Between Transcriptional and Posttranscriptional Regulation. *Arteriosclerosis, Thrombosis and Vasular Biology*. 2001;21(5):804-809. http://www.atvbaha.org

12. Laufs U, Fata V La, Plutzky J, Liao JK. Upregulation of Endothelial Nitric Oxide Synthase by HMG CoA Reductase Inhibitors. *Circulation*. 1998;97(12):1129-1135. http://ahajournals.org

13. Taddei S, Virdis A, Ghiadoni L, Magagna A, Salvetti A. Vitamin C Improves Endothelium-Dependent Vasodilation by Restoring Nitric Oxide Activity in Essential Hypertension. *Circulation*. 1998;97:2222-2229. http://ahajournals.org

14. Koppenol WH, Moreno JJ, Pryor WA, Ischiropoulos H, Beckman JS. *Peroxynitrite, a Cloaked Oxidant Formed by Nitric Oxide and Superoxide*. Vol 5.; 1992. https://pubs.acs.org/sharingguidelines

15. Rui W, Guan L, Zhang F, Zhang W, Ding W. PM2.5-induced oxidative stress increases adhesion molecules expression in human endothelial cells through the ERK/AKT/NF-κB-dependent pathway. *Journal of Applied Toxicology*. 2016;36(1):48-59. doi:10.1002/jat.3143

16. Kontush Anatol, Chapman MJ. *High-Density Lipoproteins : Structure, Metabolism, Function, and Therapeutics*. John Wiley & Sons, Inc; 2012.

17. Kontush A, Lhomme M, Chapman MJ. Thematic review series: High density lipoprotein structure, function, and metabolism: Unraveling the complexities of the HDL lipidome. *J Lipid Res*. 2013;54(11):2950-2963. doi:10.1194/jlr.R036095

18. Tran-Dinh A, Diallo D, Delbosc S, et al. HDL and endothelial protection. *Br J Pharmacol*. 2013;169(3):493-511. doi:10.1111/bph.12174

19. Bisoendial RJ, Hovingh GK, Levels JHM, et al. Restoration of endothelial function by increasing high-density lipoprotein in subjects with isolated low high-density lipoprotein. *Circulation*. 2003;107(23):2944-2948. doi:10.1161/01.CIR.0000070934.69310.1A

20. Uittenbogaard A, Shaul PW, Yuhanna IS, Blair A, Smart EJ. High density lipoprotein prevents oxidized low density lipoprotein- induced inhibition of endothelial nitric-oxide synthase localization and activation in caveolae. *Journal of Biological Chemistry*. 2000;275(15):11278-11283. doi:10.1074/jbc.275.15.11278

21. Yuhanna IS, Zhu Yan, Cox BE, et al. High-density lipoprotein binding to scavenger receptor-BI activates endothelial nitric oxide synthase. *Nat Med*. 2001;7:853-857. doi:https://doi.org/10.1038/89986

22. Mineo C, Deguchi H, Griffin JH, Shaul PW. Endothelial and antithrombotic actions of HDL. *Circ Res*. 2006;98(11):1352-1364. doi:10.1161/01.RES.0000225982.01988.93

23. Dimmeler S, Haendeler J, Zeiher AM. Regulation of endothelial cell apoptosis in atherothrombosis. *Curr Opin Lipodol*. 2002;13(5):531-536. http://journals.lww.com/co-lipidology

24. Sugano M, Tsuchida K, Makino N. High-density lipoproteins protect endothelial cells from tumor necrosis factor-α-induced apoptosis. *Biochem Biophys Res Commun*. 2000;272(3):872-876. doi:10.1006/bbrc.2000.2877

25. Tardif JC, Ballantyne CM, Barter P, et al. Effects of the high-density lipoprotein mimetic agent CER-001 on coronary atherosclerosis in patients with acute coronary syndromes: a randomized trial. *Eur Heart J*. 2014;35:3277-3286. doi:10.1093/eurheartj/ehu194

26. Nicholls SJ, Andrews J, Kastelein JJP, et al. Effect of serial infusions of CER-001, a pre-β High-density lipoprotein mimetic, on coronary atherosclerosis in patients following acute coronary syndromes in the CER-001 atherosclerosis regression acute coronary syndrome trial: A randomized clinical trial. *JAMA Cardiol*. 2018;3(9):815-822. doi:10.1001/jamacardio.2018.2121

27. Tricoci P, D'Andrea DM, Gurbel PA, et al. Infusion of Reconstituted High-Density Lipoprotein, CSL112, in Patients With Atherosclerosis: Safety and Pharmacokinetic Results From a Phase 2a Randomized Clinical Trial. *J Am Heart Assoc*. 2015;4(8):e002171. doi:10.1161/JAHA.115.002171

28. Fawaz M V., Kim SY, Li D, et al. Phospholipid component defines pharmacokinetic and pharmacodynamic properties of synthetic high-density lipoproteins. *Journal of Pharmacology and Experimental Therapeutics*. 2020;372(2):193-204. doi:10.1124/JPET.119.257568

29. Hong K, Yu M, Crowther J, et al. Effect of Lipid Composition on the Atheroprotective Properties of HDL-Mimicking Micelles. *Pharmaceutics*. 2022;14(8). doi:10.3390/pharmaceutics14081570

30. Su EJ, Fredriksson L, Kanzawa M, et al. Imatinib treatment reduces brain injury in a murine model of traumatic brain injury. *Front Cell Neurosci*. 2015;9(OCT). doi:10.3389/fncel.2015.00385

31. Koynova R, Caffrey M. Phases and Phase Transitions of the Phosphatidylcholines. *Biocheimica et Biophysica Acta.* 1998; 1(29):91-145. doi:10.1016/S0304-4157(98)00006-9

32. Kim SY, Kang J, Fawaz M V, et al. Phospholipids impact the protective effects of HDL-mimetic nanodiscs againsts lipopolysaccharide-induced inflammation . *Nanomedicine.* Published online 2024.

33. Schwendeman A, Sviridov DO, Yuan W, et al. The effect of phospholipid composition of reconstituted HDL on its cholesterol efflux and anti-inflammatory properties. *J Lipid Res*. 2015;56(9):1727-1737. doi:10.1194/jlr.M060285

34. Tousoulis D, Kampoli AM, Tentolouris Nikolaos Papageorgiou C, Stefanadis C. The Role of Nitric Oxide on Endothelial Function. *Curr Vasc Pharmacol*. 2012;10(1):4-18.

35. Chikani G, Zhu W, Smart EJ. Lipids: potential regulators of nitric oxide generation. *Am J Physiol Endocrinol Metab*. 2004;287:386-389. doi:10.1152/ajpendo.00106.2004.

36. Rämet ME, Rämet M, Lu Q, et al. High-density lipoprotein increases the abundance of eNOS protein in human vascular endothelial cells by increasing its half-life. *J Am Coll Cardiol*. 2003;41(12):2288-2297. doi:10.1016/S0735-1097(03)00481-9

37. Zhang YP, Cai J, Shields LBE, Liu N, Xu XM, Shields CB. Traumatic Brain Injury Using Mouse Models. *Transl Stroke Res*. 2014;5(4):454-471. doi:10.1007/s12975-014-0327-0

38. Greve MW, Zink BJ. Pathophysiology of traumatic brain injury. *Mount Sinai Journal of Medicine*. 2009;76(2):97-104. doi:10.1002/msj.20104

39. Werner C, Engelhard K. Pathophysiology of traumatic brain injury. *Br J Anaesth*. 2007;99(1):4-9. doi:10.1093/bja/aem131

40. Algattas H, Huang JH. Traumatic Brain Injury pathophysiology and treatments: Early, intermediate, and late phases post-injury. *Int J Mol Sci*. 2014;15(1):309-341. doi:10.3390/ijms15010309

Chapter 4 - Understanding Synthetic High-Density Lipoprotein Remodeling Ex Vivo Using Human Serum

4.1 Abstract

Synthetic high-density lipoproteins (sHDL) have been developed to mimic the natural cardioprotective behaviors of endogenous high-density lipoproteins (HDL). Endogenous HDL is remodeled by various transfer proteins and lipases, which play a role in HDL maturation, heterogeneity, and the exchange of lipids between HDL and other endogenous lipoproteins, such as very low-density lipoproteins (VLDL) and low-density lipoproteins (LDL). In this study, we sought to investigate how sHDLs remodel in the presence endogenous lipoproteins in human serum. We synthesized a library of sHDLs composed of different phosphatidylcholine (PC) lipids, as well as dye- or drug-loaded sHDLs, and monitored the movement of sHDL components and cargo to different lipoprotein populations to better understand how lipid properties influence the stability and remodeling of sHDLs in human serum. In the present study, remodeling of sHDL occurred to the largest extent for POPC-sHDL. DSPC-sHDLs remained the most intact, where PC lipid and 22A remained in HDL elution times to a larger extent than POPC-, DMPC-, and DPPC-sHDLs. DiD dye movement to different lipoprotein populations followed similar trends as PC lipid, where sHDLs formulated with DSPC showed smallest percentage of dye movement to other lipoproteins. Lastly, GW3965-sHDLs remodeled over time, where GW3965 was detected in larger lipoprotein populations for GW3965-POPC after 2 and 24 hours but mainly stayed within HDL eluting fractions for DMPC-, DPPC- and DSPC-sHDLs. Overall, the

lipid composition affects the extent of remodeling of the sHDL and movement of sHDL cargo to larger endogenous lipoprotein populations found in human serum.

4.2 Introduction

Synthetic high-density lipoproteins (sHDLs) have been designed to mimic the structure and activity of endogenous high-density lipoprotein (HDL), whose main physiological function is to carry cholesterol effluxed from peripheral tissue to the liver for elimination in a process called reverse cholesterol transport [1–3]. sHDL are 8-12 nm in size and contain phospholipids complexed with apolipoprotein A-I (ApoA-I) or ApoA-I mimetic peptides, which forms a discoidal nanoparticle that mimics the structure of endogenous pre-β HDL. sHDLs have been tested in clinical trials, where candidates have been shown to increase cholesterol efflux and reduce atheroma volume in patients suffering from cardiovascular disease [4–6]. Due to it's small size and biocompatibility, the use of sHDLs as drug delivery systems has also been proposed [7–9]. Hydrophobic drugs can be incorporated into the membrane of sHDL and work synergistically with its drug vehicle.

Though sHDLs show promise as drug candidates alone and as delivery systems, it is important to note that endogenous HDL are very dynamic systems that can exchange components with other lipoproteins, such as very low-density lipoproteins (VLDL) and low-density lipoproteins (LDL) in circulation [1,10–12]. HDL remodeling is facilitated by different enzymes that change the size and composition of the particle. For example, phospholipid transfer protein (PLTP) transfer phospholipids between HDL and other lipoproteins, altering the size and composition of HDL [10,11]. Other proteins and enzymes, such as cholesteryl ester transfer protein (CETP) and hepatic lipase (HL) can aid in the transfer and detachment of other lipids,

like triglycerides, from VLDLs, chylomicrons, and HDL [12–14]. Due to the remodeling nature of endogenous HDL, changes in the structure and composition of synthetic HDL could also occur, affecting the overall therapeutic effect and/or drug delivery capabilities of the particle.

In the present study, we sought to investigate the remodeling of sHDL in the presence of human serum containing other endogenous lipoproteins populations. Previous studies from our lab have shown that the composition of sHDLs and sHDL mimetic nanoparticles can affect the stability, pharmacokinetics and overall therapeutic activity of the particle [15–17]. We hypothesize that the lipid composition of the sHDL will impact the stability of the particle and the efficiency of drug encapsulation into the membrane, which will affect the rate of remodeling and the movement of sHDL components and sHDL cargo to other endogenous lipoprotein populations found in human serum. To test this hypothesis, we created a library of sHDLs formulated with one of four different phosphatidylcholine (PC) lipids complexed with 22A peptide. Three different sHDL groups were created. The first group of sHDLs were blank sHDL nanoparticles. Secondarily, sHDLs encapsulating DiD dye (DiD-sHDLs) were formulated. Lastly, we used GW3965 as a model drug and formulated sHDL carrying GW3965 (GW3965-sHDL). All sHDLs were incubated with human serum for various timepoints, lipoprotein populations were separated out by size exclusion chromatography, and concentration of sHDL components were measured by liquid chromatography-mass spectrometry (LC-MS) analysis to track the movement of components over time.

4.3 Materials and methods

4.3.1 Materials

The compounds 1-palmitoyl-2-oleoyl-glycero-3phosphocholine (POPC), 1,2-dimyristoyl-*sn*-glycero-3-phosphocholine (DMPC), 1,2-dipalmitoyl-*sn*-glycero-3-phosphocholine (DPPC) and 1,2-distearoyl-*sn*-glycero-3-phosphocholine (DSPC) were purchased from NOF corporation (White Plains, NY, USA). 22A (PVLDLFRELLNELLEALKQKLK) peptide was synthesized by GenScript (Piscataway, NJ) and purity was approximately 87.5% as determined by HPLC. GW3965 hydrochloride was purchased from Cayman Chemical (Ann Arbor, MI). 1,1'-Dioctadecyl-3,3,3',3'-Tetramethylindodicarbocyanine Perchlorate ($DiIC_{18}(5)$ oil) was purchased from Thermo Fisher (Carlsbad, CA). Pooled human serum was purchased from MP Biomedicals (Irvine, CA).

4.3.2 Preparation of sHDL library

All sHDLs were prepared using the co-lyophilization method as described previously. Phosphatidylcholine (PC) lipids (POPC, DMPC, DPPC, or DSPC) and 22A were dissolved in acetic acid and mixed at a weight ratio of 2:1. For sHDLs containing DiD dye, a 0.4% molar ratio of dye to lipid was dissolved in acetic acid and mixed with PC lipid and 22A. For sHDLs containing GW3965, GW3965 hydrocholoride was dissolved in DMSO to achieve a concentration of 20 mg/mL, and then added to the sHDL mixture at a 10:20:1 weight ratio of 22A:lipid:GW3965 to achieve a final concentration of 1 mg/mL GW3965. The resulting mixture was flash-frozen in liquid nitrogen and lyophilized overnight to remove the organic solvent. The lyophilized powder was rehydrated with phosphate-buffered saline (PBS) and thermo-cycled 3 times repeatedly where the solution was heated above and cooled below the transition temperature of the phospholipid for 5 min. The pH of all formulations was adjusted to 7.4 using NaOH. For sHDLs incorporating DiD dye or GW3965, unincorporated dye or drug was removed by passing the solution through a 3k

MWCO Zeba desalting column. All final sHDL solutions were filtered using a 0.22 μm syringe filter as the final step. All sHDL concentrations are expressed in terms of 22A peptide concentration.

4.3.3 Characterization of sHDL

The particle size of all sHDL were determined using dynamic light scattering (DLS) on Malvern Zetasizer Nano ZSP (Westborough, MA). sHDLs were diluted to a concentration of 1 mg/mL in PBS. Gel permeation chromatography (GPC) was used to determine the purity of the sHDL. At a diluted concentration of 1 mg/mL in PBS, the samples were run on a Waters 1525 HPLC equipped with a Tosoh TSKgel G3000SWxl column (Tosoh Bioscience**,** King of Prussia, PA), with UV detection at 220 nm with PBS as the mobile phase at 1mL/min.

To determine the encapsulation efficiency and concentration of GW3965 incorporated in the sHDL, sHDLs were diluted 400-fold in methanol and centrifuged at 17200g for 5 minutes. The supernatant was collected for LC-MS analysis. 5μL of the supernatant was injected on an Acquity UPLC equipped with a QDa detector (Waters, Milford, MA). The samples were separated on an Acquity UPLC BEH C18 column (1.7 μm, 20.1 x 50 mm) with a flow rate of 0.3 mL/min. The initial conditions of the mobile phase were 0.1% formic acid in water (A), 0.1% formic acid in acetonitrile (B), and 0.1% formic acid in methanol (C) at a ratio of 50:33:17 of A:B:C. A linear gradient to 0:67:33 of A:B:C at 2 minutes was used, followed by a hold for 2 minutes, and a return to initial conditions through a linear gradient after 4.5 minutes. Mass spectra was acquired in the negative ion mode with a cone voltage of 15V at a M/Z ratio of 580.09. The encapsulation efficiency was calculated by taking the concentration of GW3965 after desalting and filtration and dividing by the concentration prior to purification.

4.3.4 Determination of sHDL component concentrations overtime in human serum

sHDLs were mixed with human serum at a ratio of 1:9 to obtain a final sHDL concentration of 1 mg/mL. sHDL and human serum were incubated for 0, 1, 2, 4, 6, 12, and 24 hours at 37°C. After incubation, the mixtures were diluted in 100-fold in 0.9% sodium chloride and 0.02% sodium azide in water, then further diluted 4-fold in methanol. Samples were centrifuged for 5 minutes at a speed of 17200g. The supernatant was collected for LC-MS analysis.

4.3.5 sHDL remodeling in human serum

sHDLs were mixed with human serum to obtain a final sHDL concentration of 1 mg/mL, and incubated for 0, 2 or 24 hours at 37°C. Size exclusion chromatography was used to separate out the lipoprotein populations in human serum alone, sHDL alone, and 0, 2, and 24h incubation sHDL/human serum mixtures. 50µL of the sHDL/human serum mixture was injected on a Waters 1525 HPLC equipt with a Superose 6, 10/300 GL column (GE healthcare, Piscataway, NJ), with 0.9% sodium chloride and 0.02% sodium azide in water as the mobile phase delivered at 1 mL/min.

For blank sHDLs and GW3965-sHDLs, fractions were collected every minute from 5 – 30 minutes using Waters fraction collector III. Fractions were then diluted 4-fold with methanol and centrifuged at 17200g for 5 minutes. The supernatant was collected for LC-MS quantification. For DiD-sHDLs, fluorescence was measured on the Waters 1525 HPLC equipped with a Acquity Fluorescence Detector. Fluorescence data was collected at an excitation wavelength of 646 nm and emission wavelength of 663 nm.

4.3.6 LC-MS quantification of sHDL components

sHDL components, PC lipid, 22A and GW3965 (if applicable), were quantified using Acquity UPLC equipped with a QDa detector (Waters, Milford, MA). For PC lipid quantification, 2 µL of samples were injected and lipids were separated out on a Acquity UPLC BEH HILIC Column (130Å, 1.7 µm, 2.1 mm X 50 mm) using an initial mobile phase condition of 0.1% formic acid in water (A), 0.1% formic acid in acetonitrile (B) and 200 mM ammonium formate in H2O (D) at a ratio of 5:90:5 of A:B:D. A linear elution gradient was used, where the mobile phase changed to 17:78:5 of A:B:D at 0.70 minutes, and back to initial conditions at 0.71 minutes. The flow rate was set at 0.650 mL/min. PC lipids were detected at the following M/Z ratios in positive scan mode at a cone voltage of 21V: POPC (761.60), DMPC (678.62), DPPC (734.71), DSPC (790.60).

An Acquity UPLC Protein BEH C4 Column, (300 Å, 1.7 µm, 2.1 mm x 100 mm) was used for separation of 22A peptide. 5 µL was the injection volume. A gradient elution with initial conditions of 0.1 formic acid in H2O (A) and 0.1% formic acid in methanol (C) at a ratio of 40:60 of A:C, followed by a linear gradient to 10:90 A:C at 1 minute, holding for 2 minutes, and return to initial starting composition at 3.10 minutes was used. The flow rate of the mobile phase was 0.3 mL/min. 22A was detected at a M/Z ratio of 656.85 in the positive scan mode with a cone voltage of 15V.

For quantification of GW3965, samples were analyzed by LC-MS under the same injection volume, mobile phase, cone voltage and M/Z ratio conditions as described under *Characterization of sHDL*.

4.3.7 Statistical Analysis

For all experiments, samples were run in triplicates. All data are presented as mean values. Significance between different groups assessed by ordinary two-way ANOVA with Fishers multiple comparisons test. Statistical difference was considered at $p < 0.05$.

4.4 Results

4.4.1 Preparation and characterization of blank sHDL and sHDL containing cargo

All sHDLs were prepared using the co-lyophilization method. Briefly, 22A and PC lipid were dissolved in acetic acid. For sHDLs containing DiD dye, dye was dissolved in acetic acid. For sHDLs incorporating GW3965, GW3965 was dissolved in DMSO. After mixture of components at specified ratios, the solution was freeze-dried overnight, and the resulting lyophilized powder was rehydrated with PBS. The solution was then heated and cooled above and below the transition temperature of the PC lipid and pH was adjusted to 7.4 to obtain the final sHDL product. LC-MS analysis was used to determine the encapsulation efficiency of GW3965 in sHDLs, following the removal of free drug from the sHDL using a 3k MWCO desalting column. The encapsulation efficiency of GW3965 in sHDL ranged from 78-98%, depending on the type of PC lipid used in the formulation.

The size of the sHDLs **(Figure 4.1A)** and GW3965-sHDLs **(Figure 4.1B)** were determined using dynamic light scattering. All sHDLs were 9-12 nm, with the exception of POPC-sHDL which was 13.4 nm and GW3965-POPC-sHDL, which was 16.0 nm in diameter. Gel permeation chromatography was used to analyze the purity of the sHDLs (**Figure 4.1C-E)**. POPC-sHDLs show a less uniform and broader peak as compared to other formulations,

indicating a more heterogenous particle distribution. For DiD-POPC-sHDLs and GW3965-POPC-sHDLs, GPC analysis showed presence of larger particles in the solution eluting around 5 minutes.

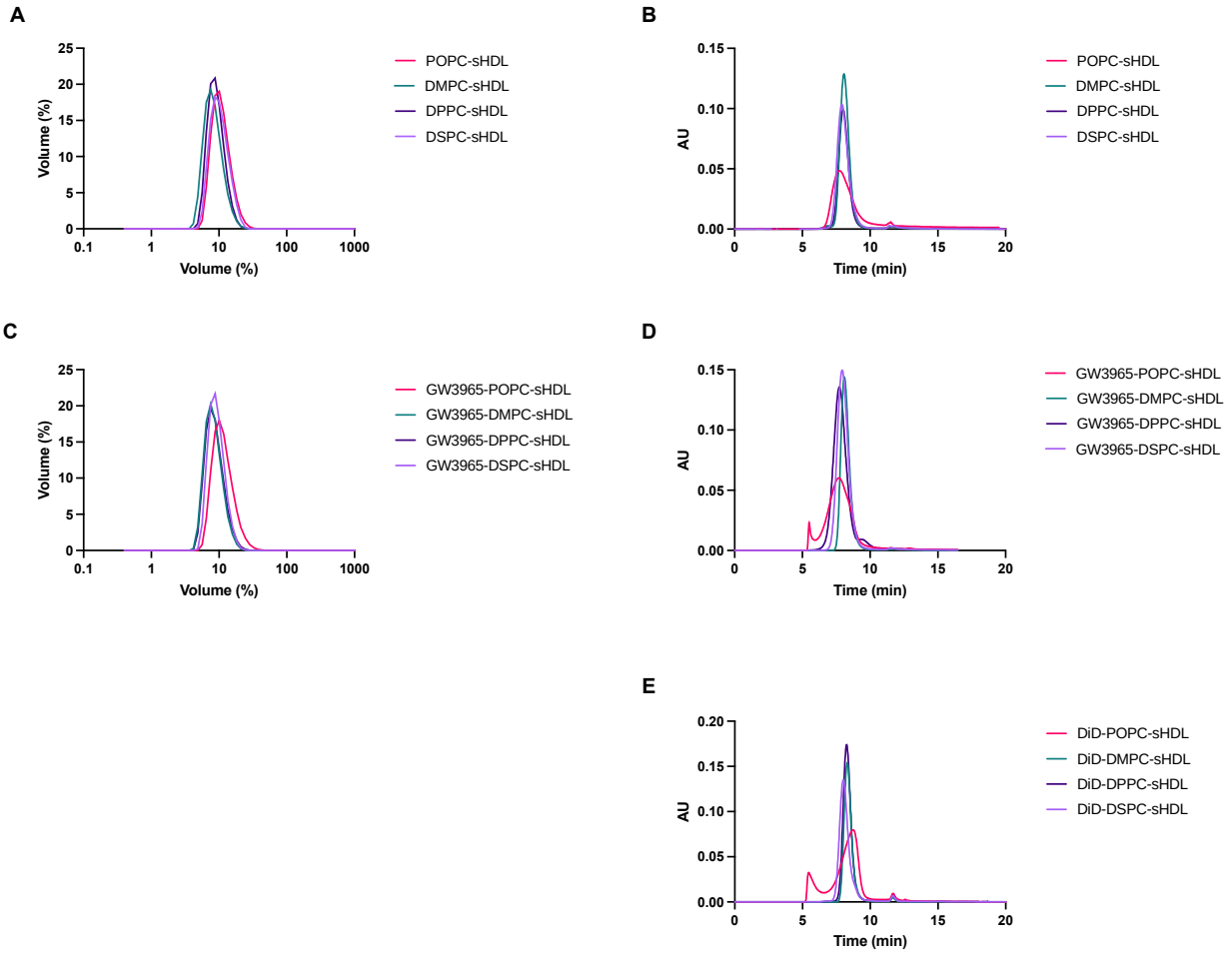

Figure 4.1 Characterization of blank sHDLs, DiD-sHDLs and GW3965-sHDLs. Particle size distribution determined by dynamic light scattering (DLS) for blank sHDLs (A) and GW3965-sHDLs (C). Purity of sHDLs determined using gel permeation chromatography (GPC) analysis for blank sHDLs (B), GW3965-sHDLs (D) and DiD-sHDLs (E).

4.4.2 Remodeling of blank sHDL in human serum

The concentration of PC lipid and 22A were assessed after incubation of blank sHDLs with human serum for different timepoints between 0 and 24 hours. Concentrations were quantified by LC-MS analysis. For all sHDLs, the concentration of PC lipid remained constant throughout the 24 hours incubation with human serum (**Figure 4.2A**). However, the 22A concentration declined over the 24 hours, suggesting that the 22A degraded when incubated with human serum over time (**Figure 4.2B**). After 6-, 12-, and 24-hours incubation, DSPC-sHDL and human serum mixture had a significantly higher percentage of initial concentration of 22A when compared to POPC-sHDLs and DMPC-sHDLs. This data demonstrates that 22A degrades to a lesser extent in DSPC-sHDL than in POPC-sHDL and DMPC-sHDL.

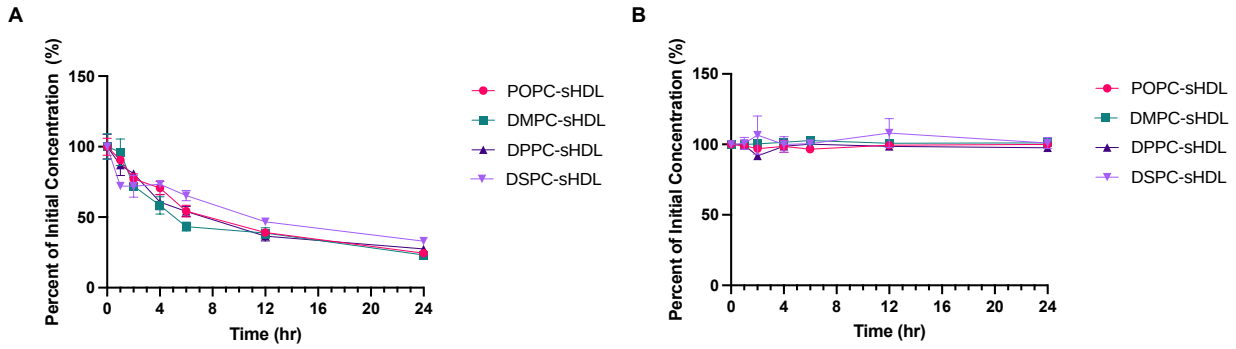

Figure 4.2 Percent of initial concentrations of 22A peptide (A) and PC lipid (B) measured by LC-MS after incubation of sHDLs with human serum at 37°C for various timepoints between 0 and 24 hours. The data represent mean ± SD (n =3).

To assess the effect of lipid composition on the extent of remodeling of sHDLs in human serum, the concentration of PC lipid and 22A peptide was quantified by LC-MS in fractions collected using size exclusion chromatography (SEC) to separate out different lipoprotein populations. During SEC separation, VLDLs elute from 7-9 minutes, LDL elute from 10-13 minutes, and endogenous and synthetic HDL elute from 14-19 minutes. To look at remodeling

and movement of components to other endogenous lipoprotein populations in human serum, concentration of PC lipid and 22A were quantified in human serum alone, sHDLs alone, and in mixtures of sHDL with human serum after incubation for 0, 2 and 24 hours. All sHDLs remodeled after 24 hours incubation with human serum to varying extents.

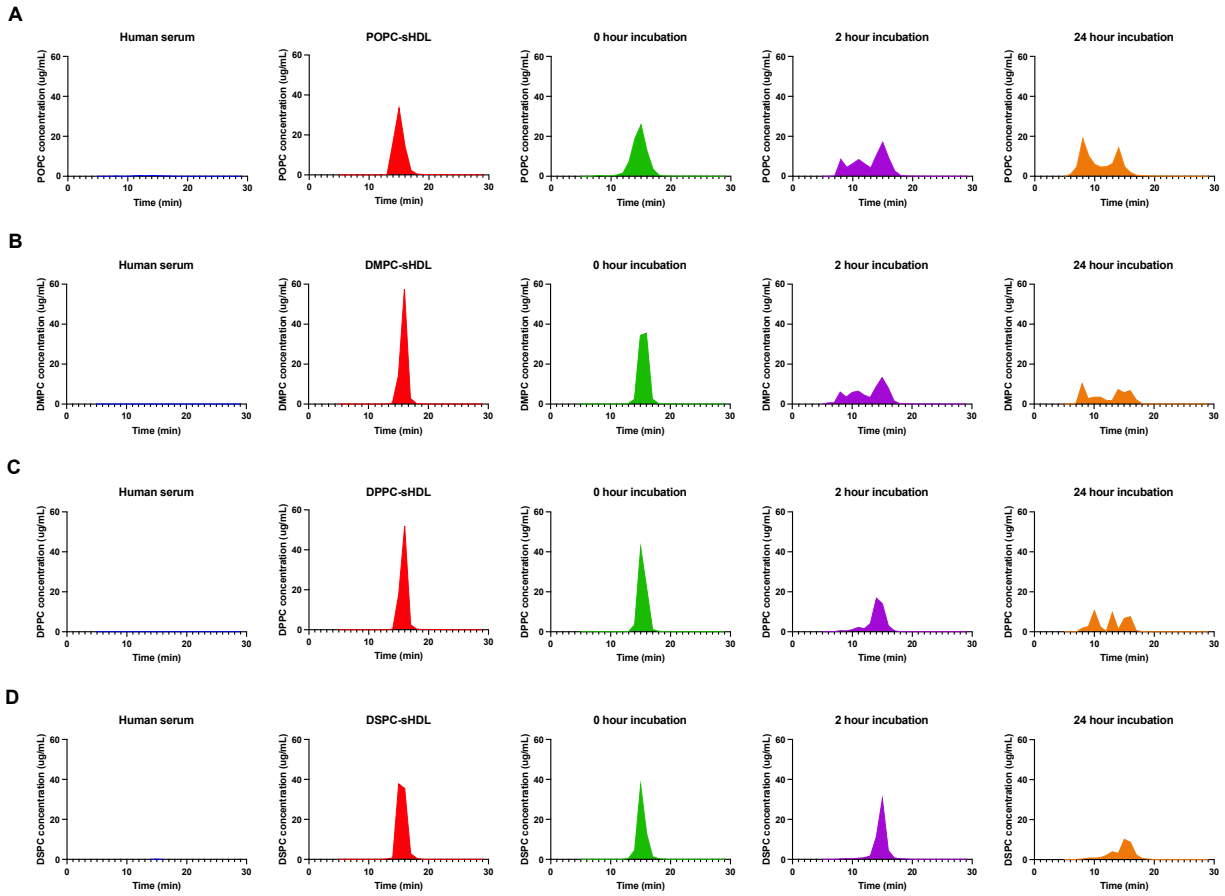

Figure 4.3 PC lipid concentrations in human serum alone, sHDLs alone, and after incubation of sHDLs with human serum for 0, 2 and 24 hours. SEC was used to separate out different lipoprotein populations found in human serum and concentrations of PC lipid in elution fractions were measured for POPC-sHDL (A), DMPC-sHDL (B), DPPC-sHDL (C), and DSPC-sHDL (D) by LC-MS analysis. Data is represented as the mean (n=3).

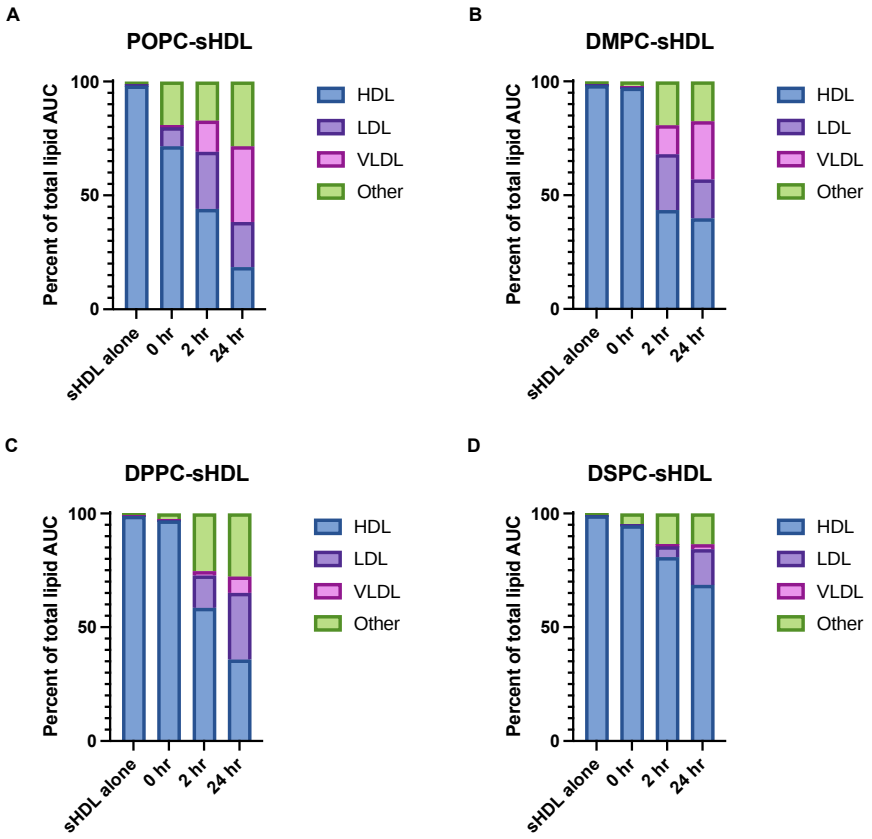

Figure 4.4 Percent of PC lipids measured within HDL, LDL, VLDL or other elution times for POPC-sHDL (A), DMPC-sHDL (B), DPPC-sHDL (C) and DSPC-sHDL (D), and after incubation of sHDLs with human serum for 0, 2 and 24 hours with subsequent separation of lipoprotein populations by SEC. Data is represented as the mean (n=3).

For PC lipids, very low levels of all lipids were detected in human serum alone. PC lipid was detected in fractions eluting from the SEC column at 13-18 minutes for sHDLs alone. For sHDLs mixed with human serum, POPC-sHDLs **(Figure 4.3A)** and DMPC-sHDLs **(Figure 4.3B)** showed movement of PC lipid and remodeling after 2 hours. Both formulations showed similar patterns, where around 50% of the PC lipid was detected in sHDL eluting fractions, while the other 50% was detected in VLDL and LDL eluting fractions **(Figure 4.4A,B)**. DPPC-sHDLs **(Figure 4.3C)** and DSPC-sHDLs **(Figure 4.3D)** appeared to remain more intact after 2 hours incubation with human serum, as compared to POPC- and DMPC-sHDLs. Around 58% of total

DPPC and over 81% of total DSPC quantified was detected in HDL eluting fractions after 2-hours incubation of sHDLs with human serum **(Figure 4.4C,D)**.

After 24 hours incubation with human serum, all sHDLs showed signs of remodeling through lipid detection in eluting fractions that correspond to larger lipoprotein populations. For POPC-sHDLs, a large majority of the total POPC lipid detected (33%) was measured in VLDL fractions, whereas only 19% of total POPC detected remained in HDL eluting fractions . For sHDLs other than POPC-sHDL, the majority of PC lipid detected was measured in HDL eluting fractions: 40% of total DMPC, 36% of total DPPC and 69% of total DSPC quantified. In contrast to POPC-sHDLs, a larger percentage of DPPC detected was measured in LDL eluting fractions (29%) than VLDL eluting fractions (8%). DSPC-sHDL appeared to remodel to the least extent when compared with other sHDLs, where only around 18% of total DSPC detected was measured in LDL and VLDL eluting fractions.

Very low to no levels of 22A were detected in fractions of human serum alone. 22A was detected in fraction eluting from the SEC column at 13-19 minutes in HDLs alone, with maximum 22A concentrations measured at 15 minutes for POPC-sHDL **(Figure 4.5A)** and 16 minutes for DMPC-sHDL **(Figure 4.5B)**, DPPC-sHDL **(Figure 4.5C)**, and DSPC-sHDL **(Figure 4.5D)**. After 2 hours of incubation with human serum, a large percentage of total 22A was still detected between 13-19 minutes for all sHDLs: 90% for POPC-sHDL, 82 % for DMPC-sHDL, 67% for DPPC-sHDL, and 80% for DSPC-sHDL, with some movement towards earlier eluting fractions **(Figure 4.6A-D)**. After 24 hours incubation of sHDLs with human serum, of the 22A quantified, 50% of 22A remained in HDL eluting fractions for POPC-sHDL, 55% for DMPC-sHDL, 50% for DPPC-sHDL and 84% for DSPC-sHDL. A similar distribution was observed in both POPC-sHDL and DMPC-sHDL fractions, where the percentage of 22A detected in VLDL

eluting fractions (16%, and 13%, respectively) was slightly higher than 22A detected in LDL eluting fractions (15% and 10%) after incubation with human serum. On the contrary, total 22A after 24 hours was detected to a larger extent in in LDL fractions (17%) than VLDL fractions (12%) for DPPC-sHDL. Similar to its lipid movement, DSPC-sHDL showed the least remodeling, where 22A detected after 24 hours incubation with human serum remained largely in HDL eluting fractions, with only 4% detected in LDL fractions and less than 1% in VLDL eluting fractions. In summary, 22A stayed within sHDL fractions after 24 hours for DSPC-sHDL to the highest extent, which suggests DSPC-sHDL stayed the most intact and the least remodeled in human serum over 24 hours as compared to POPC-, DMPC-, and DPPC-sHDLs.

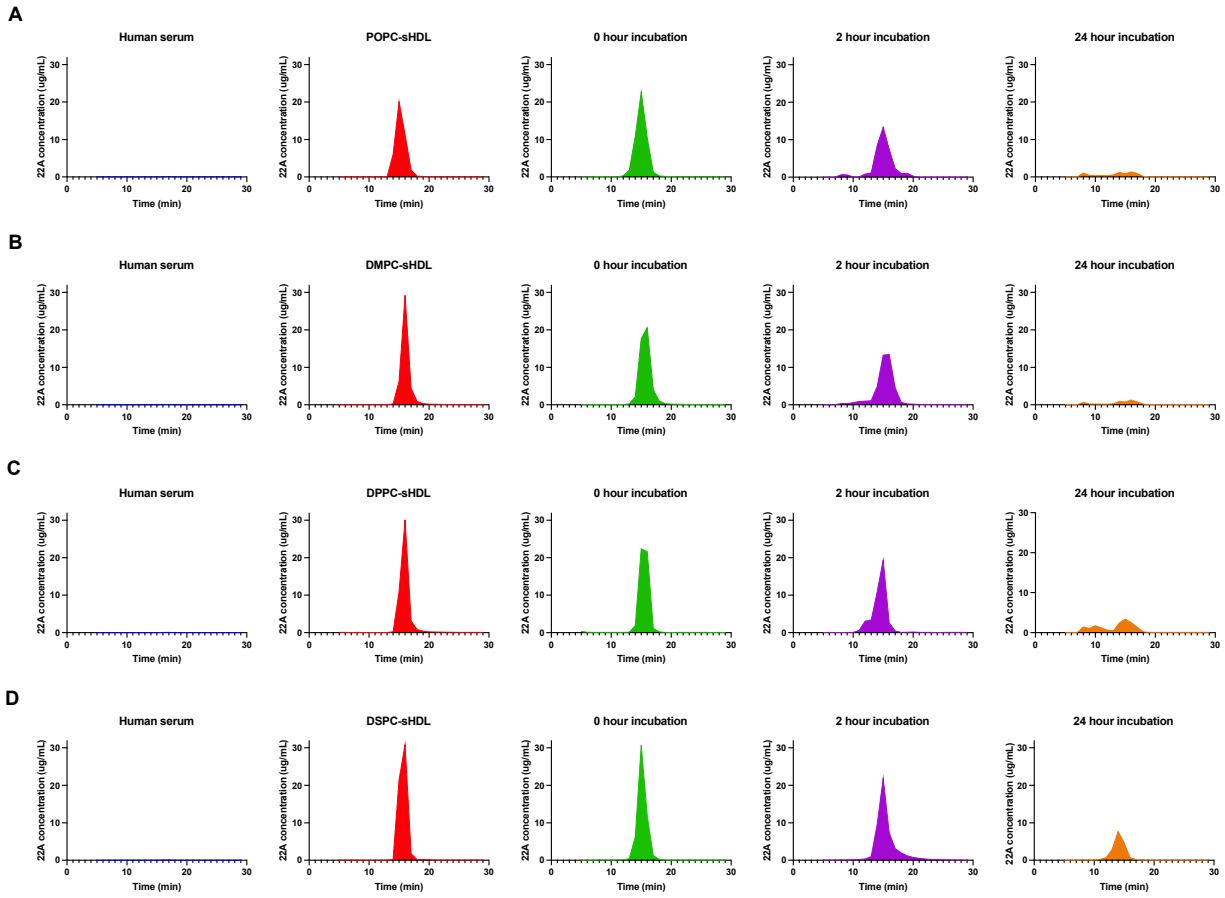

Figure 4.5 Detection of 22A peptide in fractions resulting from separation of lipoprotein populations by SEC for human serum alone, sHDLs alone, and after incubation of sHDLs with human serum for 0, 2 and 24 hours. Movement of 22A was measured for POPC-sHDL (A), DMPC-sHDL (B), DPPC-sHDL (C), and DSPC-sHDL (D) in the conditions described above. Data is represented as the mean (n=3).

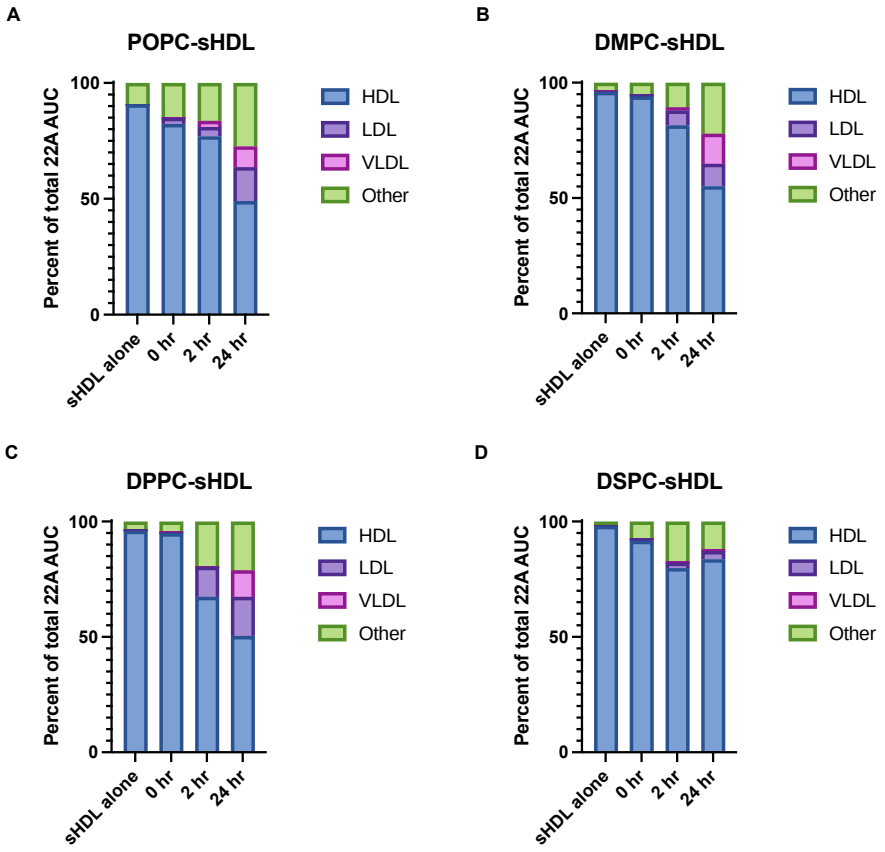

Figure 4.6 Percent of total 22A measured within HDL, LDL, VLDL or other elution times for POPC-sHDL (A), DMPC-sHDL (B), DPPC-sHDL (C) and DSPC-sHDL (D) alone, and after incubation of sHDLs with human serum for 0, 2 and 24 hours with subsequent separation of lipoprotein populations by SEC. Data is represented as the mean (n=3).

4.4.3 Remodeling of DiD-sHDLs in human serum

To assess the effect of lipid composition on the movement of hydrophobic DiD dye from sHDLs when incubated with human serum, mixtures of human serum and DiD-sHDLs were separated by SEC and fluorescence intensity was simultaneously measured during separation. In human serum alone, there was no fluorescent signal from the DiD dye. For DiD-sHDLs alone, dye was detected at 11-18 minutes for DiD-POPC-sHDL **(Figure 4.7A)**, and 15-18 minutes for DiD-DMPC-sHDL **(Figure 4.7B)**, DiD-DPPC-sHDL **(Figure 4.7C)**, and DiD-DSPC-sHDLs

(**Figure 4.7D).** The fluorescent spectra after 0 hours incubation with human serum and DiD-sHDLs with subsequent SEC separation remained similar to DiD-sHDLs alone.

After 2 hours incubation with human serum, overall fluorescent intensity decreased for all DiD-sHDLs. A large portion of DiD fluorescence signal was detected in HDL elution times for DiD-DPPC-sHDLs and DiD-DSPC-sHDLs **(Figure 4.8C,D)**, with a slight left shift in peak for both formulations towards earlier eluting times. In addition to detection at HDL elution times between 14-18 minutes after 2 hours incubation with human serum (53% of total fluorescence measured), a percentage of fluorescence signal was detected in both VLDL (14%) and LDL (32%) elution times for DiD-DMPC-sHDL **(Figure 4.8B)**. For DiD-POPC-sHDLs, DiD dye was detected largely at elution times between 8-9 minutes (41%), suggesting that dye leaked out from sHDLs and became associated with VLDL populations **(Figure 4.8A)**. Less total fluorescence was detected in LDL (24%) and HDL (34%) elution times.

Incubation of DiD-sHDL and human serum for 24 hours lead to more movement of dye to larger lipoprotein fractions and a large reduction in fluorescence signal. Fluorescence detected after incubation of DiD-POPC-sHDL with human serum for 24 hours was largely measured in VLDL elution times (60%), with only 23% of the total fluorescence signal remained within the HDL elution times. For DiD-DMPC-sHDLs, a larger percentage of total fluorescence detected was also found in VLDL (31%) and HDL (36%) elution times with a smaller percent detected in LDL elution times (24%). On the contrary, for DiD-DPPC-sHDL and DiD-DSPC sHDL, very little fluorescence signal was detected in VLDL elution times (7% and 2%, respectively), while larger percentages of fluorescence signal were measured in LDL elution times for DiD-DPPC-sHDL (40%) and DiD-DSPC-sHDL (35%). While the percentage of total fluorescence was detected in HDL eluting fractions was 47% for DiD-DPPC-sHDL, DID-DSPC-sHDL showed the

largest percentage of total fluorescence still detected in HDL fractions, at around 62% of total fluorescence measured after 24 hours incubation with human serum.

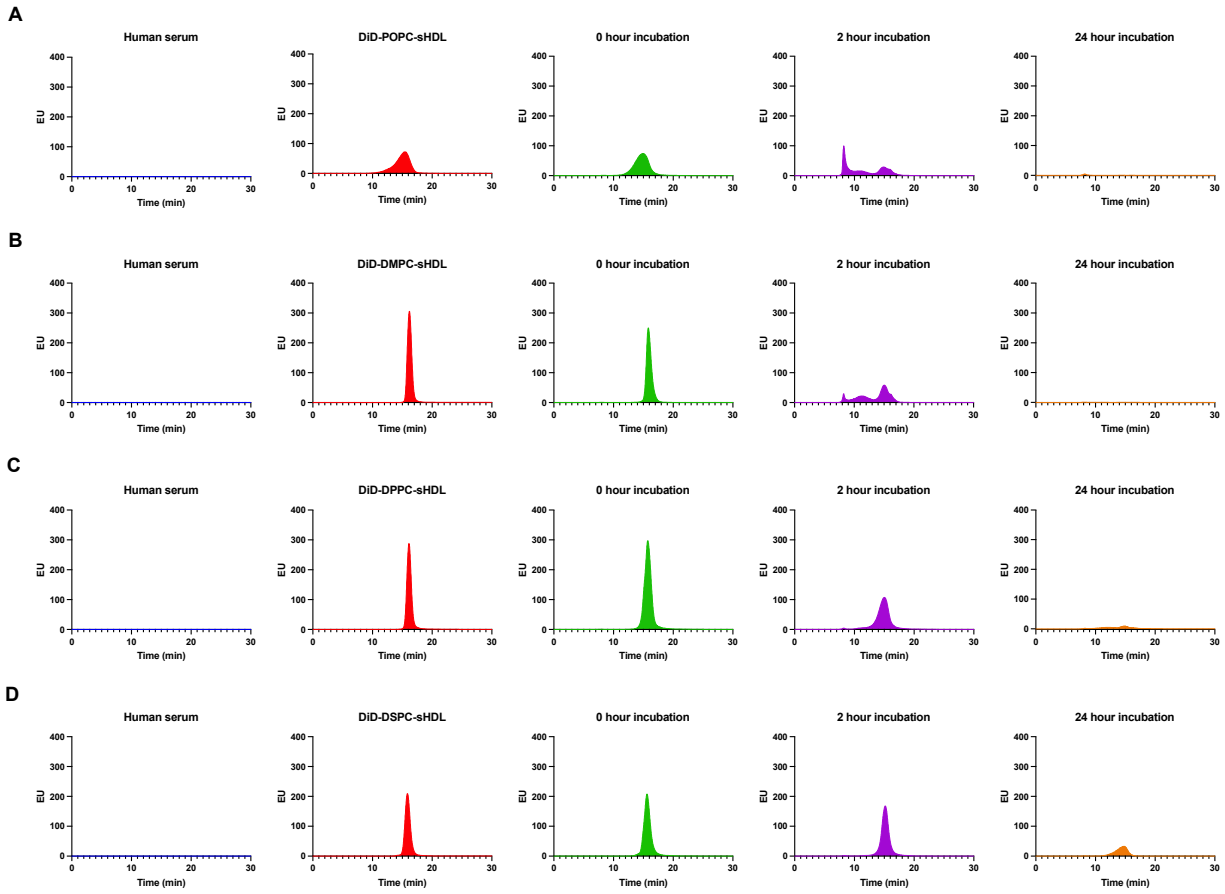

Figure 4.7 DiD fluorescence measured during SEC separation in human serum alone, DiD-sHDLs alone, and after incubation of DiD-sHDLs with human serum for 0, 2, and 24 hours for DiD-POPC-sHDL (A), DiD-DMPC-sHDL (B), DiD-DPPC-sHDL (C), and DiD-DSPC-sHDL (D). DiD fluorescence was measured at an excitation wavelength of 646 nm and emission wavelength of 663 nm. Data is represented as the mean (n=3).

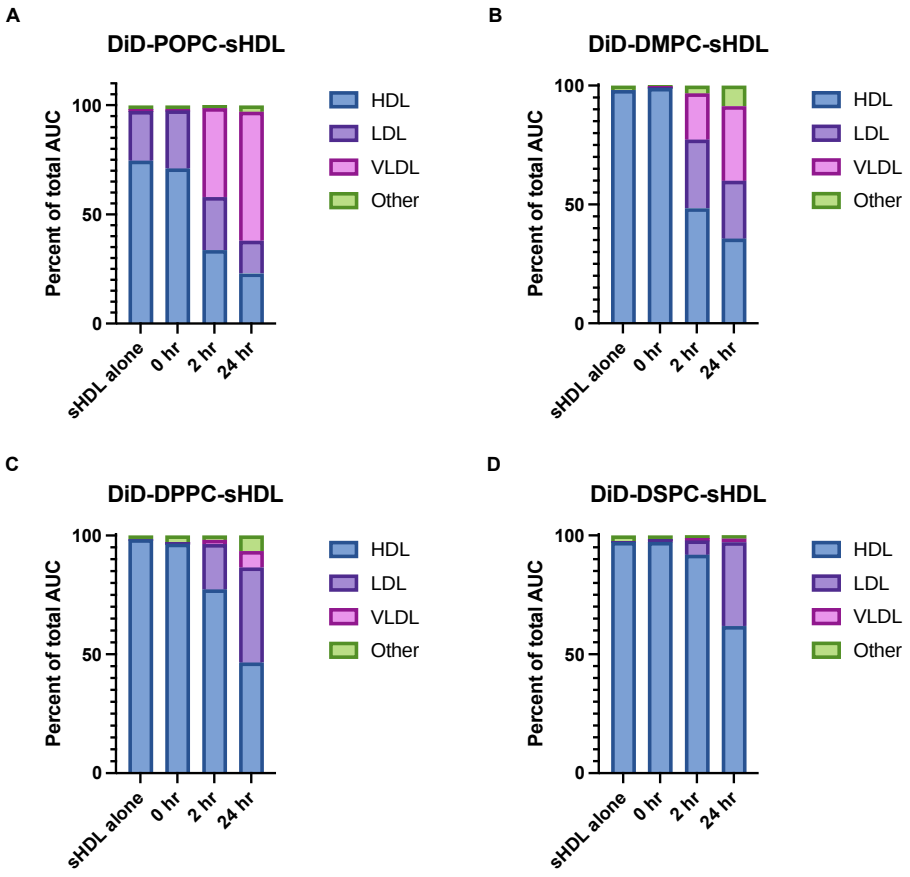

Figure 4.8 Percent of total DiD fluorescence measured within HDL, LDL, VLDL or other elution times for POPC-sHDL (A), DMPC-sHDL (B), DPPC-sHDL (C) and DSPC-sHDL (D) alone, and after incubation of sHDLs with human serum for 0, 2 and 24 hours with subsequent separation of lipoprotein populations by SEC. Data is represented as the mean (n=3).

4.4.4 Remodeling of GW3965-sHDLs in human serum

To assess the concentration of GW3965 after incubation of GW3965-sHDLs with human serum over time, GW3965-sHDLs were incubated with human serum for various timepoints between 0 and 24 hours. The concentration of GW3965 over the time course did not change, showing that GW3965 does not degrade in human serum after 24 hours **(Figure 4.9)**. Next, GW3965-sHDLs were incubated with human serum for 0, 2 and 24 hours to understand the effect of lipid composition on the movement of GW3965 during sHDL remodeling in human

serum. Lipoproteins were separated out by SEC, and LC-MS was used to quantify to concentration of GW3965 in each fraction. No GW3965 was detected in any fractions of human serum alone. GW3965 was detected in fractions eluting from 11-18 minutes for GW3965-POPC-sHDL **(Figure 4.10A)** with a maximum concentration at 15 minutes and 13-18 minutes for GW3965-DMPC-sHDL **(Figure 4.10B)**, GW3965-DPPC-sHDL **(Figure 4.10C)** and GW3965-DSPC-sHDLs **(Figure 4.10D)** with maximum concentrations at 16 minutes. After 0 hours incubation of GW3965-sHDLs with human serum, and SEC separation, the fractions in which GW3965 was detected increased, where the drug was found in fractions eluting at 10-18 minutes for all sHDLs. After 2 hours of sHDL incubation with human serum, the total GW3965 measured remain largely in HDL eluting fractions (63% for GW3965-POPC-sHDL, 72% for GW-3965-DMPC-sHDL, 70% for GW3965-DPPC-sHDL, 67% for GW3965-DSPC-sHDL) **(Figure 4.11A-D)**. GW3965-POPC-sHDL had a higher percentage of total GW3965 detected in LDL fractions, (14%), as compared to the other sHDL formulations (8-9%). After 24 hours incubation with human serum, GW3965 was detected in all lipoprotein fractions, suggesting that GW3965 was partially released from sHDLs after 24 hours from all formulations. While most of the GW3965 still remained in HDL eluting fractions, some of the drug was also detected in VLDL and LDL eluting fractions. Larger percentages of the total GW3965 measured after 24 hours was measured in VLDL (12%) and LDL (16%) eluting fraction for GW3965-POPC-sHDLs as compared to other formulation, with 50% still detected in HDL eluting fractions. GW3965-DMPC-sHDL, GW3965-DPPC-sHDL, GW3965-DSPC-sHDL showed similar trends to each other, where around 6% was detected in VLDL, 7-13% detected in LDL and 62-70% detected in HDL eluting fractions.

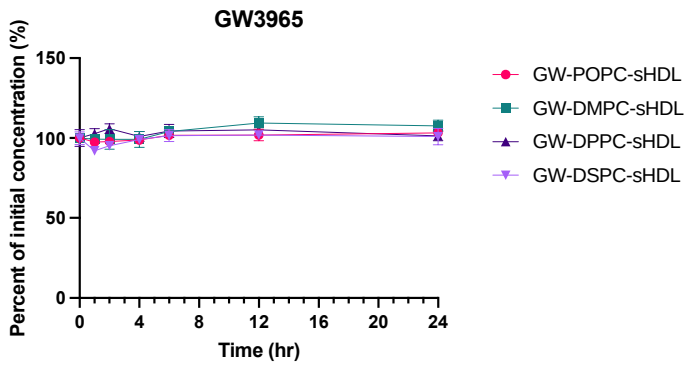

Figure 4.9 Percent of initial concentrations of GW3965 determine by LC-MS after incubation of GW3965-sHDLs with human serum at 37°C for various timepoints between 0 and 24 hours. The data represent mean ± SD (n =3).

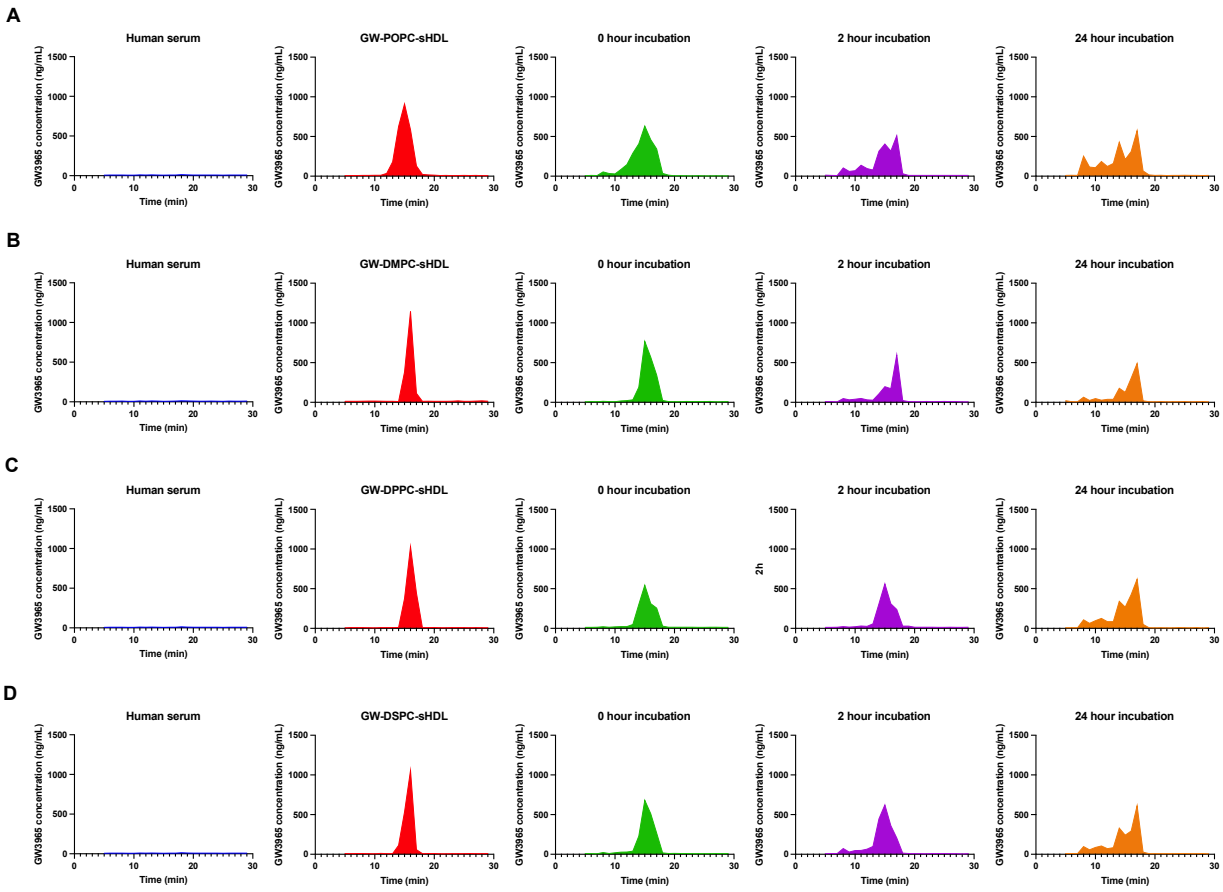

Figure 4.10 GW3965 concentrations in human serum alone, GW3965-sHDLs alone, and after 0-, 2- and 24-hour incubation of GW3965-sHDLs with human serum. POPC-sHDL (A), DMPC-sHDL (B), DPPC-sHDL (C), and DSPC-sHDL (D) were subjected to the conditions above, lipoprotein populations were separated out by SEC, and concentrations of GW3965 were measured by LC-MS analysis. Data is represented as the mean (n=3).

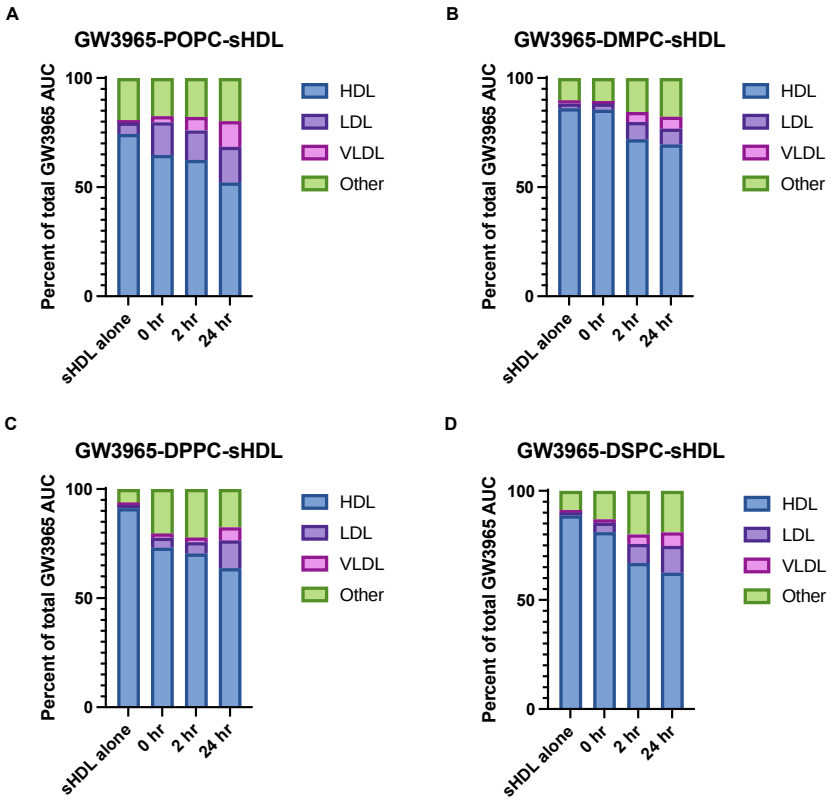

Figure 4.11 Percent of total GW3965 measured within HDL, LDL, VLDL or other elution times for POPC-sHDL (A), DMPC-sHDL (B), DPPC-sHDL (C) and DSPC-sHDL (D) alone, and after incubation of sHDLs with human serum for 0, 2 and 24 hours with subsequent separation of lipoprotein populations by SEC. Data is represented as the mean (n=3).

4.5 Discussion

sHDLs have been extensively studied and explored as therapeutics alone, as well as drug delivery systems for a multitude of indications such as cardiovascular-related diseases [16,18] different cancer types [19,20], and autoimmune disease [21]. To further evaluate the therapeutic potential of sHDL, remodeling of sHDL in human serum was assessed in the present study. Remodeling can ultimately affect the ability of sHDLs to reach the target site or to deliver its cargo to the desired area of interest, therefore impacting the overall benefit and therapeutic efficacy of the particle.

In this study, we investigated the effect of lipid composition on sHDL remodeling in the presence of human serum containing endogenous lipoproteins. We first chose to monitor the movement of sHDL components, PC lipid and 22A, after incubation of blank sHDL with human serum to understand if sHDL components migrate in the presence of human serum and to which other lipoproteins populations these components will migrate. To assess how remodeling affects the movement of hydrophobic dyes incorporated in sHDLs, we monitored DiD fluorescence after incubation of DiD-sHDLs in human serum. DiD is a lipophilic carbocyanine dye that has been long used as a tool to help track nanoparticle biodistribution in in vivo studies [22–24] . Using hydrophobic dye as an indicator of sHDL movement or accumulation in vivo could be misleading if dye leaks from sHDL while in circulation. Furthermore, to investigate how remodeling can affect sHDL drug release and movement of drugs in circulation, we formulated sHDLs carrying GW3965, which was chosen as our model drug in this study. GW3965 is a Liver-X-Receptor (LXR) agonist which works by increasing the expression of ABCA1 cholesterol efflux transporter, resulting in an increase in excess cholesterol effluxed from peripheral tissues [25,26]. LXR agonists have been shown to have therapeutic effects against atherosclerosis by increasing reverse cholesterol transport [27,28] and have recently shown early promise in treating inflammatory diseases and cancer [29,30] . Due to the hydrophobicity of GW3965, the drug can be incorporated into the membrane of sHDLs.

The lipid composition has been shown to have an effect on biological activity, stability, and pharmacokinetics of sHDL [15–17]. Phosphatidylcholine lipids used in this study all have different degrees of saturation and lipid tail lengths, which affects its transition temperature, or the temperature in which the lipids change phases. POPC and DMPC, exist in the liquid crystalline phase a physiological temperature, whereas DPPC and DSPC, exist at a gel ordered

phase at physiological temperature [31,32]. In the liquid crystalline phase, lipids are randomly oriented and fluid. In contrast, lipids are tightly packed and fully extended in the gel ordered phase. Ultimately, the phase in which lipids exist within the sHDL can affect its stability in circulation. Our results highlight that the lipid composition of the sHDLs affects the remodeling of the nanoparticle and extent of component movement to different lipoprotein populations found in human serum. POPC-sHDL had the most movement of PC lipid and 22A to larger lipoprotein eluting fractions when compared to the other sHDL formulations after 2 hours and 24 hours, where the majority of DSPC and 22A were detected in HDL eluting fractions for DSPC-sHDLs incubated with human serum after 24 hours. DiD dye seemed to follow a similar trend as PC lipid and 22A. Overall, sHDLs formulated with DSPC lipid seem to remodel at slower rates when compared to sHDL formulated with POPC lipid. We predict these trends may be attributed to the fact that lipids with higher transition temperatures, such as DSPC can cause the lipid structure to be less fluid and more ridged at physiological temperatures, leading to more stable particles and less remodeling, while POPC creates a less table membrane at room temperature due to it's low transition temperature and fluidity at 37°C.

Our group has previously investigated the effect of lipid composition on the in vivo pharmacokinetics and pharmacodynamics of sHDLs in Sprague Dawley rats and found that DSPC-sHDLs showed a higher half-life, leading to an increase in sHDL circulation time and a significantly higher free cholesterol mobilized as compared to POPC-sHDL, DMPC-sHDL and DPPC-sHDL formulations. The authors also found that after 1 hour incubation with human plasma, DSPC-sHDLs showed insertion of endogenous ApoA-I was reduced as compared to the three other sHDL formulations, suggesting DSPC-sHDL was less remodeled in the presence of endogenous HDL, which may explain the higher stability and circulation half-life seen in the

PK/PD study [15]. Furthermore, Petersbæk et. al. found that fluorophores DSPE-Cy5 and DPPE-atto488, desorbed from sHDLs with different lipid compositions to differing degrees after 2 hours. DPPC-sHDLs showed the lowest fluorophore desorption, followed by POPC, then DMPC. The author attributed this pattern to difference in phase transition temperatures and rigidity of the lipid bilayer [33]

While the lipid composition influenced the rate of remodeling of the sHDLs, it also impacted where the components were migrating to. When tracking PC lipid and DiD dye movement after sHDL incubation with human serum, components were found in VLDL elution times to a larger extent than LDL elution time for sHDLs formulated with POPC and DMPC after 24 hours incubation with human serum. On the contrary, movement of PC lipid and dye from sHDLs formulated with DPPC and DSPC were detected in LDL elution times, with a very small percent being detected VLDL elution times after 2 and 24 hours incubation with human serum. Therefore, we can hypothesize that the lipid composition may impact where PC lipids and DiD dye migrate and to which lipoprotein populations, VLDL or LDL, components migrate to. Further mechanistic studies are required to understand this phenomenon.

When tracking the movement of GW3965 to different lipoprotein fractions in human serum over time, we observed that the pattern of movement of the drug when compared to the PC lipid and 22A, was not the same. This led us to hypothesize that some sHDL particle were breaking apart, leading to the release of the drug. GW3965-POPC-sHDL showed more movement of the drug to VLDL and LDL eluting fractions after incubation with human serum for 2 and 24 hours as compared to the other sHDL formulations. The pattern of movement of GW3965 observed was similar for DMPC-, DPPC-, and DSPC-sHDLs encapsulating GW3965,

where GW3965 was largely detected in HDL eluting fractions, with a small percentage detected in LDL eluting fractions after 24 hours incubation with human serum.

The phospholipid composition of GW3965 sHDLs not only affected the movement of GW3965 to other lipoproteins in human serum, but also impacted the ease of sHDL preparation and encapsulation of the drug into the sHDL membrane. DMPC-sHDLs had the highest encapsulation of GW3965, over 98%, followed by DPPC-sHDL and DSPC-sHDL, and finally POPC-sHDL having the lowest encapsulation efficiency at 78%. DLS and GPC analysis also showed that GW3965-POPC-sHDLs had a larger particle size and were more heterogenous, maybe due to the fluidity of the particle at physiological temperature which is way above the transition temperature of the lipid. These factors may have played a role in the release of GW3965 from POPC-sHDL to larger lipoprotein fractions and may help explain why more drug was detected in fractions outside of HDL eluting fractions to a larger extent than the other sHDL formulations. Others have found that the phospholipid composition of sHDL can affect stability of sHDLs as drug vehicles and release of the drug from the carrier [34–36]. For example, addition of sphingomyelin to the lipid bilayer of sHDLs has also been suggested to improve the stability and cholesterol binding of the particles, which extends the idea of using SM lipids to tightly hold cholesterol-anchored drugs in the sHDL drug vehicle [34]. While the results from our study show the movement of drug after incubation of drug-loaded sHDLs with human serum, it is important to note that all small molecule drugs have different physiochemical properties that affect the encapsulation efficacy and release of the drug from the sHDL membrane. Thus, we cannot assume that all drugs would behave in a similar manner as GW3965 in our study. Individual remodeling studies will need to be done for each unique drug-loaded sHDL formulation.

4.6 Conclusion

In summary, the present study shows that the lipid composition of sHDLs can impact the extent of sHDL remodeling in human serum and movement of components to other lipoprotein populations time. In terms of blank sHDLs and DiD-sHDLs, remodeling in human serum occurred to the largest extent for sHDLs formulated with POPC lipid, while sHDLs formulated with DSPC lipid remained the most intact. Movement of PC lipid and DiD dye was more preferential to VLDL for sHDLs composed of POPC and DMPC lipid, while sHDLs composed of DPPC and DSPC favored movement to LDL populations. Release of GW3965 and movement to other lipoprotein populations may be dependent on remodeling of the sHDL drug vehicle, as well as other physiochemical properties that contribute to the ease of drug encapsulation into particle and release of drug from the particle. The results of this study highlight the importance of lipid composition considerations when developing sHDLs as therapeutic candidates and as drug carriers.

4.7 References

1. Kontush Anatol, Chapman MJ. *High-Density Lipoproteins : Structure, Metabolism, Function, and Therapeutics*. John Wiley & Sons, Inc; 2012.

2. Trajkovska KT, Topuzovska S. High-density lipoprotein metabolism and reverse cholesterol transport: Strategies for raising HDL cholesterol. *Anatol J Cardiol*. 2017;18(2):149-154. doi:10.14744/AnatolJCardiol.2017.7608

3. Ouimet M, Barrett TJ, Fisher EA. HDL and reverse cholesterol transport: Basic mechanisms and their roles in vascular health and disease. *Circ Res*. 2019;124(10):1505-1518. doi:10.1161/CIRCRESAHA.119.312617

4. Gille A, D'Andrea D, Tortorici MA, Hartel G, Wright SD. CSL112 (Apolipoprotein A-I [Human]) Enhances Cholesterol Efflux Similarly in Healthy Individuals and Stable Atherosclerotic Disease Patients. *Arterioscler Thromb Vasc Biol*. 2018;38(4):953-963.

5. Nicholls SJ, Andrews J, Kastelein JJP, et al. Effect of serial infusions of CER-001, a pre-β High-density lipoprotein mimetic, on coronary atherosclerosis in patients following acute coronary syndromes in the CER-001 atherosclerosis regression acute coronary syndrome trial: A randomized clinical trial. *JAMA Cardiol*. 2018;3(9):815-822. doi:10.1001/jamacardio.2018.2121

6. Tardif JC, Ballantyne CM, Barter P, et al. Effects of the high-density lipoprotein mimetic agent CER-001 on coronary atherosclerosis in patients with acute coronary syndromes: a randomized trial. *Eur Heart J*. 2014;35:3277-3286. doi:10.1093/eurheartj/ehu194

7. Kuai R, Li D, Chen YE, Moon JJ, Schwendeman A. High-Density Lipoproteins: Nature's Multifunctional Nanoparticles. *ACS Nano*. 2016;10(3):3015-3041. doi:10.1021/acsnano.5b07522

8. Raut S, Mooberry L, Sabnis N, Garud A, Dossou AS, Lacko A. Reconstituted HDL: Drug delivery platform for overcoming biological barriers to cancer therapy. *Front Pharmacol*. 2018;9(OCT). doi:10.3389/fphar.2018.01154

9. Mei Y, Tang L, Xiao Q, et al. Reconstituted high density lipoprotein (rHDL), a versatile drug delivery nanoplatform for tumor targeted therapy. *J Mater Chem B*. 2021;9(3):612-633. doi:10.1039/d0tb02139c

10. Pownall HJ, Rosales C, Gillard B, Ferrari M. Native and Reconstituted Plasma Lipoproteins in Nanomedicine: Physicochemical Determinants of Nanoparticle Structure, Stability and Metabolism. *Methodist Debakey Cardiovasc J*. 2016;12(3):146-150. doi:10.14797/mdcj-12-3-146

11. Von Eckardstein A, Kardassis D. *High Density Lipoproteins From Biological Understanding to Clinical Exploitation*.; 2015.

12. Ong KL, Cochran BBiotech BJ, Manandhar B, Thomas S, Rye KA. HDL maturation and remodelling. *Biochim Biophys Acta Mol Cell Biol Lipids*. 2022;1867(4). doi:10.1016/j.bbalip.2022.159119

13. Ji A, Wroblewski JM, Webb NR, Van Der Westhuyzen DR. Impact of phospholipid transfer protein on nascent high-density lipoprotein formation and remodeling. *Arterioscler Thromb Vasc Biol*. 2014;34(9):1910-1916. doi:10.1161/ATVBAHA.114.303533

14. Pussinen PJ, Metso J, Malle E, et al. The role of plasma phospholipid transfer protein (PLTP) in HDL remodeling in acute-phase patients. *Biochim Biophys Acta*. 2001;1533(2):153-163. doi:doi.org:10.1016/S1388-1981(01)00153-6

15. Furtado JD, Ruotolo G, Nicholls SJ, Dullea R, Carvajal-Gonzalez S, Sacks FM. Pharmacological Inhibition of CETP (Cholestery Ester Transfer Protein) Increases HDL (High-Density Lipoprotein) That Contains ApoC3 and Other HDL Subspecies Associated With Higher Risk of Coronary Heart Disease. *Arterioscler Thromb Vasc Biol*. 2022;42(2):227-237. doi:10.1161/ATVBAHA.121.317181

16. Schilcher I, Stadler JT, Lechleitner M, et al. Endothelial lipase modulates paraoxonase 1 content and arylesterase activity of HDL. *Int J Mol Sci*. 2021;22(2):1-15. doi:10.3390/ijms22020719

17. Carr MC, Ayyobi AF, Murdoch SJ, Deeb SS, Brunzell JD. Contribution of hepatic lipase, lipoprotein lipase, and cholesteryl ester transfer protein to LDL and HDL heterogeneity in healthy women. *Arterioscler Thromb Vasc Biol*. 2002;22(4):667-673. doi:10.1161/01.ATV.0000013284.47317.95

18. Fawaz M V., Kim SY, Li D, et al. Phospholipid component defines pharmacokinetic and pharmacodynamic properties of synthetic high-density lipoproteins. *Journal of Pharmacology and Experimental Therapeutics*. 2020;372(2):193-204. doi:10.1124/JPET.119.257568

19. Schwendeman A, Sviridov DO, Yuan W, et al. The effect of phospholipid composition of reconstituted HDL on its cholesterol efflux and anti-inflammatory properties. *J Lipid Res*. 2015;56(9):1727-1737. doi:10.1194/jlr.M060285

20. Kim SY, Kang J, Fawaz M V, et al. Phospholipids impact the protective effects of HDL-mimetic nanodiscs againsts lipopolysaccharide-induced inflammation . *Nanomedicine*. Published online 2024.

21. Guo Y, Yuan W, Yu B, et al. Synthetic High-Density Lipoprotein-Mediated Targeted Delivery of Liver X Receptors Agonist Promotes Atherosclerosis Regression. *EBioMedicine*. 2018;28:225-233. doi:10.1016/j.ebiom.2017.12.021

22. Scheetz L, Kadiyala P, Sun X, et al. Synthetic High-density Lipoprotein Nanodiscs for Personalized Immunotherapy against Gliomas. *Clinical Cancer Research*. 2020;26(16):4369-4380. doi:10.1158/1078-0432.CCR-20-0341

23. Kuai R, Ochyl LJ, Bahjat KS, Schwendeman A, Moon JJ. Designer vaccine nanodiscs for personalized cancer immunotherapy. *Nat Mater*. 2017;16(4):489-498. doi:10.1038/NMAT4822

24. Tiniakou I, Drakos E, Sinatkas V, et al. High-Density Lipoprotein Attenuates Th1 and Th17 Autoimmune Responses by Modulating Dendritic Cell Maturation and Function. *The Journal of Immunology*. 2015;194(10):4676-4687. doi:10.4049/jimmunol.1402870

25. Scully MA, Wilkins DE, Dang MN, Hoover EC, Aboeleneen SB, Day ES. Cancer Cell Membrane Wrapped Nanoparticles for the Delivery of a Bcl-2 Inhibitor to Triple-Negative Breast Cancer. *Mol Pharm*. 2023;20(8):3895-3913. doi:10.1021/acs.molpharmaceut.3c00009

26. Lee Y, Lee D, Park E, et al. Rhamnolipid-coated W/O/W double emulsion nanoparticles for efficient delivery of doxorubicin/erlotinib and combination chemotherapy. *J Nanobiotechnology*. 2021;19(1). doi:10.1186/s12951-021-01160-4

27. Schaack B, Hindré T, Quansah N, Hannani D, Mercier C, Laurin D. Microbiota-Derived Extracellular Vesicles Detected in Human Blood from Healthy Donors. *Int J Mol Sci*. 2022;23(22). doi:10.3390/ijms232213787

28. Algattas H, Huang JH. Traumatic Brain Injury pathophysiology and treatments: Early, intermediate, and late phases post-injury. *Int J Mol Sci*. 2014;15(1):309-341. doi:10.3390/ijms15010309

29. Di D, Wang Z, Liu Y, et al. ABCA1 upregulating apolipoproein M expression mediates via the RXR/LXR pathway in HepG2 cells. *Biochem Biophys Res Commun*. 2012;421(1):152-156. doi:10.1016/j.bbrc.2012.04.022

30. Zanotti I, Potì F, Pedrelli M, et al. The LXR agonist T0901317 promotes the reverse cholesterol transport from macrophages by increasing plasma efflux potential. *J Lipid Res*. 2008;49(5):954-960. doi:10.1194/jlr.M700254-JLR200

31. Savla SR, Prabhavalkar KS, Bhatt LK. Liver X receptor: a potential target in the treatment of atherosclerosis. *Expert Opin Ther Targets*. 2022;26(7):645-658. doi:10.1080/14728222.2022.2117610

32. Tavazoie MF, Pollack I, Tanqueco R, et al. LXR/ApoE Activation Restricts Innate Immune Suppression in Cancer. *Cell*. 2018;172(4):825-840.e18. doi:10.1016/j.cell.2017.12.026

33. Wang Q, Wang J, Wang J, Zhang H. Molecular mechanisms of liver X receptors in cancer therapeutics. *Life Sci*. 2021;273. doi:doi:10.1016/j.lfs.2021.119287

34. Dmitriev AA, Surovtsev N V. Temperature-Dependent Hydrocarbon Chain Disorder in Phosphatidylcholine Bilayers Studied by Raman Spectroscopy. *Journal of Physical Chemistry B*. 2015;119(51):15613-15622. doi:10.1021/acs.jpcb.5b07502

35. Pentak D. Alternative methods of determining phase transition temperatures of phospholipids that constitute liposomes on the example of DPPC and DMPC. *Thermochim Acta*. 2014;584:36-44. doi:10.1016/j.tca.2014.03.020

36. Pedersbæk D, Kræmer MK, Kempen PJ, et al. The Composition of Reconstituted High-Density Lipoproteins (rHDL) Dictates the Degree of rHDL Cargo- A nd Size-Remodeling via Direct Interactions with Endogenous Lipoproteins. *Bioconjug Chem*. 2019;30(10):2634-2646. doi:10.1021/acs.bioconjchem.9b00552

37. Kučerka N, Marquardt D, Harroun TA, et al. Cholesterol in bilayers with PUFA chains: Doping with DMPC or POPC results in sterol reorientation and membrane-domain formation. *Biochemistry*. 2010;49(35):7485-7493. doi:10.1021/bi100891z

38. Yancey PG, De La Llera-Moya M, Swarnakar S, et al. High density lipoprotein phospholipid composition is a major determinant of the bi-directional flux and net movement of cellular free cholesterol mediated by scavenger receptor BI. *Journal of Biological Chemistry*. 2000;275(47):36596-36604. doi:10.1074/jbc.M006924200

39. Mcmullen TPW, Lewis RNAH, Mcelhaney RN. Differential Scanning Calorimetric Study of the Effect of Cholesterol on the Thermotropic Phase Behavior of a Homologous Series of Linear Saturated Phosphatydlcholines. *Biochemistry*. 1993;32(2):516-522. https://pubs.acs.org/sharingguidelines

Chapter 5 Conclusions and Perspectives

The work presented in this dissertation expands on the utility of sHDL and HDL mimetic micelles as potential therapeutics for cardiovascular disease. Given the prevalence of cardiovascular disease mortality, and the innate ability of HDL to modulate several aspects of endothelial cellular function, inflammatory cascades, and cholesterol mobilization, the development of sHDLs and HDL mimetic micelles for targeting the pathophysiology of endothelial dysfunction and atherosclerosis holds great potential. Here, the impact of lipid composition on the biological activity, pharmacokinetics, stability, and remodeling of these lipid-based nanoparticle was evaluated.

In chapter 2, we examined how the phospholipid composition of HDL-mimicking micelles impacts the atheroprotective properties of the nanoparticle. Micelles were proposed as a biomimetic of HDL to overcome the potential clinical scalability limitations of sHDLs. We successfully formulated a library of micelles, with varying phosphatidylcholine (PC) lipid types and extent of PEGylation of the particle. While changing the PC lipid did not affect the size of the particles, increasing the PEGylation lead to a decrease in micelle size. Our results showed that micelles are a promising therapeutic agent for treating atherosclerosis due to their ability to reduce cytokine production, promote cholesterol efflux and dissolve cholesterol crystals. While all micelles showed similar cholesterol efflux capacities, the anti-inflammatory activity and cholesterol crystal dissolution capabilities of the particles were impacted by lipid composition in vitro. Micelles composed of POPC and DMPC, and micelles with less PEGylation, were the

most potent in reducing TNF- α and IL-6 proinflammatory cytokine levels. DMPC micelles and micelles with moderate PEGylation showed the greatest ability to dissolve cholesterol crystals. The lipid composition also impacted the pharmacokinetics and cholesterol mobilization in vivo, where micelles with increased PEGylation showed a longer drug exposure and total cholesterol mobilized over 48 hours.

In future work, we would like to further elucidate the impact of lipid composition on the overall therapeutic potential of micelles by testing micelles with different lipid compositions in an in vivo murine model of atherosclerosis. Evaluating how lipid composition may impact the biodistribution, accumulation in plaque areas, and reduction of overall plaque volume may help us further optimize micelles for atherosclerosis treatment. Micelles may also hold potential as drug delivery carriers due to their lipid core and biocompatibility. LXR agonists or PCSK9 inhibitors could be incorporated into micelles and work synergistically to target atherosclerosis pathophysiology. We foresee that the lipid composition of micelles may affect the encapsulation efficiency of these small molecule drugs, therefore, composition may also need to be optimized when using micelles as drug delivery systems to ensure the drugs stay incorporated within the particles and have favorable release kinetics. Further optimization of micelle composition could also include addition of targeting moieties incorporated into the lipid monolayer to improve micelle targeting to atherosclerotic plaques.

In chapter 3, we evaluated the endothelial protective properties of sHDL. We first synthesized a library of sHDLs composed of one of four different PC lipids: POPC, DMPC, DPPC and DSPC. All sHDLs showed ability to reduce adhesion molecule expression in HUVECs challenged with LPS and TNF-α. DMPC-, DPPC-, and POPC-sHDLs showed more potent effects in reducing expression of E-selectin, VCAM1 and ICAM1 in HUVECs challenged

with LPS than DSPC-sHDLs. For HUVECs challenged with LPS and TNF-α, only DMPC-sHDLs were able to partially restore eNOS expression. Furthermore, DMPC-sHDLs showed ability to increase NO production in HUVECs. In a TBI murine model, treatment with DMPC-sHDLs after injury lead to a decrease in Evan blue dye leakage into the injured hemisphere of the brain, suggesting potential positive effects of DMPC-sHDLs on endothelial barrier integrity. The data derived from chapter 3 shows that DMPC-sHDLs have protective effects on the endothelium and promotes proper endothelial function through reduction of adhesion molecules expression and partial restoration of eNOS expression in HUVECs challenged with LPS and TNF-α, increasing NO production in HUVECs, and decreasing Evan blue dye leakage into the brain after TBI, which promotes further development of DMPC-sHDL as a therapeutic to target endothelial dysfunction.

While we observed that sHDLs could increase NO levels in HUVECs, additional studies need to be conducted to elucidate the mechanism behind this activity and subsequent loss of activity in the presence of L-NAME, an eNOS inhibitor. Many mechanisms have been proposed to explain the effects of HDL on eNOS activity, expression and activation, for example, maintaining the lipid environment in caveole where eNOS is localized or activation of kinase signaling cascades through SR-BI. Furthermore, a more defined animal model may be used to specifically evaluate sHDLs therapeutic effect on endothelial barrier integrity, endothelial cell function, and inflammation reduction. We hypothesize that LPS injection in the brain to disrupt the barrier integrity may be a more reasonable model to use. In order to strengthen the therapeutic effects of sHDLs on endothelial function, addition of sphingosine-1-phosphate (S1P) may also be investigated. S1P is a signaling lipid that is present in endogenous HDL and has

been shown to promote endothelial cell growth and reduce expression of adhesion molecules on endothelial cells. Therefore, usage of sHDLs as a delivery system for S1P could be explored.

Chapter 4 focused on evaluating the effect of lipid composition on the remodeling of sHDL in human serum. Due to the dynamic nature of endogenous HDL and exchange of component with LDL and VLDL through transfer proteins and enzymes, assessing how sHDL remodel in human serum is vital to understanding the stability and pharmacokinetics of the nanoparticle as a stand-alone therapy or drug delivery carrier. In our study, we found that sHDLs remodel in the presence of human serum and remodel to varying extents based on lipid composition. By tracking the movement of sHDL components to different lipoprotein populations using SEC and LC-MS analysis, we found that sHDLs formulated with POPC remodeled to the largest extent, while sHDLs formulated with DSPC stayed the most intact after 24 hours of incubation with human serum for blank sHDLs and sHDLs labeled with DiD dye. These trends were slightly different when tracking movement of our model drug, GW3965, after incubation of GW3965-sHDLs with human serum, where POPC-sHDLs showed the largest movement of drug to other lipoprotein populations, while the extent of drug movement was similar for GW3965-DMPC-, DPPC-, and DSPC-sHDLs. We predict that drug encapsulation efficiency and physiochemical properties may also play a role in the extent of drug movement in human serum. Our studies highlight the importance of considering lipid composition and remodeling kinetics when developing sHDLs as therapeutics.

In future studies, we would like to continue to evaluate other properties that affect the movement of drugs carried by sHDLs. We would also like to expand on our current findings and investigate the remodeling of sHDLs containing therapeutic peptides and targeting antibodies in human serum. When adding targeting antibodies to sHDLs, it is important to know if the

antibodies stay intact or become detached or cleaved from sHDLs to determine the effectiveness of the targeting antibody to get sHDLs to their target site. Furthermore, next steps of this research could involve understanding the mechanisms behind sHDL remodeling, focused on the activity of the enzyme and proteins that are responsible for the exchange of components between HDL, LDL and VLDL in circulation. More studies evaluating PLTP and CETP activity and how inhibition of these transfer proteins affects the remodeling of sHDLs could lead to further insights on the mechanisms behind remodeling of sHDLs with endogenous lipoproteins.

Together, the work from this dissertation gives rise to new insights on the application of sHDL and HDL-mimetic micelle therapies for cardiovascular disease and sheds light on the importance of phospholipid composition considerations when developing these lipid-based therapeutics. We hope that these new insights can facilitate further development of sHDLs and HDL-mimetic micelles with optimal therapeutic properties.